Geoscience BC

MINERALS

Summary of Activities 2021

Geoscience BC

GEOSCIENCE BC
SUMMARY OF ACTIVITIES 2021: MINERALS

Geoscience BC Report 2022-01

Geoscience BC

This publication is also available, free of charge, as colour digital files in Adobe Acrobat® PDF format from the Geoscience BC website: http://www.geosciencebc.com/updates/summary-of-activities/.

Every reasonable effort is made to ensure the accuracy of the information contained in this report, but Geoscience BC does not assume any liability for errors that may occur. Source references are included in the report and the user should verify critical information.

When using information from this publication in other publications or presentations, due acknowledgment should be given to Geoscience BC. The recommended reference is included on the title page of each paper. The complete volume should be referenced as follows:

Geoscience BC (2022): Geoscience BC Summary of Activities 2021: Minerals; Geoscience BC, Report 2022-01, 92 p.

Summary of Activities: Minerals (Geoscience BC)
Annual publication

ISSN 2562-8623 (Print)
ISSN 2562-8631 (Online)

Geoscience BC
1101–750 West Pender Street
Vancouver, British Columbia V6C 2T7
Canada

Front cover photo and credit: Ph.D. candidate and *Summary of Activities* author V.K. Kuppusamy collects a sample as part of a coal-leaching experiment at the Norman B. Keevil Institute of Mining Engineering (The University of British Columbia). Photo by D. Stenzel (April 2021).

Foreword

Geoscience BC is pleased to once again present results from our ongoing projects and scholarship recipients in our annual *Summary of Activities* publication. Papers are published in two separate volumes: *Energy and Water*, and this volume, *Minerals*. Both volumes are available in print and online via www.geosciencebc.com.

Summary of Activities 2021: Minerals

This volume, *Summary of Activities 2021: Minerals*, contains nine papers from Geoscience BC–funded projects and scholarship recipients that are within Geoscience BC's strategic focus area of minerals. The papers are divided into two sections, based on Geoscience BC's strategic objectives of

1) Identifying New Natural Resource Opportunities, and
2) Advancing Science and Innovative Geoscience Technologies.

The 'Identifying New Natural Resource Opportunities' section starts off with Sacco et al. providing an update on a surficial exploration program, part of the Central Interior Copper-Gold Research series, with a focus on the innovative use of the Talon Drill™ that has been modified with custom purpose-built tooling to sample subglacial till. The remaining three papers are contributions from Geoscience BC Scholarship recipients. Damant and Enkelmann consider the burial and exhumation history of the Intermontane Belt and related implications for preservation of porphyry deposits, and Voegeli and Lecumberri-Sanchez examine the spatial distribution of the hydrothermal system at the Lawyers property, as well as the broader structural/lithological controls within the Toodoggone region. Finally, Kuppusamy and Holuszko present an update on ongoing research into extracting rare-earth elements from southeastern British Columbia coals.

The 'Advancing Science and Innovative Geoscience Technologies' section features five papers from Geoscience BC Scholarship recipients. Iulianella Phillips et al. describe continuing research into using microbial-community fingerprinting to explore for mineral deposits, and Williams et al. consider both traditional Indigenous knowledge and contemporary ecological theory, as they relate to using fire, as a tool in post-mining reclamation activities. Yang et al. examine rock-engineering standards and the feasibility of integrating them with machine learning, and Hendi et al. present results from an investigation on the response of fibre optic cables used in monitoring geological stresses underground. Finally, Adria et al. explore the application of the parametric-breach method for modelling two tailings-dam breaches and the resultant flows.

Geoscience BC Minerals Publications 2021

Geoscience BC published the following six interim and final reports and maps in 2021:

- Fifteen technical papers in the **Geoscience BC Summary of Activities 2020: Minerals** volume (Geoscience BC Report 2021-01)
- **Surficial Geology, Drift Thickness and Till Sampling Suitability Maps (NTS 093J/03, 047; 093K/09, 16; 093O/03, 04), British Columbia,** by Palmer (Geoscience BC Report 2021-03)
- **Logging SEDAR: A Review of the Contribution of NI 43-101 Reports to Public Geoscience Data,** by N.D. Barlow, J.R. Barlow, K.E. Flower, E.D. Hardie and J.G. McArthur (Geoscience BC Report 2021-04)
- **Geochemical and Indicator Mineral Data from a Regional Bulk Stream-Sediment Survey, Boundary District, South-Central British Columbia**, by W. Jackaman (Geoscience BC Report 2021-05)
- **Smithers Exploration Group's Rock Room Project: Geoscience BC Final Report,** by A. Ledwon, C. Ogryzlo and L. Farrell (Geoscience BC Report 2021-06)
- **Geochemical Reanalysis of Archived Till Samples, CICGR Surficial Exploration Project, Interior Plateau, North Central BC (parts of NTS 093A, B, G, J, K, O),** W. Jackaman, D.A. Sacco and R.E. Lett (Geoscience BC Report 2021-09)
- **Golden Triangle Geophysics Data Compilation Project Summary Report,** by B.K. Clift, T.A. Ballantyne and C.L. Pellett (Geoscience BC Report 2021-15)

All releases of Geoscience BC reports, maps and data are published on our website and announced through our website and e-mail updates. Most final reports and data can be viewed or accessed through our Earth Science Viewer at https://gis.geosciencebc.com/esv/?viewer=esv.

Acknowledgments

Geoscience BC would like to thank all authors and reviewers of the *Summary of Activities* for their contributions to this volume. COVID-19 once again made this a challenging year for all our field programs and laboratory research, and Geoscience BC continues to be grateful for the perseverance of our researchers and scholarship recipients in continuing their projects.

RnD Technical is also acknowledged for its work in editing and assembling both volumes. As well, Geoscience BC would like to acknowledge the Province of British Columbia and our project funding partners for their ongoing support of public geoscience, and express our appreciation for the leaders and volunteers in British Columbia's mineral exploration, mining and energy sectors who support our organization through their guidance, use and recognition of the data and information that we collect and distribute.

Christa Pellett
Vice President, Minerals
Geoscience BC
www.geosciencebc.com

Contents

Identifying New Natural Resource Opportunities

Advancing Science and Innovative Geoscience Technologies

Mineral Exploration in the Central Interior Copper-Gold Research Projects Area, Central British Columbia (Parts of NTS 093A, B, G, J, K, O): New Tools for a Proven Approach to Exploration Under Cover

D.A. Sacco, Palmer, Vancouver, British Columbia, dave.sacco@pecg.ca

B. Janzen, Palmer, Vancouver, British Columbia

W. Jackaman, Noble Exploration Services Ltd., Jordan River, British Columbia

Sacco, D.A., Janzen, B. and Jackaman, W. (2022): Mineral exploration in the Central Interior Copper-Gold Research projects area, central British Columbia (parts of NTS 093A, B, G, J, K, O): new tools for a proven approach to exploration under cover; *in* Geoscience BC Summary of Activities 2021: Minerals, Geoscience BC, Report 2022-01, p. 1–10.

Introduction

Geoscience BC's Central Interior Copper-Gold Research (CICGR) projects area occupies a large region in central British Columbia (BC) between the communities of Mackenzie and Williams Lake (Figure 1a). The region has significant mineral potential, however, exploration is hindered by extensive Quaternary sediments that obscure bedrock. The objective of the CICGR projects is to investigate the potential for undiscovered mineral deposits buried beneath thick glacial sediments.

Drift prospecting is an effective method to identify exploration targets in areas covered by thick glacial sediments and can be optimized when applied within a comprehensive understanding of the glacial history and surficial geology (e.g., Levson et al., 1994; Levson, 2001; Plouffe et al., 2001; Sacco et al., 2018). As such, Geoscience BC has initiated this multiyear surficial exploration program targeting specific areas (surficial study areas; Figure 1a, b) within the larger CICGR projects area. The program is modelled after Geoscience BC's highly successful Targeting Resources through Exploration and Knowledge (TREK; e.g., Jackaman and Sacco, 2014; Jackaman et al., 2014, 2015; Sacco and Jackaman, 2015; Sacco et al., 2018) and Quesnellia Exploration Strategy (QUEST; e.g., Sacco et al., 2010; Ward et al., 2011, 2012, 2013) surficial exploration programs (Figure 1). The CICGR program is generating high-quality baseline data integral to promoting and supporting successful mineral exploration in this challenging setting. Combined with data from the TREK (Jackaman et al., 2015) and QUEST (Ward et al., 2013) projects, the results of this study extend the coverage of directly comparable geochemical and mineralogical data and 1:50 000 scale surficial mapping to a large, nearly continuous portion of central BC (Figure 1c).

This publication is also available, free of charge, as colour digital files in Adobe Acrobat® PDF format from the Geoscience BC website: http://geosciencebc.com/updates/summary-of-activities/.

This program is designed to generate a geochemical and mineralogical database and an understanding of the surficial geology necessary to collect and interpret these data, such that they can be integrated into and guide private-sector exploration. The scope of the program defines three objectives:

1) produce 1:50 000 scale surficial geology maps and derive till sampling suitability (TSS) and drift thickness maps to support mineral exploration;
2) compile relevant historical data and reanalyze archived till survey samples; and
3) build upon the historical dataset through new and infill till geochemical and mineralogical surveys.

A summary of the three objectives along with the results from the first two years of the program are presented herein. A more detailed account of these objectives and prior years' activities is available in previous Geoscience BC Summary of Activities publications (Sacco et al., 2020, 2021). The project is currently in its third and final year, during which the focus has largely been on completing the till sampling, field verification and finalization of the surficial geology interpretations, and preparing the survey results for release.

A new program objective was added in 2021 that aims to determine how a hand-portable, shallow-drilling system can be integrated into till sampling programs for regional- to property-scale surveys. The use of a portable, shallow-drilling system to collect till samples is not a new concept. Several groups, including the Geological Survey of Canada (GSC), have tested off-the-shelf products for this purpose (e.g., Plouffe 1995; McMartin and McClenaghan, 2001). Limited success has been realized due to the complex nature of subglacial till; it requires a system that can penetrate overconsolidated sediments containing cobbles and boulders. As a result, industry's only option has been to use larger, more expensive systems, which are not always a feasible option (e.g., reverse circulation or rotosonic systems) to collect till samples in unfavourable conditions. The Talon Drill™ (manufactured by Quantum Machine Works

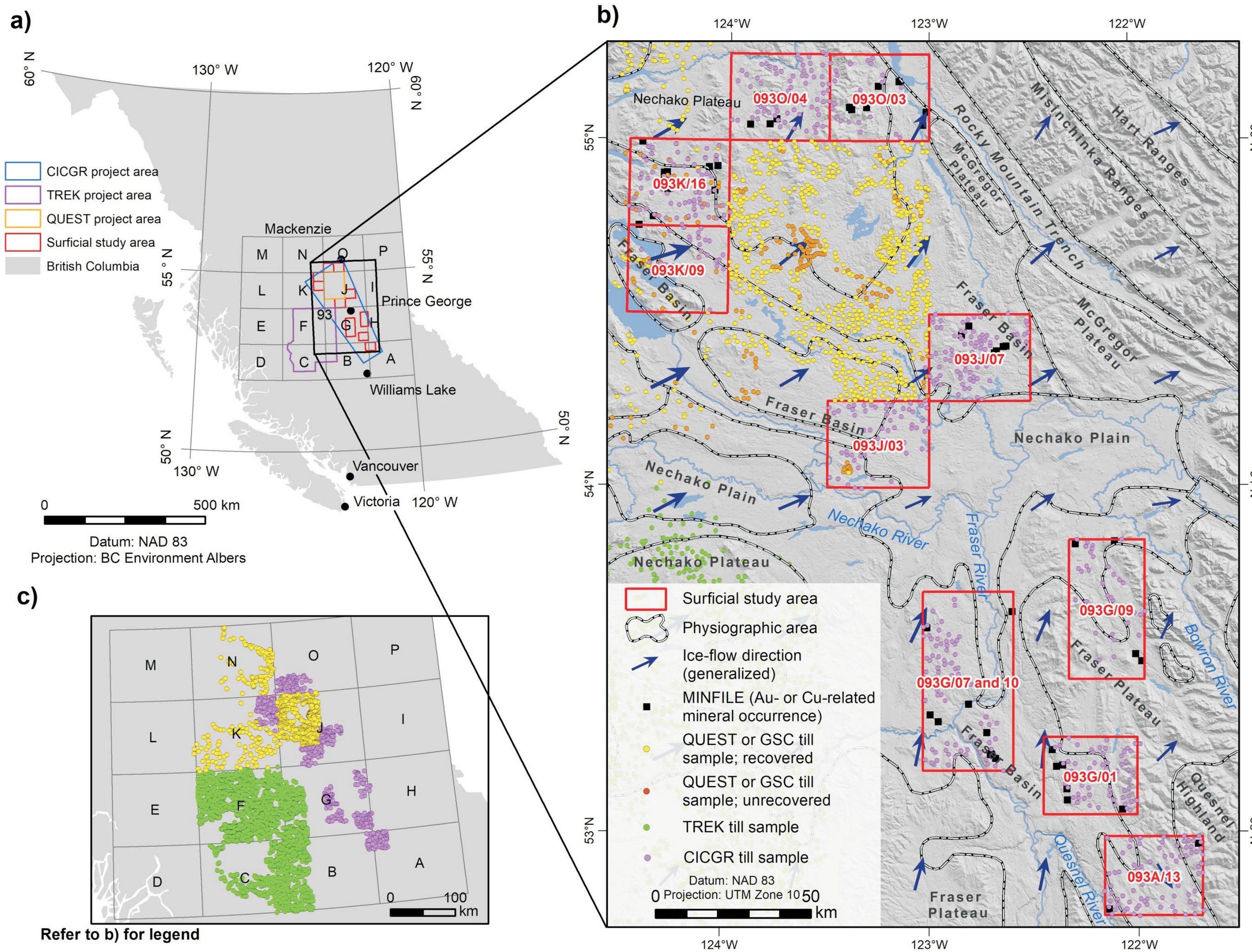

Figure 1. a) Location of Central Interior Copper-Gold Research (CICGR), Targeting Resources through Exploration and Knowledge (TREK) and Quesnellia Exploration Strategy (QUEST) projects areas. **b)** Surficial study areas; physiographic areas (Holland, 1976; Mathews, 1986); MINFILE occurrences (BC Geological Survey, 2020); locations of historical surface sediment samples proposed for reanalysis from QUEST (Ward et al., 2013) and Geological Survey of Canada (GSC) programs (Plouffe and Ballantyne, 1993; Plouffe, 1995; Plouffe and Williams, 1998); TREK till sample locations (Jackaman et al., 2015); and till samples collected during this study. **c)** Distribution of recovered historical till samples (yellow symbols) in central British Columbia, which have been reanalyzed to produce data comparable to existing data from the TREK (green symbols) and current (purple symbols) projects.

Ltd.), modified with custom purpose-built tooling, has proven effective in drilling through subglacial till and has the potential to streamline till sampling programs and improve sampling distribution and coverage, ultimately providing more robust datasets to support explorers in BC.

Project Area and Previous Work

Within the CICGR projects area, the surficial exploration study areas include parts of NTS 093A, B, G, J, K and O and cover approximately 9700 km^2 (Figure 1c). There are 52 MINFILE mineral occurrences related to gold or copper mineralization within the surficial study areas (BC Geological Survey, 2020), although significantly more occur within the larger CICGR projects area. The surficial study areas were determined based on

1) prospective geology,
2) avoidance of private land, and
3) applicability of till sampling.

Some of the study area boundaries are not the same as the NTS map area boundaries to account for these factors. For continuity of the till database, the compilation of historical till data and reanalysis of archived samples extends beyond the CICGR projects area to include the full extent of previous surveys (Figure 1).

The surficial study areas are within the Interior Plateau physiographic region and consist of parts of the Fraser Basin, Fraser Plateau, Nechako Plain, Nechako Plateau, Rocky Mountain Trench and Quesnel Highland (Holland, 1976; Mathews, 1986). Bedrock exposures are commonly obscured by thick surficial deposits, composed dominantly of till, glaciolacustrine and glaciofluvial sediments. Small-scale surficial geology mapping has previously been completed in some parts of the project area, providing an important regional context for the higher resolution interpretations being completed as part of this project. A complete list of regional surficial geology maps that overlap the study areas is available in Sacco et al. (2020).

The regional surficial setting is largely a result of the coalescence and subsequent divergence of glaciers in and around the northern part of the CICGR area during the last (Fraser) glaciation. This dynamic glacial environment resulted in a complex landscape with thick surficial deposits, which have hindered exploration efforts. The coalescence of advancing ice masses caused significant variations in ice flow that affected the depositional patterns of till and altered drainage systems resulting in the development of extensive glacial lakes (Clague, 1988; Plouffe, 1997; Sacco et al., 2017). During deglaciation, ice retreated toward the source areas leaving behind ablating ice masses that again altered drainage resulting in the deposition of large outwash deposits and the development of glacial Lake Fraser: an extensive body of water that changed shape and size throughout deglaciation and in which significant amounts of sediment accumulated. These thick sediment units obscure the underlying bedrock and till, which typically provide a basis for exploration, hindering the collection of high-quality surface data. As a result, the CICGR area is underexplored and its potential mineral resources are largely unknown. Previous till sampling programs have been conducted in the northwestern part of the CICGR area (Figure 1), for which descriptions are provided in Sacco et al. (2020).

In the first two years of this program, the surficial geology, TSS and drift thickness mapping products were drafted. The maps provided the foundation to plan and execute a till sampling program focused mostly in the northern study areas (NTS 093J/03, 07, 093K/09, 16, 093O/03, 04). The historical data were compiled and the archive samples from the GSC and Geoscience BC programs were collected and sent to the lab for reanalysis.

Methods

Objective 1: Surficial Geology Mapping and Derivative Mapping

Surficial geology mapping provides a basis for the collection and interpretation of surface sediment data. The surficial geology was interpreted from pseudo-stereo imagery at a scale of 1:50 000 using the GSC mapping protocols (Deblonde et al., 2018), which maintains consistency with existing regional mapping by the GSC and similar scale mapping by the BC Geological Survey. Specific details of the mapping protocols are provided in Sacco et al. (2020).

Till sampling suitability and drift thickness maps were derived from the surficial geology mapping using multiclass indices to reattribute the polygons. The TSS index was based on the occurrence of subglacial till and geomorphological processes that may have altered, reworked or remobilized the material. This ultimately categorized the polygons based on the proportion of subglacial till at the surface that is suitable for sampling. The drift thickness index used the mapped unit thicknesses and assumed sediment stratigraphy (e.g., glaciolacustrine material is deposited passively, so it is assumed to overlie till) to estimate relative thicknesses for the polygon attributes.

Objective 2: Compilation of Historical Data and Reanalysis of Archive Samples

Reanalyzing till samples archived from previous regional geochemical surveys is a cost-effective method to upgrade the utility of the associated geochemical datasets. Many of these historical projects were completed in the 1990s when sampling protocols were less strict, and a considerable amount of the original results were generated using analytical methods that have been replaced by new procedures that provide more accurate determinations and have lower detection limits. The reanalysis by modern laboratory techniques creates a high-quality dataset that is comprehensive and directly comparable to the standard of current provincial datasets, which support mineral exploration and environmental assessments.

Archive sample material from the silt+clay (<0.063 mm) size fraction was sent to Bureau Veritas Commodities Canada (Bureau Veritas; Vancouver, British Columbia) for analysis to elevate these datasets to current standards. Details of the analytical packages are described in the methods for objective 3 below. Prior to reanalysis, analytical duplicate and control reference samples were inserted into the sample sequence to monitor and assess the accuracy and precision of the new analytical results.

Objective 3: Till Geochemical and Mineralogical Survey

Subglacial till is the target sample media for this survey because it is a first derivative of bedrock (Schilts, 1993), is predictably transported in the direction of ice flow and provides a larger anomaly than the original bedrock source (Levson, 2001). For this program, C-horizon material was collected to reduce the influence of soil development and postdepositional processes on the geochemical concentrations of the material. As such, anomalies can be more confidently attributed to geology (i.e., mineralization) as opposed to other processes that cause spurious results in A- or B-horizon soil data. The surficial geology and TSS mapping provided the foundation to plan and collect suitable subglacial till samples at ~2 km spacing. The survey was conducted to established standards, producing high-quality field and analytical results that are consistent with, and comparable to, the existing provincial till geochemical database.

The till geochemical and mineralogical survey was completed during years two and three of the program. Most of the sampling relied on existing exposures of sediments (e.g., roadcuts), termed 'opportunistic exposures', which were targeted to reach the in situ, C-horizon subglacial till. To sample these exposures, it was necessary that the till be at or close to the surface and the site be accessible via an active road. In many areas, there are sufficient opportunistic exposures to achieve the desired sample distribution for a regional program, but in some areas this can be challenging due to a lack of optimal sampling sites. This year, a new method of sampling using a shallow-drilling system was introduced to access C-horizon till without being constrained by the occurrence of opportunistic exposures, while also providing a means to collect samples beneath veneers of other materials.

At opportunistic sites, the standard protocol was used. This involved collecting two, ~1 kg, C-horizon subglacial till samples for geochemical analysis and 50 clasts (ranging in size from large pebble to small cobble) for lithological analysis. At approximately every other site (i.e., half density), an additional 10–12 kg sample was collected for mineralogical analysis. Sacco et al. (2020) provides additional details for the field sampling and data collection protocols used at opportunistic sampling sites.

The drill-supported sampling was completed with the Talon Drill tooled with custom bits and samplers specifically designed and engineered for till sampling (Figure 2).

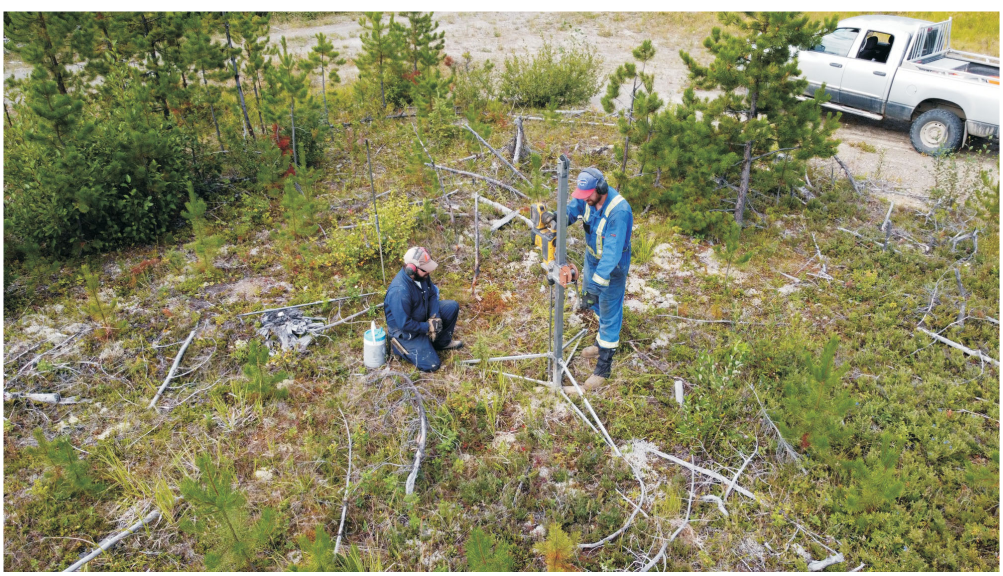

Figure 2. The Talon Drill™ system tooled with custom bits and samplers specifically designed to work within the difficult drilling conditions encountered when sampling subglacial till. This system enables the collection of high-quality till samples anywhere the till occurs at or near the surface. This method of till sampling overcomes the limitations of standard opportunistic sampling programs, which can result in suboptimal sample distributions because of the reliance on sampling existing exposures.

It is a rotary-percussion system designed to displace fine-grained material (i.e., till matrix) while the specialized bits and hammer-action are capable of pulverizing clasts and drilling through boulders that may be encountered. This system provides a nearly zero-impact method to quickly and easily access C-horizon till at surface or buried beneath a shallow deposit of other materials, which would have otherwise been inaccessible. At a typical drill-sample site, a series of pilot bits were used to penetrate to a suitable sample depth of ~1.5 m. A specialized sampler was then attached to collect an in situ sample from the bottom of the hole. Approximately 500 g of till matrix was collected at each sample site for geochemical analysis. Due to the smaller sample sizes and limited exposure of in situ material compared to the opportunistic sites, the single 500 g sample was used for all analyses and no pebble or mineralogy samples were collected.

Geochemical analysis for all samples is being performed by Bureau Veritas. The samples are dried and processed to produce clay (<0.002 mm) and silt+clay (<0.063 mm) size fraction splits. Both size fractions will be analyzed for minor and trace elements by an ultratrace, aqua-regia digestion (0.5 g sample), inductively coupled plasma–mass spectrometry (ICP-MS) package for 53 elements and by instrumental neutron activation analysis (INAA) for total gold plus 34 elements. Major and minor elements will be determined by inductively coupled plasma–emission spectrometry (ICP-ES) following a lithium metaborate-tetraborate fusion and dilute acid digestion. This analytical package will include loss-on-ignition by weight difference after ignition at 1000ºC, plus total carbon and sulphur by LECO analysis. The LECO analysis converts carbon and sulphur forms in a sample into CO_2 and SO_2 by combustion in an induction furnace. The concentrations of CO_2 and SO_2 are measured by infrared absorption and thermal conductivity to determine total concentrations of carbon and sulphur. Quality control for analytical determinations will include the use of field duplicates, analytical duplicates, reference standards and blanks, based on established protocols (Spirito et al., 2011).

Clast lithologies were grouped into broad categories that reflect the main lithologies of local bedrock to provide insight on the direction and distance of glacial transport. The bulk till samples were sent to Overburden Drilling Management Limited (Ottawa, Ontario) and processed for gold grain concentrates (<2.0 mm) and heavy and medium mineral concentrates (0.25–2.0 mm) using a combination of gravity tables and heavy liquids. Concentrates will be visually picked for gold and porphyry-copper–indicator minerals.

Progress and Future Work

The surficial geology interpretations provided the foundation to develop the CICGR surficial exploration field program strategy. Draft surficial geology, TSS and drift thickness mapping was completed in year one and revealed that TSS is most heavily influenced by the distribution of glacial lake sediments and ablation till. These deposits are also generally associated with thicker drift as they tend to accumulate in large depressions (i.e., lowlands around Prince George) and within valley fill sequences. The surficial geology interpretations and derivative products have been refined and finalized based on field observations for 093J/03, 07, 093K/09, 16, 093O/03 and 04. These map products were released as Geoscience BC Report 2021-03 (Palmer, 2021), which is a compilation of 18 georeferenced PDF maps. The field observations collected for the study areas associated with 093A/13, 093G/01, 07, 09 and 10 are currently being compiled and used to finalize the respective mapping products. The release of the remaining surficial map sets is planned for early 2022. The release will include georeferenced PDF map sets of surficial geology, TSS and drift thickness, and spatial data for the complete map series, including the already released map sets.

A total of 1039 archive samples or pulps (i.e., representative 2 g splits of the silt+clay [<0.063 mm] size fraction) were recovered for reanalysis. Six hundred and seventy-two of these were archive samples originally collected in the late 2000s as part of Geoscience BC's QUEST project (Ward et al., 2013). Three hundred and sixty-seven were pulps retained from regional till surveys completed by the GSC in the 1990s (Plouffe and Ballantyne, 1993; Plouffe, 1995; Plouffe and Williams, 1998). Approximately 330 pulps and 153 archive till samples could not be located. The reanalysis has been completed and the results have been released in Geoscience BC Report 2021-09 (Jackaman et al., 2021).

The 2020 and 2021 till sampling programs were complicated by the COVID-19 pandemic. Field crews adhered to WorkSafeBC guidelines with a focus on the maintenance of working-group bubbles to reduce the risk of crew exposure and community spread of COVID-19. Lodging and travel options were restricted, resulting in longer daily commutes to the study areas and driving rather than flying to field sites. Although these complications had an impact on daily productivity, the goals of completing the till sampling program throughout all map areas and verifying the mapping with field-based information were achieved.

Six hundred and thirty-four new till samples were collected in the survey area. The expected sample density has been achieved throughout most of the individual study areas; however, some regions are lacking adequate coverage (Figure 1c). The main factors inhibiting till sample collection were a lack of road access, limited opportunistic sampling sites and/or materials of another genesis overlying the till and impeding sampling. Few till samples were collected from the eastern portion of 093O/03 due to the extensive outwash deposits and a lack of road access. Sample coverage in much of 093K/09 is poor due to extensive mantles of thin glaciolacustrine material that cover the till, and low relief that results in few roadcuts. Similarly, sample coverage in 093G/07 and 10 is limited due to the extensive glaciolacustrine mantles overlying the till, particularly in the Fraser River Valley where till has largely been eroded or buried through glaciofluvial activity. The desired sample density was also not achieved on the east side of 093J/07 and throughout 093G/09. Deglacial sediments impeded access to till in both map areas, but a lack of road access was the biggest issue in 093G/09.

Testing of the Talon Drill system was focused mainly on the northern part of 093J/03. This area was chosen because road access is relatively good, opportunistic exposures are rare and till generally occurs either at surface or buried under a thin veneer of glaciolacustrine material throughout much of the area. This area provided optimal testing conditions for the drill system because of the combination of factors that hindered standard opportunistic sampling here.

In 2020, 29 opportunistic samples were collected in 093J/03 and the map area was considered finished because no other existing exposures could be located for sampling. In 2021, 31 additional samples were collected using the shallow-drilling system, doubling the sample density for the map area and greatly improving the coverage and distribution of sampling (Figure 3). Average sampling times were about 90 minutes, including the set up and tear down of the drill. This average time would likely be lower during a production-focused program because additional time was spent at some sites testing different tooling and some suboptimal sites were chosen in order to determine how the drill would perform. Nevertheless, drill-supported sampling rates averaged only 0.3 samples per day lower than the standard opportunistic approach with hand tools, and the resulting sample distribution and coverage were significantly better, demonstrating the efficacy and value of the system.

Many of the drill-supported samples were collected in areas where till was predicted to occur but existing exposures were lacking to verify the surficial material type. Due to

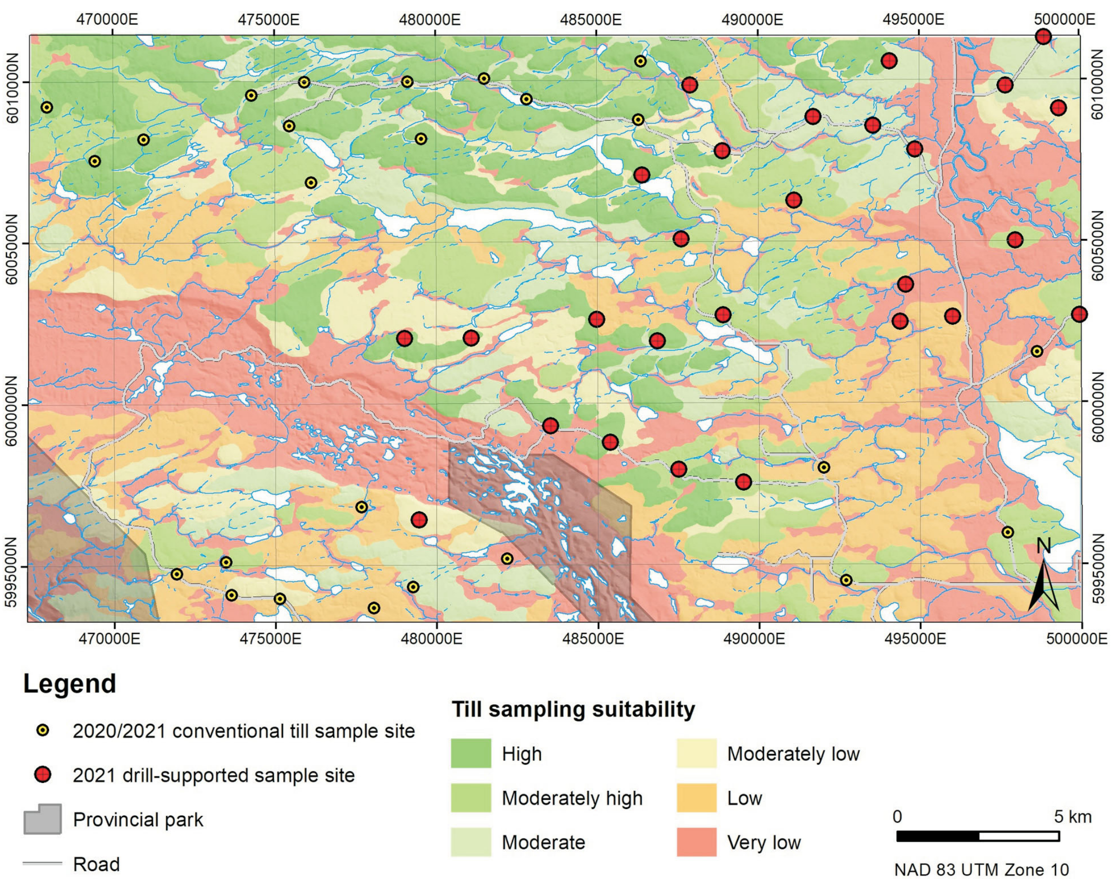

Figure 3. Sample distribution attained using the standard ‘opportunistic’ method of till sampling (yellow symbols) with hand tools from existing sediment exposures, such as roadcuts, and using the Talon Drill™ shallow-drilling system (red symbols) in the northern part of NTS map area 093J/03. Till sampling suitability classifications are defined in Sacco et al. (2020).

this lack of exposures, knowledge that till is present at the sample sites was integral to success, which was largely accomplished through the examination of shallow test pits and the experience of the sampling crew. The 1:50 000 scale mapping completed for this program provides an understanding of the general setting but lacks the detail to determine the conditions at a specific site. In the absence of higher resolution mapping, the ability of sampling crews to interpret the landscape will be critical in future programs that employ drill-supported sampling.

The drilling system was tested to determine how much of the till profile can be effectively sampled and the maximum thickness of overlying materials below which samples can be collected. In general, the first metre of till requires less than 10 minutes to drill through, whereas the second metre requires an additional 15 minutes. The third and the fourth metres require about 25 and 40 minutes, respectively. The maximum depth reached in till was 3.9 m. Further depths could be reached, but it was decided that enough information had been gained and the time was better spent sampling other sites. Reaching a depth of 4 m in about 90 minutes is impressive, but the decreased drilling rate with depth makes drilling deeper counterproductive for a regional program. For target-scale work, the value of the data would necessitate the extra time, but in general an ~2 m depth is considered optimal for a regional survey.

The clast content of the till was the largest factor contributing to drilling rates. The drill advanced through most clasts that were encountered in the till. Pebble- to medium cobble-sized (2–15 cm) clasts were quickly surpassed, although rounded quartzite pebbles and cobbles posed a challenge as the hardness and rounding caused the bit to move laterally, binding the rod string against the hole. Clasts can usually be penetrated to about 10 cm within five minutes, at which time they will typically fracture and displace. If the clast has not been surpassed within five minutes, it could be too large to advance through in a reasonable amount of time. In these cases, it was determined to be more efficient to move the drill a metre or two and start a new hole. There is no way of predicting how large the clast is and it is likely faster to drill through a new section of till than risk spending too much time slowly advancing through a boulder.

The drill advanced through softer sediments considerably faster than through till. At numerous locations, 1 to 2.5 m of glaciolacustrine sand and silt were smoothly advanced through in 5 to 30 minutes. When suitable till was encountered, which is demarcated by an obvious change in drilling rates, samples could be collected immediately below the fine-grained material. In general, fine-grained glaciolacustrine materials were not a hindrance to sampling; however, accurately predicting their depth when thicker than a few metres can be difficult. As such, it is recommended to only attempt sampling beneath areas interpreted as having thin mantles (e.g., <2 m) of glaciolacustrine sediment, to avoid the potential of beginning a hole that would require more time than anticipated and lowering production rates. Nonetheless, the results of this testing indicate that the Talon Drill system provides a means to extend till sampling into areas that are mapped as glaciolacustrine veneer overlying till, which were previously identified as poorly suited for sampling.

In 2021, 38 samples were collected using the Talon Drill and 140 samples were collected from roadcut exposures. These samples have been sent to Bureau Veritas and Overburden Drilling Management Ltd. for geochemical and mineralogical analyses, respectively. The geochemical, mineralogical and pebble data from the new samples will be evaluated and compiled before they are released as digital databases, which will include all analytical results and quality control data. The data are expected to be ready for release in mid 2022.

Conclusions

The Central Interior Copper-Gold Research (CICGR) surficial exploration program has produced over 9700 km^2 of new surficial geology, till sampling suitability and drift thickness mapping to support mineral exploration. Using these products, 634 new subglacial till samples were collected that infill gaps within the existing historical datasets and extend coverage into new areas. From the archives, 1039 samples were reanalyzed. The project results, combined with data from the earlier Targeting Resources through Exploration and Knowledge (TREK) and Quesnellia Exploration Strategy (QUEST) projects, extend the coverage of comprehensive geochemical and mineralogical data to a nearly continuous portion of central British Columbia, and will promote increased awareness in a highly prospective region, assist in the identification of new exploration targets and support follow-up activities.

The data-driven approach to this program contributes heavily to its success. A foundational understanding of the surficial geology not only informs the design and execution of the program, but also identifies the characteristics of the areas that are not suitable for the standard sampling methodologies. Low relief, resulting in a lack of opportunistic exposures, and mantles of deglacial materials overlying the till are recurring challenges to achieving optimal sample distributions. A new method of sampling using a hand-portable, ultra-lightweight drill was tested this year to overcome these challenges. The testing revealed that the Talon Drill™, tooled with customized bits and samplers, effectively extended sample coverage into areas where standard opportunistic sampling methods were not successful. These results suggest that the use of this method can be extended to the east part of NTS 093O/03, the majority of 093K/09, southeast corner of 093J/07 and much of 093G/07 and 10 to improve data coverage in those regions, and the overall success of the CICGR surficial exploration program.

Acknowledgments

This program was funded by Geoscience BC. The authors would like to thank A. Plouffe from the Geological Survey of Canada for his heroic efforts to recover archive samples from storage in Ottawa and his support in the development of this project. Assistance in archive sample recovery was also provided by R. Lett, B. Ward and T. Ferbey. The fieldwork would not have been possible without the hard work by field assistants H. Bains and J. Constandinou. A special thank you to D. Turner for his thorough review and thoughtful comments that improved the quality of this paper.

References

BC Geological Survey (2020): MINFILE BC mineral deposits database; BC Ministry of Energy, Mines and Low Carbon Innovation, BC Geological Survey, URL <http://minfile.ca/> [October 2020].

Clague, J.J. (1988): Quaternary stratigraphy and history, Quesnel, British Columbia; Géographie physique et Quaternaire, v. 42, p. 279–288.

Deblonde, C., Cocking, R.B., Kerr, D.E., Campbell, J.E., Eagles, S., Everett, D., Huntley, D.H., Inglis, E., Parent, M., Plouffe, A., Robertson, L., Smith, I.R. and Weatherston, A. (2018): Surficial data model: the science language of the integrated Geological Survey of Canada data model for surficial geology maps (ed. ver. 2.3.14); Geological Survey of Canada, Open File 8236, 50 p.

Holland, S.S. (1976): Landforms of British Columbia: a physiographic outline (second edition); BC Ministry of Energy, Mines and Low Carbon Innovation, Bulletin 48, 138 p.

Jackaman, W. and Sacco, D. (2014): Geochemical and mineralogical data, TREK project, Interior Plateau, British Columbia; Geoscience BC, Report 2014-10, 13 p., URL <http://www.geosciencebc.com/reports/gbcr-2014-10/> [October 2020].

Jackaman, W., Sacco, D. and Lett, R.E. (2014): Geochemical reanalysis of archived till samples, TREK project, Interior Plateau, central BC (parts of NTS 093C, 093B, 093F & 093K); Geoscience BC, Report 2015-09, 5 p., URL <http://www.geosciencebc.com/reports/gbcr-2015-09/> [October 2020].

Jackaman, W., Sacco, D.A. and Lett, R.E. (2015): Regional geochemical and mineralogical data, TREK project – year 2, Interior Plateau, British Columbia; Geoscience BC, Report 2015-12, 13 p., URL <http://www.geosciencebc.com/reports/gbcr-2015-12/> [October 2020].

Jackaman, W., Sacco, D.A. and Lett, R.E. (2021): Geochemical reanalysis of archived till samples, CICGR surficial exploration project, Interior Plateau, north central BC (parts of NTS 093A, B, G, J, K, O); Geoscience BC, Report 2021-09, 13 p., URL <http://geosciencebc.com/i/project_data/GBCReport2021-09/GBC%20Report%202021-09%20Geochemical%20Reanalysis%20of%20Archived%20Till%20Samples%20Report%20and%20Data.zip> [October 2021].

Levson, V.M. (2001): Regional till geochemical surveys in the Canadian Cordillera: sample media, methods, and anomaly evaluation; *in* Drift Exploration in Glaciated Terrain, M.B. McClenaghan, P.T. Bobrowsky, G.E.M. Hall and S.J. Cook (ed.), Geological Society, Special Publication No. 185, p. 45–68.

Levson, V.M., Giles, T.R., Cook, S.J. and Jackaman, W. (1994): Till geochemistry of the Fawnie Creek area (93F/03); BC Ministry of Energy, Mines and Low Carbon Innovation, BC Geological Survey, Open File 1994-18, 40 p., URL <https://www2.gov.bc.ca/gov/content/industry/mineral-exploration-mining/british-columbia-geological-survey/publications/openfiles-1999-1990#1994> [October 2020].

Mathews, W.H. (1986): Physiographic map of the Canadian Cordillera; Geological Survey of Canada, "A" Series Map 1710A, scale 1:5 000 000.

McMartin, I. and McClenaghan, B. (2001): Till geochemistry and sampling techniques in glaciated shield terrain: a review; *in* Drift Exploration in Glaciated Terrain, M.B. McClenaghan, P.T. Bobrowsky, G.E.M. Hall and S.J. Cook (ed.), Geological Society, Special Publication No. 185, p. 19–43.

Palmer (2021): Surficial geology, drift thickness and till sampling suitability maps (NTS 093J/03, 07; 093K/09, 16; 093O/03, 04), British Columbia; Geoscience BC, Report 2021-03, 18 maps, scale 1:50 000, URL <http://geosciencebc.com/i/project_data/GBCReport2021-03/GBC%20Report%202021-03%20Surficial%20Geology,%20Drift%20Thickness%20and%20Till%20Sampling%20Suitability%20Maps.zip> [October 2021].

Plouffe, A. (1995): Geochemistry, lithology, mineralogy and visible gold grain content of till in the Manson River and Fort Fraser map areas, central British Columbia (NTS 093K, N); Geological Survey of Canada, Open File 3194, 119 p.

Plouffe, A. (1997): Ice-flow and late-glacial lakes of the Fraser glaciation, central British Columbia; *in* Current Research 1997-A/B, Geological Survey of Canada, p. 133–143.

Plouffe, A. and Ballantyne, S.B. (1993): Regional till geochemistry, Manson River and Fort Fraser area, British Columbia (NTS 093K, N), silt plus clay and clay size fractions; Geological Survey of Canada, Open File 2593, 224 p.

Plouffe, A. and Williams, S.P. (1998): Regional till geochemistry of the northern sector of Nechako River map area, British Columbia (NTS 093F); Geological Survey of Canada, Open File 3687, scale 1:400 000.

Plouffe, A., Levson, V.M. and Mate, D.J. (2001): Till geochemistry of the Nechako River map area (NTS 93F), central British Columbia; Geological Survey of Canada, Open File 4166, 66 p.

Sacco, D.A. and Jackaman, W. (2015): Targeted geochemical and mineralogical surveys in the TREK project area, central British Columbia (parts of NTS 093B, C, F, G): year two; *in* Geoscience BC Summary of Activities 2014, Geoscience BC, Report 2015-01, p. 1–12, URL <http://cdn.geosciencebc.com/pdf/SummaryofActivities2014/SoA2014_Sacco.pdf> [October 2020].

Sacco, D.A., Jackaman, W. and Knox, C. (2021): Proven approach to mineral exploration in thick surficial deposits applied to the Central Interior Copper-Gold Research projects area, central British Columbia (parts of NTS 093A, B, G, J, K, O); *in* Geoscience BC Summary of Activities 2020: Minerals, Geoscience BC, Report 2021-01, p. 1–10, URL <http://

www.geosciencebc.com/i/pdf/SummaryofActivities2020/Minerals/Project%202018-050_MineralsSOA2020.pdf> [October 2021].

Sacco, D.A., Jackaman, W. and McGregor, C. (2020): Mineral exploration in central British Columbia's thick surficial deposits: surficial mapping to inform surface sediment data compilation and till sample reanalysis and collection in the Central Interior Copper-Gold Research project area (parts of NTS 093A, B, G, J, K, O); *in* Geoscience BC Summary of Activities 2019: Minerals, Geoscience BC, Report 2020-01, p. 83–92, URL <http://www.geosciencebc.com/i/pdf/SummaryofActivities2019/Minerals/Project%202018-050_Minerals_SOA2019.pdf> [October 2020].

Sacco, D.A., Lett, R., Jackaman, W. and Elder, B. (2018): Advanced processing of the TREK project geochemical data: identifying and enhancing geochemical anomalies in the TREK project area using sediment transport modeling combined with multimedia and multivariate analysis; Geoscience BC, Report 2018-07, 56 p., URL <http://www.geosciencebc.com/i/project_data/GBCReport2018-07/GBCReport2018-07.pdf> [October 2020].

Sacco, D.A., Ward, B.C., Lian, O.B., Maynard, D.E. and Geertsema, M. (2017): Quaternary geology of part of the McLeod Lake map area (NTS 093J), central British Columbia: lithostratigraphy, glacial history, and chronology; Canadian Journal of Earth Sciences, v. 54, no. 10, p. 1063–1084.

Sacco, D.A., Ward, B.C., Maynard, D., Geertsema, M. and Reichheld, S. (2010): Terrain mapping, glacial history and drift prospecting in the northwest corner of McLeod Lake map area (part of NTS 093J), central British Columbia; *in* Geoscience BC Summary of Activities 2009, Geoscience BC, Report 2010-01, p. 33–42, URL <http://cdn.geosciencebc.com/pdf/SummaryofActivities2009/SoA2009_Sacco.pdf> [October 2020].

Shilts, W. (1993): Geological Survey of Canada's contributions to understanding the composition of glacial sediments; Canadian Journal of Earth Sciences, v. 30, p. 333–353.

Spirito, W.A., McClenaghan, M.B., Plouffe, A., McMartin, I., Campbell, J.E., Paulen, R.C. and Hall, G.E.M. (2011): Till sampling and analytical protocols for GEM projects: from field to archive; Geological Survey of Canada, Open File 6850, 83 p.

Ward, B.C., Leybourne, M.I. and Sacco, D.A. (2011): Drift prospecting within the QUEST project area, central British Columbia (NTS 093J): potential for porphyry copper-gold, volcanogenic massive sulphide mineralization and gold-copper veins; *in* Geoscience BC Summary of Activities 2010, Geoscience BC, Report 2011-01, p. 73–96, URL <http://cdn.geosciencebc.com/pdf/SummaryofActivities2010/SoA2010_Ward_etal.pdf> [October 2020].

Ward, B.C., Leybourne, M.I. and Sacco, D.A. (2012): Heavy mineral analysis of till samples within the QUEST project area, central British Columbia (NTS 093J); *in* Geoscience BC Summary of Activities 2011, Geoscience BC, Report 2012-01, p. 59–68, URL <http://cdn.geosciencebc.com/pdf/SummaryofActivities2011/SoA2011_Ward.pdf> [October 2020].

Ward, B.C., Leybourne, M.I., Sacco, D.A., Lett, R.E. and Struik, L.C. (2013): Drift prospecting for porphyry copper-gold, volcanogenic massive sulphide mineralization and precious and base metal veins within the QUEST project area, central British Columbia (NTS 093J); Geoscience BC, Report 2013-15, 59 p., URL <http://www.geosciencebc.com/reports/gbcr-2013-15/> [October 2020].

Upper-Crustal Cooling History of the Intermontane Belt in Southern British Columbia (Parts of NTS 082E, 092I, P, 093A, B, C)

K.A. Damant[1], **Department of Geoscience, University of Calgary, Calgary, Alberta, kade.damant@ucalgary.ca**

E. Enkelmann, Department of Geoscience, University of Calgary, Calgary, Alberta

Damant, K.A. and Enkelmann, E. (2022): Upper-crustal cooling history of the Intermontane Belt in southern British Columbia (parts of NTS 082E,092I, P, 093A, B, C); *in* Geoscience BC Summary of Activities 2021: Minerals, Geoscience BC, Report 2022-01, p. 11–20.

Introduction

Porphyry deposits are large (10–100 km^3), low to medium grade ore deposits which supply approximately 70% of the world's copper and most of the molybdenum (Dilles and John, 2021). As the demand for raw materials increases, identification and development of new porphyry deposits will prove essential to the support of a growing global population. Porphyry deposits typically form at shallow depths (1–4 km), where metalliferous fluids circulate through the tops of the intrusions and deposit metals (Seedorff et al., 2005; Singer et al., 2008). Most porphyries preserved today are Cenozoic in age, likely due to the effective erosion of the upper crust in older settings (Sillitoe, 2010). Therefore, porphyry deposits can be used as a proxy for identifying regions of limited erosion and exhumation, particularly in Mesozoic and older terranes.

The Intermontane Belt of the Canadian Cordillera is an economically significant region in British Columbia (BC) due to an abundance of Cu-Au-Mo porphyry deposits (Figure 1; McMillan et al., 1996). A problem facing mineral exploration efforts in southern BC is the widespread Cenozoic basalt and Pleistocene glacial till that cover the porphyry targets (Mihalynuk, 2007; Thomas et al., 2011; Sacco et al., 2021). This cover sequence not only impairs geophysical imaging techniques, but precludes relying on surface observations and geological mapping as exploration options. Working toward a better understanding of the evolution of the porphyry-bearing bedrock underlying the cover rocks will help mitigate this problem and may lead to more targeted exploration efforts. The aim of this project is to investigate the upper-crustal cooling history of the southern Intermontane Belt.

In the Intermontane Belt, porphyry deposits hosted within accreted terranes primarily formed ca. 205–195 Ma (Mortensen et al., 1995), which suggests that limited erosion or rock exhumation (<4 km) has taken place in the Intermontane Belt since the Jurassic. This idea is supported by the low metamorphic grade and low-relief landscape of the Interior Plateau, which dominates the southern Intermontane Belt (Church and Ryder, 2010). Alternatively, the Intermontane Belt may have been buried and shielded from erosion by sediments derived from the adjacent mountain belts, which were subsequently removed prior to formation of an Eocene unconformity surface (Tribe, 2005). Regardless, their presence suggests the southern Intermontane Belt has experienced a markedly different history than the adjacent Omineca and Coast belts.

The aim of this project is to measure the timing and magnitude of exhumation in the southern Intermontane Belt. To quantify exhumation, apatite and zircon (U-Th)/He and fission-track thermochronology will be used to measure the timing and rate at which rocks cooled from 190 to 40°C. This regional multimethod approach will make it possible to examine spatial patterns in rock exhumation from depths of 7 to 2 km across the Intermontane Belt and identify potential reheating events, such as those due to burial or volcanism. More specifically, the goal is to answer the following questions:

- When and how did the Interior Plateau form?
- How does the regional exhumation pattern relate to the preservation of porphyry deposits?
- Why didn't the Intermontane Belt experience exhumation equivalent to the surrounding belts?

Determining the regional exhumation patterns of bedrock underlying the Cenozoic cover will assist Cu-porphyry exploration efforts by helping in identifying regions of possible porphyry exposure. Quantifying the thermal history of the Intermontane Belt will also inform models of the evolution and interaction of the different morphogeological belts over geological time. Understanding the burial and erosional history of the Intermontane Belt is therefore crucial to mineral exploration and contributes as well to a better understanding of the evolution of the Cordillera.

Regional Geology

The Intermontane Belt is the central belt of the Canadian Cordillera and comprises an amalgam of magmatic arcs and

[1] *The lead author is a 2021 Geoscience BC Scholarship recipient.*

This publication is also available, free of charge, as colour digital files in Adobe Acrobat® PDF format from the Geoscience BC website: http://geosciencebc.com/updates/summary-of-activities/.

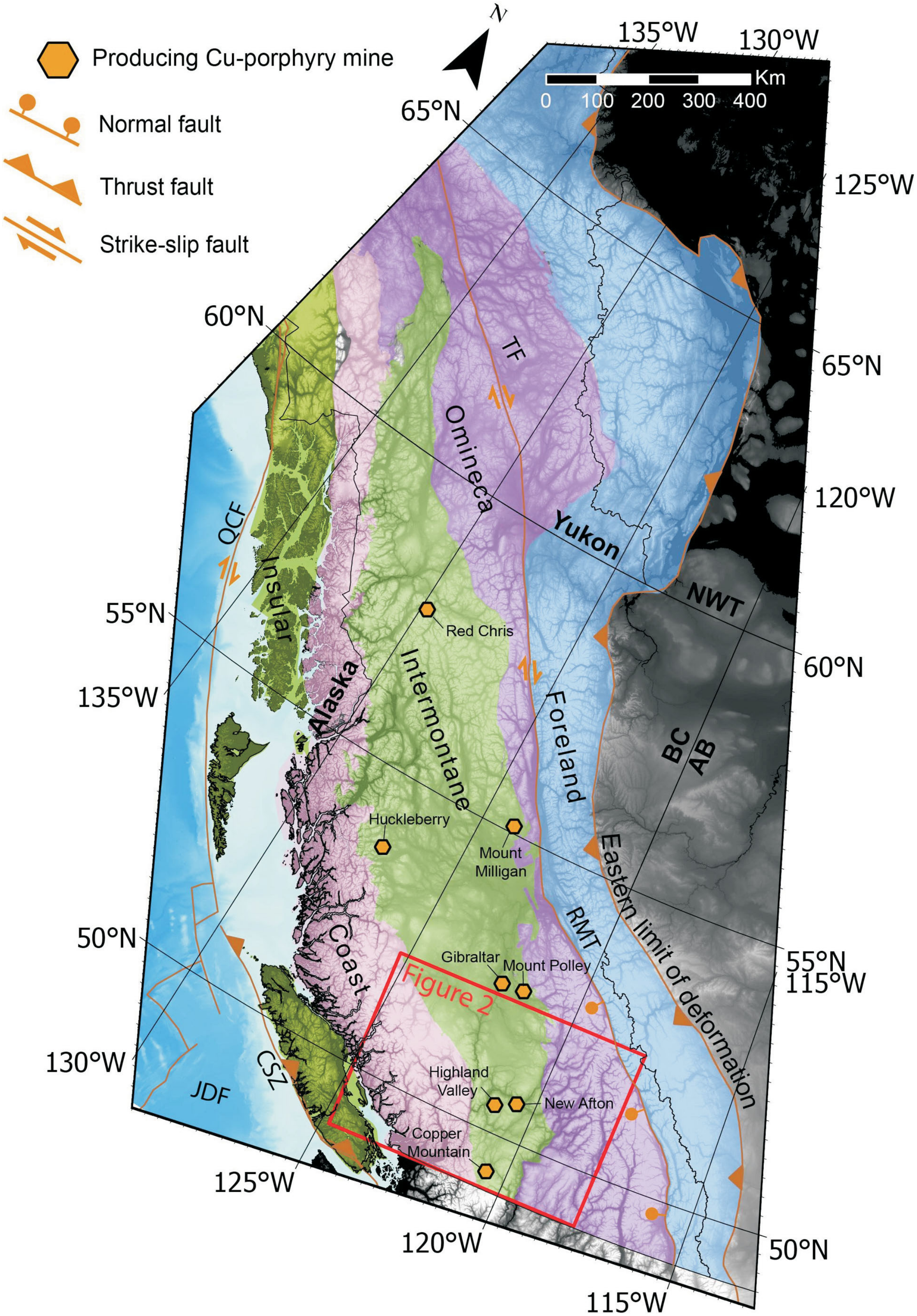

Figure 1. Morphogeological belts of the Canadian Cordillera, showing major structures. The study area of this project is outlined in red. Location of currently producing porphyry mines in British Columbia is shown by orange dots (location of Figure 2 is also shown). Abbreviations: AB, Alberta; BC, British Columbia; NWT, Northwest Territories; JDF, Juan de Fuca Plate; CSZ, Cascadia subduction zone; QCF, Queen Charlotte fault; RMT, Rocky Mountain trench; TF, Tintina fault. Base map modified after Cui et al., (2017) and Yukon Geological Survey (2020b).

oceanic terranes accreted to North America during the Jurassic. Accretion of these exotic terranes to the North American margin has been considered the driving force behind the eastward translation of continental margin deposits and terranes, and the thickening of the Canadian Cordillera (Sigloch and Mihalynuk, 2017). Alternatively, Monger and Gibson (2019) suggested that mountain building was the result of the westward motion of the North American continent, driven by seafloor spreading along the mid-Atlantic ridge, and that accretion was not a driving force but rather a product of this motion.

The Stikine and Quesnel arc terranes constitute the majority of the southern Intermontane Belt and formed outboard of the North American margin in the late Paleozoic to early Mesozoic (Figure 2; Unterschutz et al., 2002). Intervening oceans between these arcs and North America are preserved by the accreted Cache Creek and Slide Mountain terranes. These terranes amalgamated together prior to accretion onto the edge of the craton, thus forming the Intermontane Superterrane. Rocks of these Intermontane terranes are much lower in metamorphic grade and show sparser magmatism relative to the adjacent Omineca and Coast belts. Faulting in the southern Intermontane Belt is also dominated by dextral strike-slip faults concentrated along terrane boundaries and the eastern Coast Belt (Figure 2). Major shear zones, such as the Fraser–Straight Creek fault, Yalakom fault and Pinchi fault, were active in the Late Cretaceous to Eocene, with displacement estimates reaching up to 125 km (Umhoefer and Kleinspehn, 1995).

The Coast and Omineca belts constitute two crystalline belts within the Cordillera dominated by high-grade metamorphic and intrusive rocks, separated by the volcanic and sedimentary rocks of the Intermontane Belt. Previous thermochronology studies in the southern Canadian Cordillera focused on the deeply exhumed Omineca and Coast belts, but very little data exists for the Intermontane Belt. In the Omineca Belt, Eocene postorogenic extension exhumed

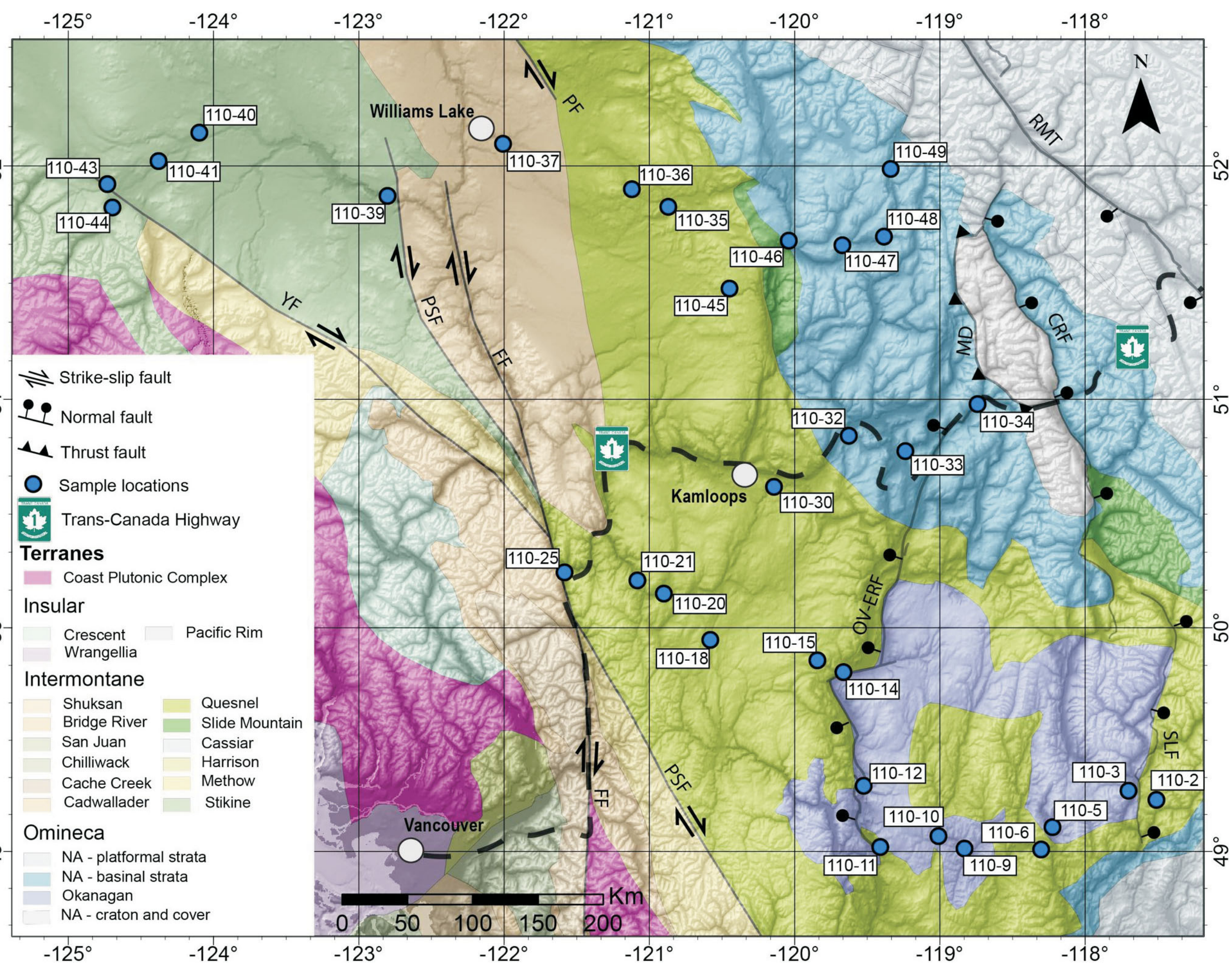

Figure 2. Terrane map of the study area in the Intermontane Belt of southern British Columbia, showing sample locations (blue dots) and identification numbers (e.g., 110-2) as well as major faults: CRF, Columbia River fault; FF, Fraser–Straight Creek fault; MD, Monashee décollement; OV-ERF, Okanagan Valley–Eagle River fault; PF, Pinchi fault; PSF, Pasayten fault; RMT, Rocky Mountain trench; SLF, Slocan Lake fault; YF, Yalakom fault. Base map from Yukon Geological Survey (2020a).

amphibolite- to granulite-facies metamorphic core complexes from depths of up to 25 km with cooling rates exceeding 100°C/m.y. (Parrish, 1995; Vanderhaeghe and Teyssier, 1997; Vanderhaeghe et al., 2003; Spear, 2004). Thermochronological results from the Coast Belt suggest increased cooling rates since <4 Ma, associated with deep glacial incision and exhumation of the Coast Mountains (Farley et al., 2001). Exhumation in the Omineca and Coast belts is estimated at upward of 25 km during the Cenozoic, whereas the Intermontane Belt shows no evidence for such a degree of denudation (Parrish, 1995; Farley et al., 2001).

The geomorphology of the southern Intermontane Belt is characterized by a low-relief region of plateaus and highlands known as the Interior Plateau (Holland, 1976; Church and Ryder, 2010), which has an average surface elevation >1000 m and hosts a variety of landscapes across its area (Figure 3). The western margin maintains a low-relief-plateau surface until reaching the eastern Coast Mountains (Figure 3, cross-section A–A') In contrast, the southeastern margin of the Interior Plateau is dominated by a higher relief transition zone of highlands along the Columbia Mountains (Figure 3, cross-section B–B'). As the Interior Plateau and Intermontane Belt narrow in the south, the low-relief landscape gives way to more incised highlands between the deeply exhumed Coast and Omineca belts (Figure 3, cross-section C–C').

The Interior Plateau was covered by widespread volcanism from the Eocene to early Pleistocene (Bevier, 1983; Mathews, 1989). The most prominent volcanic sequence is the Chilcotin Group, a series of Miocene–Pliocene basalt flows approximately 20 m thick covering 17 500 km^2 (Dohaney et al., 2010; Andrews et al., 2011). The volcanism was the product of mantle-derived melts that ascended quickly through the crust without much crustal assimilation (Bevier, 1983). The Chilcotin Group can be considered a smaller scale counterpart to the Columbia River basalts in the northwestern United States (Mathews, 1989). The base of the Chilcotin Group is of low relief and subhorizontal, overlying an Eocene unconformity (Tribe, 2005; Andrews et al., 2011). The modern low-relief surface mimics this unconformity, with a similar distribution of highlands, plateaus and deeply incised channels, which indicate that the formation of the Interior Plateau likely predates the Eocene. Mathews (1991) proposed a model for the evolution of the Interior Plateau involving Late Cretaceous to Pliocene peneplanation, but other studies have yet to confirm this model. Glaciation across the Interior Plateau, which resulted in significantly less erosion than that observed in the Coast and Omineca belts, deposited a veneer of glacial till across the surface of the plateau (Andrews et al., 2011).

Porphyry Deposits

Within the Intermontane Belt, early Mesozoic Cu-porphyry deposits are concentrated within the Stikine and Quesnel terranes (McMillan et al., 1996). It has been suggested that many deposits formed within the active island arcs outboard of the North American margin prior to accretion and are therefore not associated with postaccretionary intrusions. Most Cu-porphyry deposits form within 4 km of the Earth's surface, where metalliferous fluids exsolved from crystallizing magmas can circulate through the upper portions of the intrusion (Singer et al., 2008; Sillitoe, 2010). A pre-accretionary origin for these porphyry deposits indicates the terranes of the Intermontane Belt have experienced very little erosion since the Jurassic, when accretion began. Alternatively, porphyry deposits within the accreted terranes may have been buried following their formation, protecting them from subaerial erosion and preserving them until today.

Fieldwork

Thirty-one samples of 5–10 kg of rock were collected during the 2019 and 2020 field seasons along two east–west transects across the Intermontane Belt (Table 1; Figures 2, 3). Target rocks were surface exposures of coarse-grained igneous, metamorphic or clastic sedimentary rocks, ideally from Mesozoic and older terranes and postaccretionary intrusions underlying the widespread basalt and glacial sediment cover. Zones of pervasive deformation or alteration were avoided where possible to increase the yield of high-quality apatite and zircon and minimize complication of the cooling signal due to fluid circulation. As exposure was limited in many parts of the study area due to the Cenozoic cover rocks and vegetation, some samples did not meet the ideal characteristics previously outlined. Of the 31 samples, 13 were collected from terranes and intrusions in the Intermontane Belt, and 13 samples were collected from North American basinal rocks and intrusions in the Omineca Belt. Five samples were collected from volcanic and sedimentary overlap assemblages in the Intermontane and Omineca belts (Figure 2). Most of the Intermontane Belt samples (8) were collected from the Quesnel terrane and postaccretionary intrusions, whereas four were collected from the Stikine terrane and one sample was collected from the Cache Creek terrane. The majority of samples collected (21) are from felsic to intermediate plutons, some of which have shown evidence of metallic mineralization, such as the Takomkane and Thuya batholiths (Table 1; Plouffe et al., 2011).

The spatial relationship of the sample transects across the Intermontane Belt was designed to facilitate examination of the longitudinal variations in exhumation from the Omineca Belt to the Coast Belt as well as the latitudinal variations of this pattern. The first transect, completed in

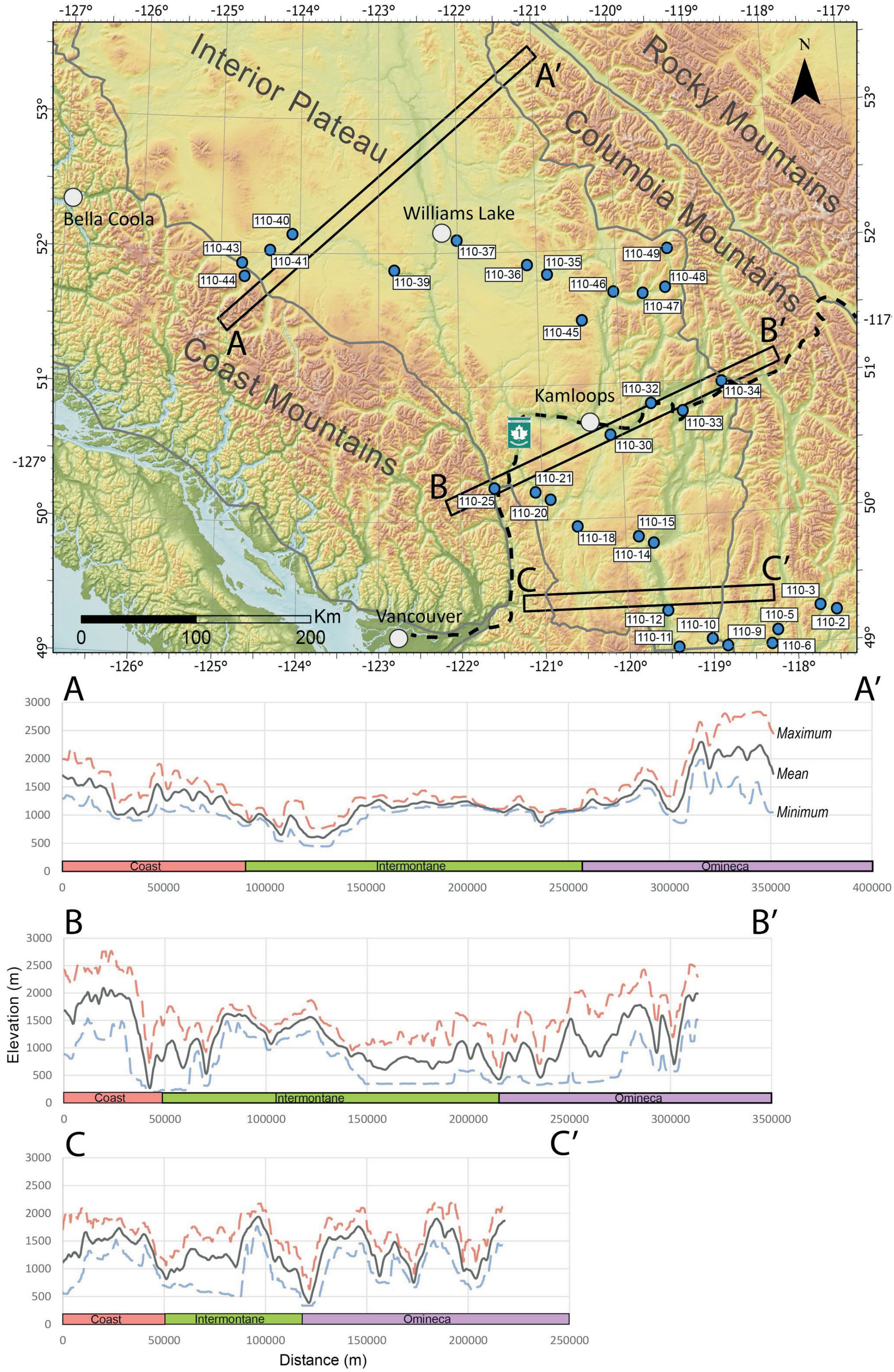

Figure 3. Physiography of southern British Columbia, showing sample locations (blue dots) and identification numbers (e.g., 110-2). Profiles show how the maximum, minimum and mean surface elevation changes from cross-section A–A', through B–B' to C–C'. Digital elevation model downloaded from gebco.net (General bathymetric chart of the oceans).

Table 1. Location and description of samples collected across the Intermontane Belt of southern British Columbia.

Sample	Latitude	Longitude	Elevation	Terrane and lithological unit	Age	Rock description
110-2	49.2325	-117.5096	1191	Postaccretionary - Bonnington pluton	Jurassic	Biotite-hornblende granodiorite
110-3	49.2736	-117.7018	768	Okanagan - Greenwood/Wallace Creek plutons	Cretaceous	Hornblende granite with megacrystic K-feldspar
110-5	49.1097	-118.2248	596	Postaccretionary - Coryell Plutonic Suite	Eocene	Foliated hornblende granodiorite
110-6	49.0090	-118.3033	517	Okanagan - Grand Forks Complex	Proterozoic	Folded gneiss with quartzofeldspathic banding
110-9	49.0130	-118.8307	594	Overlap - Penticton Group	Eocene	Hornblende diorite
110-10	49.0694	-119.0098	716	Overlap - Kettle River and Springbrook Formation	Eocene	Rounded medium- to coarsed-grain sandstone
110-11	49.0203	-119.4106	520	Postaccretionary - unnamed intrusion	Jurassic	Foliated biotite granite with quartz veining
110-12	49.2958	-119.5247	417	Okanagan - Grand Forks Complex	Proterozoic	Foliated granite
110-14	49.8033	-119.6640	444	Overlap - Penticton Group	Eocene	Biotite granite with quartz veining
110-15	49.8557	-119.8433	873	Quesnel - Quesnellia intrusion	Triassic-Jurassic	Biotite-hornblende granite
110-18	49.9463	-120.5805	1036	Quesnel - Nicola Group	Triassic	Subangular-subrounded, moderately well-sorted fine-grained lithic arkose with mudstone rip-up clasts
110-20	50.1510	-120.9004	557	Overlap - Princeton Group	Eocene	Porphyritic rhylotite lava and vesicular tuff
110-21	50.2444	-121.5838	225	Quesnel - Mount Lytton Complex	Permian-Triassic	Foliated hornblende granite
110-25	50.2091	-121.0823	460	Overlap - Spences Bridge Group-Pimainus Formation	Cretaceous	Porphyritic fine-grained intermediate lava
110-30	50.6195	-120.1420	602	Quesnel - Quesnellia intrusion	Triassic-Jurassic	Biotite granite
110-32	50.8421	-119.6271	391	North American (basin) - Mt. Ida Assemblage-Little orthogneiss	Ordovician	Foliated biotite gneiss
110-33	50.7752	-119.2378	369	North America (basin) - Mt. Ida Assemblage-Sicamous Formation	Cambrian-Silurian	Folded foliated granoblastic biotite gneiss
110-34	50.9794	-118.7405	528	North America (basin) - Horsethief Creek Group	Neoproterozoic	Folded biotite gneiss with quartz veining
110-35	51.8264	-120.8698	799	Quesnel - Quesnel monzonite suite	Jurassic	Altered hornblende-biotite granodiorite
110-36	51.9013	-121.1204	1002	Quesnel - Takomkane batholith	Jurassic	Biotite granite with hornblende-rich xenoliths
110-37	52.0936	-122.0074	597	Cache Creek - unnamed intrusion	Undated	Chloritized granite
110-39	51.8729	-122.8023	956	Stikine - dacite tuff	Jurassic	Folded green tuff
110-40	52.1408	-124.0979	1099	Stikine - Chilanko Igneous Complex	Jurassic-Cretaceous	Porphyritic hornblende tonalite
110-41	52.0205	-124.3788	1078	Postaccretionary - Tatla Lake stock	Eocene	Foliated biotite granodiorite
110-43	51.9229	-124.7310	959	Stikine - Tatla Lake Metamorphic Complex	Cretaceous	Biotite orthogneiss
110-44	51.8236	-124.6960	1044	Stikine - Sapeye Creek pluton	Triassic-Jurassic	Biotite tonalite
110-45	51.4774	-120.4483	1147	Quesnel - Thuya batholith	Jurassic	Hornblende-biotite granodiorite
110-46	51.6823	-120.0405	421	Postaccretionary - Raft batholith	Cretaceous	Hornblende-biotite granite
110-47	51.6627	-119.6714	535	Postaccretionary - Raft batholith	Cretaceous	Hornblende-biotite granite
110-48	51.6995	-119.3851	601	North America (basin) - Malton Complex	Proterozoic	Foliated biotite gneiss with quartz veining
110-49	51.9872	-119.3388	679	Postaccretionary - Blue River pluton	Cretaceous	Muscovite granite

2019, focused on southernmost BC, sampling along major highways and stretches 230 km across the southern Intermontane Belt (Figure 3). The second transect, completed in 2020, focused northward from the 2019 transect and stretches 400 km across the Intermontane Belt (Figure 3).

Methods

In this study, multiple low-temperature thermochronometers were used to quantify the timing and rate of bedrock cooling from 180 to 40°C. Apatite and zircon (U-Th)/He (AHe and ZHe, respectively) dating is based on the thermally activated diffusion of radiogenic ^{4}He from the alpha decay of ^{238}U, ^{235}U and ^{232}Th (Harrison and Zeitler, 2005). Helium retention in apatite and zircon is temperature dependent and defines a zone of partial He retention known as the 'partial retention zone'(PRZ). For the ZHe system, the PRZ is 190–170°C and for the AHe system, it is 80–40°C (Reiners et al., 2004; Flowers et al., 2009). Apatite fission-track dating (AFT) is based on the accumulation of damage zones from the fission decay of ^{238}U in the apatite crystal, known as 'fission tracks'. Fission tracks readily anneal above 120°C and are preserved when cooled below 60°C (Donelick et al., 1999; Ketcham et al., 1999). This temperature range defines the 'partial annealing zone', where fission tracks anneal at a known temperature-dependent rate. Thermal modelling of these data is used to explore possible thermal histories within these sensitivity windows.

All analyses will be conducted at the University of Calgary Geo- and Thermochronology Laboratory. As a first step, apatite and zircon were separated from whole-rock samples following standard mineral-separation techniques involving a jaw crusher, disk mill, Wilfley table, magnetic separator and heavy liquid separation using lithium heteropolytungstate and methylene iodide (Figure 4). Based on mineral-separate yields, 29 samples are currently being dated using the AHe technique, 27 samples are being dated using AFT analysis and up to 22 samples will be dated using the ZHe technique, depending on budget and time constraints. The (U-Th)/He dating procedure is outlined in detail in McKay et al. (2021), where apatite and zircon grains are picked under a stereomicroscope, aiming for euhedral, inclusion and crack-free grains >70 µm in size. Select grains are packed into Nb tubes and are first degassed in an ASI Alphachron He extraction line before inlet into a mass spectrometer to measure the number of radiogenic ^{4}He atoms in each grain. An isotopic spike solution of 15 ng/g U and 5 ng/g Th is added to each degassed grain and the number of ^{238}U, ^{235}U and ^{232}Th parent atoms is measured using an Agilent 7700x inductively coupled plasma–mass spectrometer (Evans et al., 2005; McKay et al., 2021). For AHe dating, five single-grain aliquots will be dated for each sample and a mean age will be calculated from the single-grain dates. In the case of ZHe dating, three single-grain aliquots will be dated for each sample and compiled to determine a mean age. Apatite fission-track analysis will follow the external detector and zeta-calibration method, where apatite grains are mounted in epoxy, polished and fitted with an external detector plate, and then irradiated in a nuclear reactor (Hurford and Green, 1983).

Age data derived from ZHe, AFT and AHe analyses will be numerically modelled using QTQt inverse thermal history modelling software (Gallagher, 2012). This software explores time-temperature space to identify thermal histories that agree with the input data. The multimethod approach will provide greater time-temperature constraints for modelling and allow investigation of possible thermal histories over a wider temperature and time range.

Summary

The southern Intermontane Belt is dominated by the low-relief Interior Plateau and hosts an abundance of early Mesozoic porphyry deposits. Samples were collected along two east–west transects across the Intermontane Belt in southern BC to explore the timing and pattern of exhumation as well as how the latter relates to the preservation of porphyry deposits. Currently, preparation of samples for radiometric dating is underway to produce the thermochronological dataset necessary for completing the objectives of this study. This multimethod approach will provide thermal history information over a greater temperature window and make it possible to quantify cooling rates and possible reheating events otherwise not observed using a single thermochronometer. Quantifying the thermal history of samples across the Intermontane Belt from 190 to 40°C will make it possible to investigate erosion and burial processes that affected the accreted terranes of southern BC. These processes preserved early Mesozoic porphyry deposits throughout Jurassic–Paleocene mountain building and Eocene postorogenic collapse. The results of this study will inform tectonic and geomorphic models of the Intermontane Belt, and aid future mineral-exploration efforts through their potential to identify regions of undiscovered porphyry mineralization.

Acknowledgments

The lead author would like to thank Geoscience BC for providing financial support through the Geoscience BC scholarship. Funding for this project was also provided by a Natural Sciences and Engineering Research Council of Canada (NSERC) Discovery Grant (RGPIN-2018-03932) awarded to E. Enkelmann and an NSERC Canada Graduate Scholarship–Master's (CGS-M) awarded to K. Damant. The authors also wish to thank A. MacDougall and S. Tiede for their hard work in the laboratory amid adverse circumstances. A special thank you to S. Jess for providing comments that improved the quality of this paper.

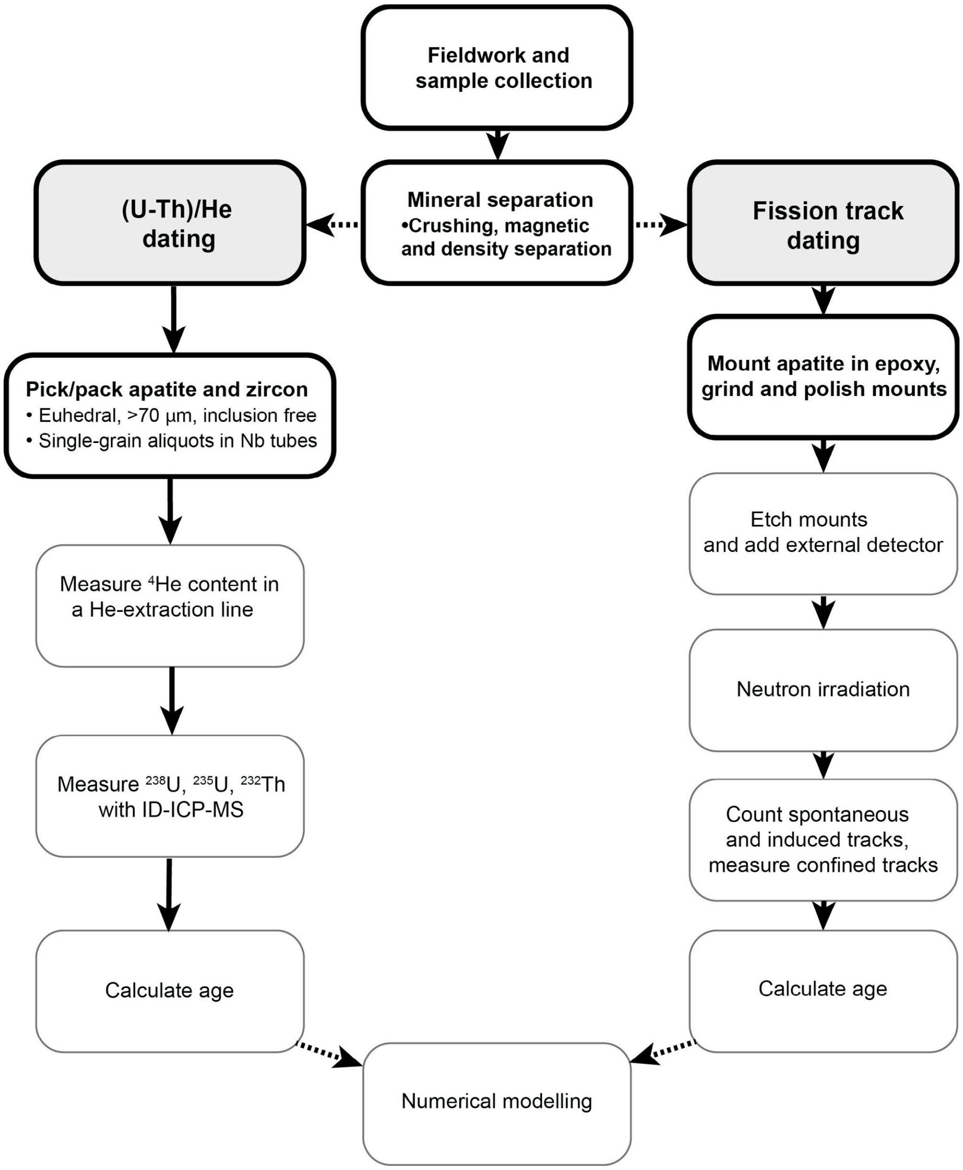

Figure 4. Flow chart of apatite and zircon (U-Th)/He and fission-track laboratory procedures. Bolded boxes indicate steps which have been completed, light grey boxes are steps which have yet to be completed as of October 2021. Abbreviation: ID-ICP-MS, isotope dilution-inductively coupled plasma–mass spectrometer.

References

Andrews, G.D.M., Plouffe, A., Ferbey, T., Russell, J.K., Brown, S.R. and Anderson, R.G. (2011): The thickness of Neogene and Quaternary cover across the central Interior Plateau, British Columbia: analysis of water-well drill records and implications for mineral exploration potential; Canadian Journal of Earth Sciences, v. 48, p. 973–986.

Bevier, M.L. (1983): Implications of chemical and isotopic composition for petrogenesis of Chilcotin group basalts, British Columbia; Journal of Petrology, v. 24, p. 207–226.

Church, M. and Ryder, J. (2010): Physiography of British Columbia; Chapter 2 *in* Compendium of Forest Hydrology and Geomorphology in British Columbia, R.G. Pike, R.D. Redding, R.D. Moore, R.D. Winkler and K.D. Bladon (ed.), BC Ministry of Energy, Mines and Low Carbon Innovation, Land Management Handbook 66, p. 17–46.

Cui, Y., Miller, D., Schiarizza, P. and Diakow, L.J. (2017): British Columbia digital geology; British Columbia Ministry of Energy, Mines and Low Carbon Innovation, British Columbia Geological Survey, Open File 2017-8, 9 p., data version 2019-12-19, URL <http://cmscontent.nrs.gv.bc.ca/geoscience/PublicationCatalogue/OpenFile/BCGS_2017-08.pdf> [November 2021].

Dilles, J.H. and John, D.A. (2021): Porphyry and epithermal mineral deposits; *in* Encyclopedia of Geology, D. Alderton and S.A. Elias (ed.), Elsevier, p. 847–866, <https://doi.org/10.1016/B978-0-08-102908-4.00005-9>.

Dohaney, J., Andrews, G.D.M., Russell, J.K. and Anderson, R.G. (2010): Distribution of the Chilcotin Group, Taseko Lakes and Bonaparte Lake map areas, British Columbia; Geological Survey of Canada, Open File 6344, scale 1:250 000.

Donelick, R.A., Ketcham, R.A. and Carlson, W.D. (1999): Variability of apatite fission-track annealing kinetics: II. Crystallographic orientation effects; American Mineralogist, v. 84, p. 1224–1234.

Evans, N.J., Byrne, J.P., Keegan, J.T. and Dotter, L.E. (2005): Determination of uranium and thorium in zircon, apatite, and fluorite: application to laser (U-Th)/He thermochronology; Journal of Analytical Chemistry, v. 60, p. 1159–1165.

Farley, K.A., Rusmore, M.E. and Bogue, S.W. (2001): Post-10 Ma uplift and exhumation of the northern Coast mountains, British Columbia; Geology, v. 29, p. 99–102.

Flowers, R.M., Ketcham, R.A., Shuster, D.L. and Farley, K.A. (2009): Apatite (U-Th)/He thermochronometry using a radiation damage accumulation and annealing model; Geochimica et Cosmochimica Acta, v. 73, p. 2347–2365.

Gallagher, K. (2012): Transdimensional inverse thermal history modeling for quantitative thermochronology; Journal of Geophysical Research: Solid Earth, v. 117, p. 1–16.

Harrison, T.M. and Zeitler, P.K. (2005): Fundamentals of noble gas thermochronometry; Reviews in Mineralogy and Geochemistry, v. 58, p. 123–149.

Holland, S.S. (1976): Landforms of British Columbia: a physiographic outline; British Columbia Ministry of Mines and Petroleum Resources, Bulletin no. 48.

Hurford, A.J. and Green, P.F. (1983): The zeta age calibration of fission-track dating; Chemical Geology, v. 41, p. 285–317.

Ketcham, R.A., Donelick, R.A. and Carlson, W.D. (1999): Variability of apatite fission-track annealing kinetics: III. Extrapolation to geologic time scales; American Mineralogist, v. 84, p. 1235–1255.

Mathews, W.H. (1989): Neogene Chilcotin basalts in south-central British Columbia: geology, ages, and geomorphic history; Canadian Journal of Earth Sciences, v. 26, p. 969–982.

Mathews, W.H. (1991) Physiographic evolution of the Canadian Cordillera; Chapter 11 *in* Geology of the Cordilleran Orogen in Canada, H. Gabrielse and C.J. Yorath (ed.), Geological Survey of Canada, Geology of Canada, no. 4, p. 405–418 (also Geological Society of America, Geology of North America, v. G-2).

McKay, R., Enkelmann, E., Hadlari, T., Matthews, W. and Mouthereau, F. (2021): Cenozoic exhumation history of the eastern margin of the northern Canadian Cordillera; Tectonics, v. 40, p. 1–18.

McMillan, W.J., Thompson, J.F.H., Hart, C.J.R. and Johnston, S.T. (1996): Porphyry deposits of the Canadian Cordillera; Geoscience Canada, v. 23, p. 125–134.

Mihalynuk, G. (2007): Evaluation of mineral inventories and mineral exploration deficit of the Interior Plateau beetle infested zone (BIZ), south-central British Columbia; *in* Geological Fieldwork 2006, BC Ministry of Energy, Mines and Low Carbon Innovation, Paper 2007-1, p. 137–142.

Monger, J.W.H. and Gibson, H.D. (2019): Mesozoic–Cenozoic deformation in the Canadian Cordillera: the record of a “Continental Bulldozer”?; Tectonophysics, v. 757, p. 153–169.

Mortensen, J.K., Ghosh, D.K. and Ferri, F. (1995): U-Pb geochronology of intrusive rocks associated with copper-gold porphyry deposits in the Canadian Cordillera; *in* Porphyry deposits of the northwestern Cordillera of North America, T.G. Schroeter (ed.), Canadian Institute of Mining, Metallurgy and Petroleum, Special Volume 46, p. 142–158.

Parrish, R.R. (1995): Thermal evolution of the southeastern Canadian Cordillera; Canadian Journal of Earth Sciences, v. 32, p. 1618–1642.

Plouffe, A., Anderson, R.G., Gruenwald, W., Davis, W.J., Bednarski, J.M. and Paulen, R.C. (2011): Integrating ice-flow history, geochronology, geology, and geophysics to trace mineralized glacial erratics to their bedrock source: an example from south-central British Columbia; Canadian Journal of Earth Sciences, v. 48, p. 1113–1130.

Reiners, P.W., Spell, T.L., Nicolescu, S. and Zanetti, K.A. (2004): Zircon (U-Th)/He thermochronometry: He diffusion and comparisons with ^{40}Ar/^{39}Ar dating; Geochimica et Cosmochimica Acta, v. 68, p. 1857–1887.

Sacco, D.A., Jackaman, W. and Knox, C. (2021): Proven approach to mineral exploration in thick surficial deposits applied to the Central Interior Copper-Gold Research projects area, central British Columbia (parts of NTS 093A, B, G, J, K, O); *in* Geoscience BC Summary of Activities 2020: Minerals, Geoscience BC, Report 2021-01, p. 1–10, URL <http://www.geosciencebc.com/summary-of-activities-2020-minerals/> [November 2021].

Seedorff, E., Dilles, J.H., Proffett, J.M., Einaudi, M.T., Zurcher, L., Stavast, W.J.A., Johnson, D.A. and Barton, M.D. (2005): Porphyry deposits: characteristics and origin of hypogene features; Economic Geology, 100th Anniversary Volume, p. 251–298.

Sigloch, K. and Mihalynuk, M.G. (2017): Mantle and geological evidence for a Late Jurassic-Cretaceous suture spanning North America; Geological Society of America, GSA Bulletin, p. 1489–1520.

Sillitoe, R.H. (2010): Porphyry copper systems; Economic Geology, v. 105, p. 3–41.

Singer, D.A., Berger, V.I. and Moring, B.C. (2008): Porphyry copper deposits of the world: database and grade and tonnage models, 2008; U.S. Geological Survey, Open File Report 2008-1155, 45 p.

Spear, F.S. (2004): Fast cooling and exhumation of the Valhalla metamorphic core complex, southeastern British Columbia; International Geology Review, v. 46, p. 193–209.

Thomas, M.D., Pilkington, M. and Anderson, R.G. (2011): Geological significance of high-resolution magnetic data in the Quesnel terrane, central British Columbia; Canadian Journal of Earth Sciences, v. 48, p. 1065–1089.

Tribe, S. (2005): Eocene paleo-physiography and drainage directions, southern Interior Plateau, British Columbia; Canadian Journal of Earth Sciences, v. 42, p. 215–230.

Umhoefer, P.J. and Kleinspehn, K.L. (1995): Mesoscale and regional kinematics of the northwestern Yalakom fault system: major Paleogene dextral faulting in British Columbia, Canada; Tectonics, v. 14, p. 78–94.

Unterschutz, J.L.E., Creaser, R.A., Erdmer, P., Thompson, R.I. and Daughtry, K.L. (2002): North American margin origin of Quesnel terrane strata in the southern Canadian Cordillera: inferences from geochemical and Nd isotopic characteristics of Triassic metasedimentary rocks; Bulletin of the Geological Society of America, v. 114, p. 462–475.

Vanderhaeghe, O. and Teyssier, C. (1997): Formation of the Shuswap metamorphic core complex during late-orogenic collapse of the Canadian Cordillera: role of ductile thinning and partial melting of the mid-to lower crust; Geodinamica Acta, v. 10, p. 41–58.

Vanderhaeghe, O., Teyssier, C., McDougall, I. and Dunlap, W.J. (2003): Cooling and exhumation of the Shuswap metamorphic core complex constrained by ^{40}Ar-^{39}Ar thermochronology; Geological Society of America, GSA Bulletin, v. 115, p. 200–216.

Yukon Geological Survey (2020a): A digital atlas of terranes for the northern Cordillera; Yukon Geological Survey, URL <https://data.geology.gov.yk.ca/Compilation/2> [October 4, 2021]

Yukon Geological Survey (2020b): Yukon digital bedrock geology; Yukon Geological Survey, URL <https://data.geology.gov.yk.ca/Compilation/3> [September 18, 2021]

Spectral and Geochemical Characterization of the Silver Pond Argillic–Advanced Argillic Alteration Lithocap, Lawyers Property, Toodoggone District, North-Central British Columbia (Part of NTS 094E)

P. Voegeli[1], **Department of Earth and Atmospheric Sciences, University of Alberta, Edmonton, Alberta, pvoegeli@ualberta.ca**

P. Lecumberri-Sanchez, Department of Earth and Atmospheric Sciences, University of Alberta, Edmonton, Alberta

Voegeli, P. and Lecumberri-Sanchez, P. (2022): Spectral and geochemical characterization of the Silver Pond argillic–advanced argillic alteration lithocap, Lawyers property, Toodoggone district, north-central British Columbia (part of NTS 094E); *in* Geoscience BC Summary of Activities 2021: Minerals, Geoscience BC, Report 2022-01, p. 21–38.

Introduction

The Toodoggone district of north-central British Columbia (BC) hosts several historical precious and base-metal producers, including the Baker (MINFILE 094E 026, MapPlace, 2021), Cheni (MINFILE 094E 066), Shasta (MINFILE 094E 050) and Kemess (MINFILE 094E 094) mines, and has emerged as a high priority exploration area with major discovery potential. The Lawyers property is the site of the historical Cheni mine and lies in the central region of the Toodoggone district (Figure 1). The Lawyers property is the site of a well-preserved epithermal system that hosts an indicated resource of 2.05 million oz. Au-Ag and is currently being explored (Benchmark Metals Inc., 2021).

The majority of known Au-Ag mineralization present at the Lawyers property is hosted in narrow multiphase quartz-carbonate, quartz-adularia, quartz-sulphide vein, stockwork and hydrothermal breccia zones, typical of low sulphidation epithermal systems (Duuring at al., 2009). Mineralization is often closely associated with narrow (~5–30 m) potassic (potassium feldspar+sericite±kaolinite) alteration zones and broad regional-scale propylitic alteration (chlorite+hematite±epidote). Proximal to the extensively developed, low sulphidation–style prospects of Cliff Creek, Amethyst Gold Breccia (AGB) and Dukes Ridge (MINFILE 094E 066), but separated from them by a regional-scale fault, there is a less explored group of prospects known as Silver Pond (MINFILE 094E 163; Figure 2). In contrast to the Lawyers property's dominant mineralization style, the Silver Pond prospects exhibit several characteristics of high sulphidation–style epithermal systems. In this system, the condensation of magmatic gas into groundwater results in the disproportionation of $S0_2$, forming H_2SO_4 and H_2S, resulting in the formation of a highly acidic solution (pH <1; Sillitoe, 1973; Arribas, 1995). The acidic solution reacts with hostrocks in a series of hydrolysis reactions that progressively neutralize acidity and form a characteristic zonation of alteration assemblages (Steven and Ratte, 1960), including a core zone of residual or vuggy quartz rimmed by an advanced argillic-alteration assemblage, which typically has a mineralogical composition dominated by alunite, pyrophyllite, dickite, quartz, anhydrite, diaspore and topaz. The narrow advanced argillic-alteration rim typically has an outer broad argillic alteration zone composed of illite, chlorite and montmorillonite (Arribas, 1995; John et al., 2018).

The Silver Pond prospects broadly resemble a 'lithocap', which is a broad subsurface alteration domain that is laterally and vertically extensive (Cooke et al., 2017) and commonly occurs as the near-surface expression of porphyry systems (Bouzari et al., 2019). Mineralogical and geochemical evidence suggest that the Silver Pond prospects are genetically distinct from the surrounding low sulphidation–style epithermal deposits present on the Lawyers property.

The main objective of this study is to determine the spatial distribution of the broad hydrothermal system (low sulphidation, high sulphidation and potential porphyry zones) with respect to the Silver Pond prospects as well as the potential structural/lithological controls that have led to the distribution of different deposit types within the Toodoggone region. This main objective is being pursued through determination of the spatial and paragenetic distribution of minerals in the Silver Pond prospects.

Geological Setting

The Toodoggone district is located in the Stikine terrane of north-central BC and is predominantly hosted in an ~2 km thick package of Lower Jurassic intermediate volcanic rocks belonging to the Toodoggone Formation, which is part of the regionally extensive Hazelton Group. The domi-

[1] *The lead author is a 2021 Geoscience BC Scholarship recipient.*

This publication is also available, free of charge, as colour digital files in Adobe Acrobat® PDF format from the Geoscience BC website: http://geosciencebc.com/updates/summary-of-activities/.

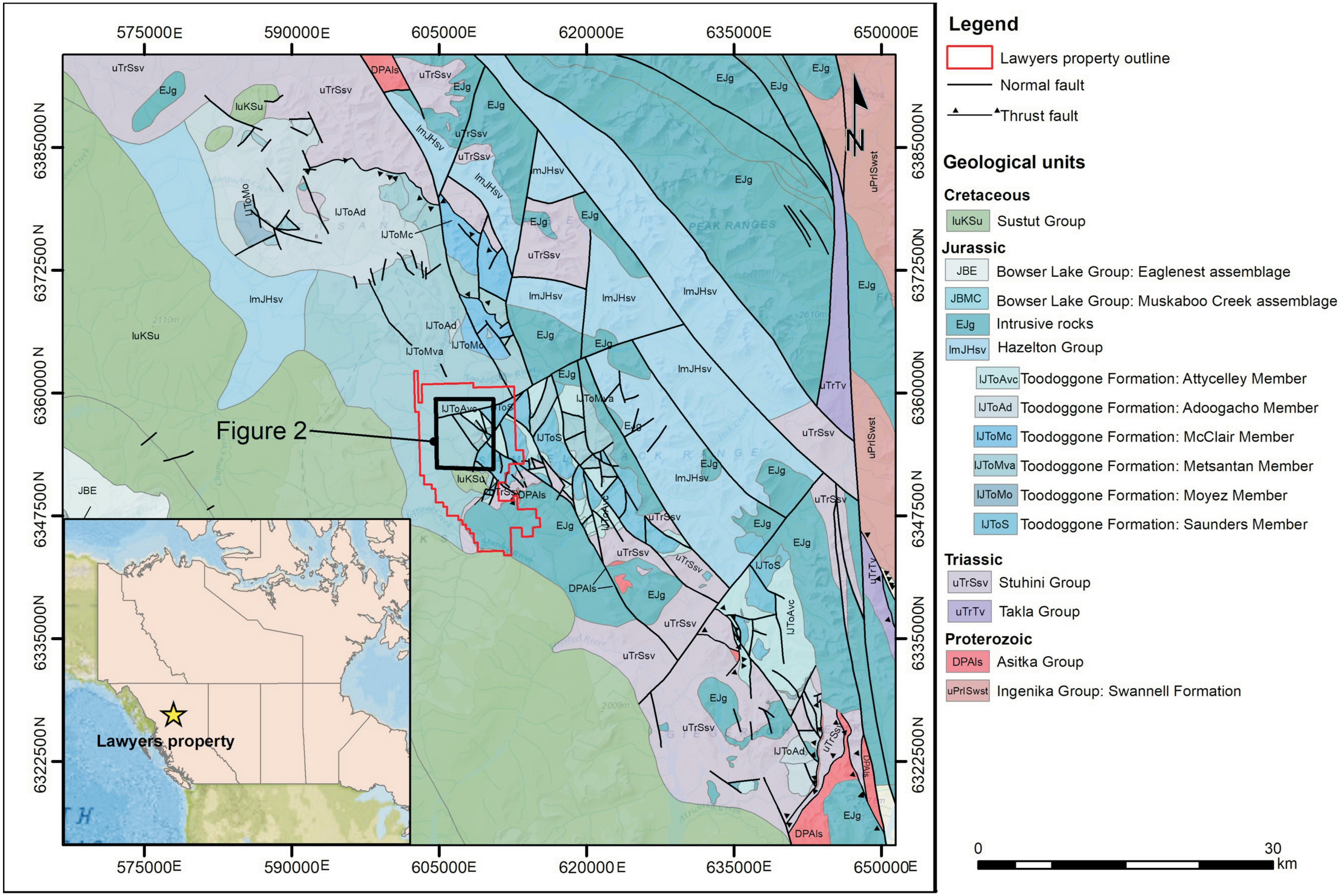

Figure 1. Regional geology of Lawyers property area in north-central British Columbia. Volcanic rocks of the Toodoggone Formation appear as the dominant lithology within the property boundary and they are truncated by a series of north-northwest-trending fault structures. Geological unit boundaries and faults are from the BC Geological Survey's MapPlace dataset (MapPlace, 2021). All co-ordinates are in UTM Zone 9, NAD 83.

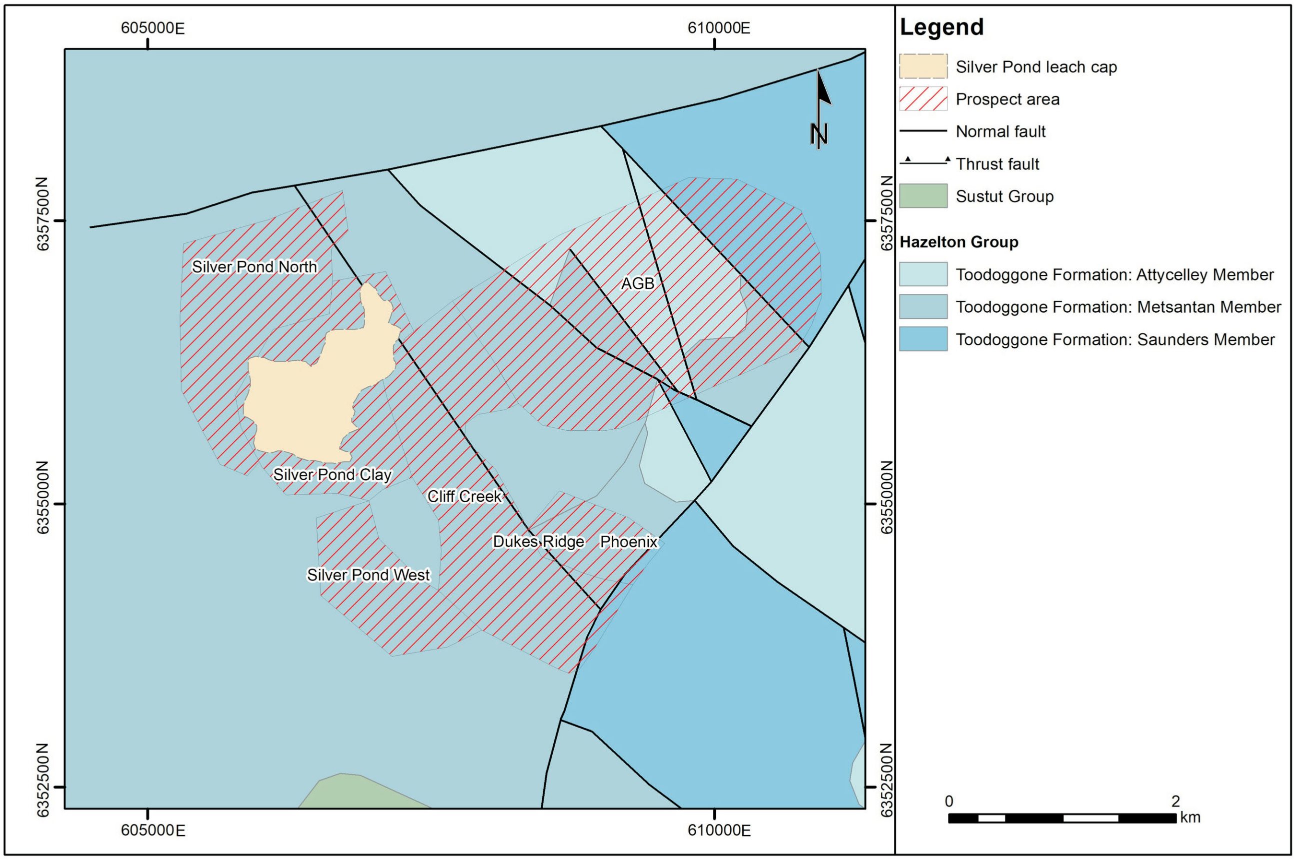

Figure 2. Geology of main prospect areas of the north-central part of the Lawyers property: Amethyst Gold Breccia (AGB), Cliff Creek, Phoenix and Dukes Ridge (MINFILE 094E 066, MapPlace, 2021). The study area is focused on the Silver Pond group of prospects (Silver Pond North, Silver Pond Clay, Silver Pond West; MINFILE 094E 163). The Silver Pond leach cap is the surface expression of the argillic alteration assemblages that define the high sulphidation–style prospect area. Geological unit boundaries and faults are from the BC Geological Survey's MapPlace dataset (MapPlace, 2021). All co-ordinates are in UTM Zone 9, NAD 83.

nant rocks of the Toodoggone Formation are latite to dacite volcanic strata deposited in a north-northwest-elongated volcano-tectonic depression of the Lower Triassic Takla Group volcanic rocks and Permian carbonate rocks (Diakow et al., 1991). Following the depositional hiatus of the Middle to Upper Jurassic, a thick package of Cretaceous sedimentary rocks known as the Sustut Group was deposited and represents the top of bedrock in the Lawyers property and surrounding region (Diakow et al., 1991). The late sedimentary units are credited with being responsible for the preservation of the epithermal deposits, hosted in the Toodoggone volcanic rocks, during subsequent uplift (Bouzari et al., 2019). A series of porphyritic plutons known as the Black Lake intrusive suite, which consists of granodiorite to quartz monzonite crosscut by a series of felsic–intermediate cogenetic dikes, occurs in the southeastern portion of the Lawyers property and crosscuts the stratigraphy of the Toodoggone district. Unaltered late basalt dikes, trending north-northwest, crosscut the volcanic and plutonic units, and appear to have exploited deep-rooted extensional faults based on their similar orientation and common appearance along fault planes throughout the Lawyers property.

The Lawyers property has a relatively simple structural history that is dominated by a brittle deformation regime. The dominant property-scale structures consist of steeply dipping, north-northwest-trending (~310–340°) synvolcanic faults, which formed during extension in the Early Jurassic. This synvolcanic faulting formed a series of horst-graben blocks (Diakow et al., 1991), which define the structural geometry and displacement of the local and regional stratigraphy. Most fault blocks exhibit normal displacement with rare kinematic indicators (conjugate riedel structures and lineations) of minimal displacement and/or strike-slip movement. Major fault gouge zones are associated with potassic and propylitic alteration assemblages and are commonly pervasively silicified. The main Lawyers trend, which hosts the known hydrothermal breccia zones and their associated Au-Ag mineralization and alteration assemblages, is strongly structurally controlled, with the north-northwest-trending fault structures functioning as key fluid conduits. Isolated dilation jogs and intersections of north-northwest- and west-trending faults appear to concentrate ore shoots within the Lawyers trend. The argillic alteration assemblages of the Silver Pond prospects appear to have a strong association with deep-rooted north-northwest-trending fault structures. These faults have similar orientations to the main regional fault structures that serve as major controls for mineralization in the adjacent low sulphidation–style prospects.

Material and Methods

Shortwave Infrared Analysis

In this study, two principal datasets were acquired for shortwave infrared (SWIR) analysis to determine mineralogical composition and the alteration assemblages present. The first dataset was collected in the 2018 field season with Malvern Panalytical Ltd's portable ASD TerraSpec® Halo spectrometer, and the second dataset was collected in the 2020 and 2021 field seasons using Malvern Panalytical Ltd's stationary ASD TerraSpec 4 Hi-Res Mineral spectrometer. All datasets were collected by APEX Geoscience Ltd staff. Surface datasets were collected with the ASD TerraSpec Halo in a 50 by 50 m grid using a GPS for navigation. Sample locations varied by up to 20 m from the grid spacing when necessary to access adequate clay exposure. Surface clay samples contained at least 1 cm of soil/clay and were scanned only when dry. In addition to surface clay, flat unweathered/unoxidized representative hostrock samples were scanned where available. The SWIR analysis of the drillcore was performed with the stationary ASD TerraSpec 4 Hi-Res unit. All drillcore SWIR analysis were performed at regular 3 m intervals on a broken flat surface of representative core, which had been dried before scanning. In order to ensure measurements were accurate and to limit noise during acquisition, the lens was regularly cleaned and calibrated with a white standard puck. The SWIR data acquired consists of 1866 spectra from 496 surface samples and 1370 core samples.

After the initial acquisition effort, all measured spectra were processed using Commonwealth Scientific and Industrial Research Organisation's The Spectral Geologist (TSG™), Spectral International Inc.'s SpecMin™ and IMDEX™ Limited's aiSIRIS™ software. The Spectral Geologist extracted spectral signatures identified at wavelengths between 350 and 2500 nanometres (nm), representing the visible, near-infrared and shortwave infrared spectral ranges. Spectra with abnormal absorption features or excessive noise likely resulted from poor calibration, a dirty lens or the scanned samples were still wet upon analysis; these spectra were therefore discarded. In order to verify mineralogy picks assigned to individual spectra by the TSG algorithm, each spectral signature was compared against and verified with reference spectrum using SpecMin software. In order to account for possible variances due to factors such as compositional differences between the analyzed spectra and the reference spectra, and/or the presence of more than one mineral type being included in the sample interval during scanning (resulting in a mixed spectra than contains signatures of more than one mineral), each spectra was compared to multiple reference samples taken from numerous different deposits. The SpecMin software's 'stacking' feature was used to overlay multiple reference spectra of one or more mineral signatures and was then compared to the spectra gathered with ASD TerraSpec to confirm the results provided by TSG. Key absorption features used to identify diagnostic mineral signatures include 1400, 1900, 2160, 2180, 2200, 2250, 2330 and 2350 nm wavelengths. The bulk of the identified signatures belonged to illite, smectite, kaolinite, pyrophyllite-talc, sulphate and chlorite group minerals.

In addition to identifying minerals, crystallinity indices for white mica and kaolinite group minerals were determined using arithmetic expressions within TSG software as well as machine learning algorithms used by aiSIRIS software. Manual processing through TSG identified the relevant samples using a filter for white mica (muscovite series, paragonite) and a filter for kaolinite group minerals (kaolinite, dickite, nacrite, halloysite), resulting in an output table of the TSG results. For white mica, the 2200 nm absorption feature was divided by the 1900 nm absorption feature to provide the white mica crystallinity index (Guggenheim et al., 2002). For kaolinite, the mean 2181 nm absorption feature was divided by the 2161 nm absorption feature to provide the kaolinite crystallinity index (Hauff et al., 1990). A subset of 1000 spectra was processed through aiSIRIS. The aiSIRIS trial output provided mineral picks for the presence of other minerals present in the initial scan and provided proportions of all other mineral types identified in the spectra. To ensure consistency between processing methods, 25 spectra from the aiSIRIS subset were also processed through TSG and similar results were obtained.

In order to validate the outputs provided by TSG and aiSIRIS, as well as help define the paragenetic relationships, compositional variances and relative abundances of the different minerals identified, samples of clay species and alteration types were analyzed with a hyperspectral core scanner. Sampling procedures included identifying sections of core with key diagnostic minerals, as identified through TSG or aiSIRIS, or interesting overprinting relationships and alteration textures. These core were then cut into 2–10 cm sections of half-core for hyperspectral analysis. All samples were then secured on plywood sheets and run through SPECIM, Spectral Imaging Ltd.'s SisuROCK hyperspectral scanning system at the Imaging Spectroscopy Laboratory, University of Alberta (Edmonton, Alberta). The core were analyzed for aluminum minerals, water and hydroxyl absorption, rock chemistry index, Fe-Mg minerals as well as sulphates and carbonates. The hyperspectral data are presented in the form of GeoTIFF files with 250 µm/pixel resolution, which provide colour-coded schemes for the spatial distribution of the wavelength of key absorption features within each sample as well as grey-scale maps indicating the relative abundances of each identified mineral type. The hyperspectral scans produced mineral (abundance) maps of the samples, which were then used to confirm representativity of field sample analysis, evaluate the abundance of each respective mineral and define paragenetic relationships of mineral assemblages, including key high temperature minerals (pyrophyllite, dickite).

Minerals identified with SWIR analysis were categorized into alteration assemblages, which grouped minerals present in similar temperature and pH conditions, and will then be used to help determine the geological setting of each alteration zone. The classification scheme summarized all processed spectra into a total of three separate alteration assemblages including propylitic (chlorite, epidote, hematite, carbonate), argillic (illite, smectite±kaolinite) and advanced argillic (alunite, dickite, kaolinite, pyrophyllite). Due to kaolinite occurring in multiple environmental settings with different genetic implications, mineral associations were used to preliminarily categorize which environment kaolinite had the most likely association with (e.g., if kaolinite occurred with dickite, alunite and pyrophyllite, the sample would be categorized as advanced argillic alteration). All processed spectral data was input into Micromine Pty Ltd's Micromine™ 2019 modelling software in order to visualize the spatial relationship for defined alteration assemblages and to overlie other datasets such as geophysics, geochemistry and core logging observations.

Geochemical Characteristics and Vectoring

Geochemical samples collected at the Silver Pond prospects include soil, rock and drillcore samples. Soil samples were collected in a 50 by 50 m grid and only samples considered to be in situ were targeted, sections with Quaternary overburden were avoided. The Silver Pond prospects generally have poor outcrop exposure, with most rock samples categorized as subcrop. Therefore, rock samples were taken at mapping stations and not at regular sampling intervals. Drillcore sampling varied depending on factors such as degree of veining, alteration and mineralization and the presence of key structural contacts. Sections of core that appeared to be relatively fresh hostrock with little to no mineralization were sampled at a 2 m interval, and samples with significant veining, increased alteration intensity and/or mineralization were sampled at a 1 m interval. In sections of core with major structural breaks, isolated mineralization and/or veining, sampling intervals were adjusted to isolate the zone of interest with a minimum sample interval of 30 cm.

All samples were analyzed by ALS-Geochemistry (Vancouver, British Columbia) for gold, silver and an additional 46 elements. Gold was analyzed by fire assay of a 30 g sample followed by inductively coupled plasma–atomic emission spectroscopy (ICP-AES), with a lower detection limit of 0.001 ppm. All samples that exceeded 10 ppm gold were reassayed by fire assay of a 30 g sample with a gravimetric finish; the upper detection limit was 10 000 ppm. The silver and additional 46 elements were analyzed by four-acid digestion followed by inductively coupled plasma–mass spectrometry (ICP-MS), with samples that returned silver assays in excess of 1500 ppm being reanalyzed by fire assay of a 30 g sample with a gravimetric finish. Quality assurance and quality control samples were inserted at a minimum of every 10 samples, with duplicates being taken in mineralized zones.

Assay data were used to evaluate depletion and addition of rock-forming elements (such as Ca, K, Na and Mg) and common pathfinder elements (such as Mo, As and Te). In particular, the epithermal elemental suite, including As, Sb, Hg, Se, Te, Tl, Mo and W, was considered. This analysis was applied to surface and drillcore data to evaluate the relationship of alteration and alteration intensity with Au-Ag pathfinders, and determine the usefulness of SWIR analyses as a field-ready pathfinder tool in the Silver Pond and geochemically similar prospects.

Isocon plots were used to observe quantitative changes in elemental concentrations of the rock-forming and epithermal suite elements as compared to immobile elements in order to determine the relationship between alteration types and addition/subtraction of elements (Grant, 2005). An unaltered reference was calculated from 10–15 m sections of unaltered core from 14 separate holes across the property with the same lithology as the Silver Pond prospects. In total, 179.9 m of core was used to calculate the unaltered reference. The mean, median and standard deviations of each of the elements analyzed were determined to help ensure that samples selected were representative of unaltered sections, and to remove any potential outliers within the selected sections. The mean value was then used as the unaltered reference against all sections of interest. Elements that experienced no net loss or gain lay on the line with a slope of 1, with enriched elements having a value greater than one and depleted elements having a value of less than one, and immobile elements (i.e., Al) generally staying on the line regardless of the influence of alteration events. Mineralized sections, alteration assemblages and individual alteration minerals identified by SWIR were plotted against the unaltered reference mean to help understand the composition of hydrothermal fluids responsible for mineralization and alteration.

Results

Spatial Distribution of Minerals

Three main alteration types are present at the Silver Pond prospects and their distinct mineralogy, spatial distribution and textural characteristics are different from the alteration types present at the low sulphidation targets on the Lawyers property. The analysis of the surficial and drillhole data revealed that the highest intensity hydrothermal alteration zoning at the Silver Pond prospects is an elongated east-west advanced argillic-alteration core, with south and north shoulder zones predominantly composed of argillic and propylitic alteration assemblages. The core of the hydrothermal alteration zone is defined by the presence of high temperature, low pH, advanced argillic-alteration assemblages identified in surface clays and at depth (Figure 3a–c; drillholes 20SPCDD004, 20SPCDD008, 20SPCDD009). The advanced argillic-alteration core zone is predominantly altered to alunite, kaolinite, dickite and high crystallinity white mica with isolated occurrences of pyrophyllite and gypsum. The south and north shoulder zones exhibit a transition from advanced argillic-alteration to argillic alteration. The argillic alteration represents low–moderate temperature and moderate pH conditions and is observed in the surface clays and at depth in drillholes 20SPCDD005, 20SPCDD006 and 20SPCDD007. These shoulder zones are surrounded by a broader regional-scale alteration zone that is defined by an argillic to propylitic transition and is altered predominantly to white mica, montmorillonite and chlorite assemblages. The majority of chlorite identified within the Silver Pond prospects has a low wavelength absorption feature (~2246–2252 nm) indicating a magnesium-rich end member, which commonly occurs in the more proximal portions of a hydrothermal system. The observed hydrothermal alteration zones and their respective assemblage classifications are complemented by key geochemical features, including a depletion in rock-forming elements and enrichment in epithermal suite elements (Figure 4a–d), which is a strong indication and proxy for the influence of hydrothermal magmatic fluids.

At the Silver Pond prospects, drillholes that intersect a range of mineral assemblages also show a transition from muscovite to phengite with increasing depth (Figure 5a, b) and a proximity to higher temperature assemblages. This transition is reflected in changes in the 2200 nm absorption feature, in which white mica of phengitic composition show a characteristic increase in the 2200 nm absorption feature to the ~2210 nm range. The 2200 nm absorption feature can also migrate to a shorter average wavelength (~2190 nm) and typically reflects a sericite-muscovite reaction (Cohen, 2011). In drillholes surrounding the central advanced argillic-alteration zone, both kaolinite and white mica crystallinity values show a trend toward increasing crystallinity with depth (Figure 5c, d) and/or proximity to advanced argillic-alteration zones.

The presence and abundance of pyrophyllite and dickite, as examples of high temperature phases with vectoring potential, was confirmed through hyperspectral core scans. Several samples contain over 90% volume of dickite or pyrophyllite (Figure 6c, d). Preliminary paragenetic relationships extracted from these scans also show that kaolinite postdates dickite (Figure 6b), with kaolinite veins crosscutting samples pervasively altered to dickite, and gypsum veins crosscutting both the kaolinite and dickite. Isolated sections of the advanced argillic-alteration core zone exhibit a pervasive alunite overprint of the groundmass and the phenocrysts of the relic hostrock (Figure 6a).

Geochemical Characteristics and Vectoring

The surface area of the Silver Pond leach cap is characterized by a systematic depletion in common rock-forming elements, such as Mg, Ca and Na, as well as enrichment in epithermal suite elements, such as Tl, Te, Se, As and Sb (Figure 4a, b, 7b–d). Similar chemical relationships were also displayed in the subsurface with the highest degree of relative enrichment closely correlating with the intensity and type of clay alteration present. Highly altered, advanced argillic-alteration assemblages generally exhibit the highest degree of enrichment in epithermal suite elements and corresponding depletion in rock-forming elements (Figure 7b), with argillic and propylitic alteration assemblages sequentially having a lower degree of enrichment/depletion of indicative element suites (Figure 7a).

Select samples within isolated mineralized intervals (0.3–1 m) from two different drillholes (20SPCDD005, 20SPCDD009) show a correlation between the occurrence of Au-Ag and W, Pb, Bi, Cu, Te, Mo and Se (Figure 7c, d). In addition, positive anomalies of Mo, Se, Te, Pb, Bi and Sn systematically increase from argillic to advanced argillic-alteration zones.

A series of modelled and logged north-northwest-trending faults appear to have an influence on the spatial distribution of geochemical trends, with areas proximal to the fault system experiencing a higher degree of enrichment in select epithermal suite elements (Figure 4c, d). Similar degrees of enrichment and elemental associations can be found within isolated Au-Ag intersections. Historical drilling on the Silver Pond prospects also indicates select zones of mineralization occur along a northern extension of the fault system, possibly indicating extensive mineralization along the strike of these major fault structures. The close spatial correlation of the enrichment of pathfinder elements with high temperature, low pH and clay assemblages provides evidence that the system at the Silver Pond site has a strong structural control.

a)

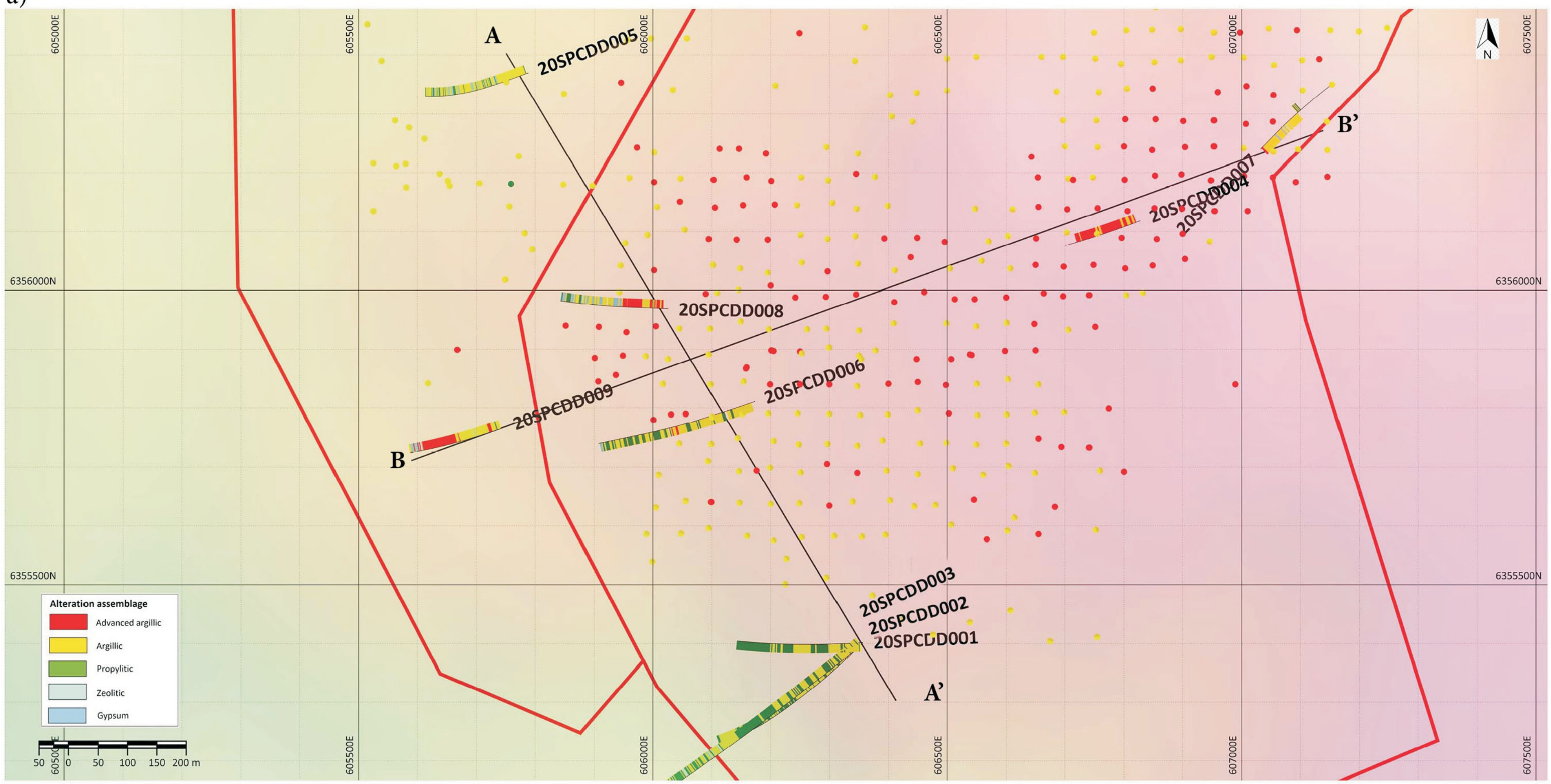

Figure 3. a) Plan view of the Silver Pond prospects shows the extent of the argillic (yellow) and advanced argillic-alteration assemblages (red) at surface, Silver Pond prospects and surrounding area. Figure includes locations of drillholes (20SPCDD00X) and cross-sections (A–A', B–B'; see Figure 3b, c). All co-ordinates are in UTM Zone 9, NAD 83.

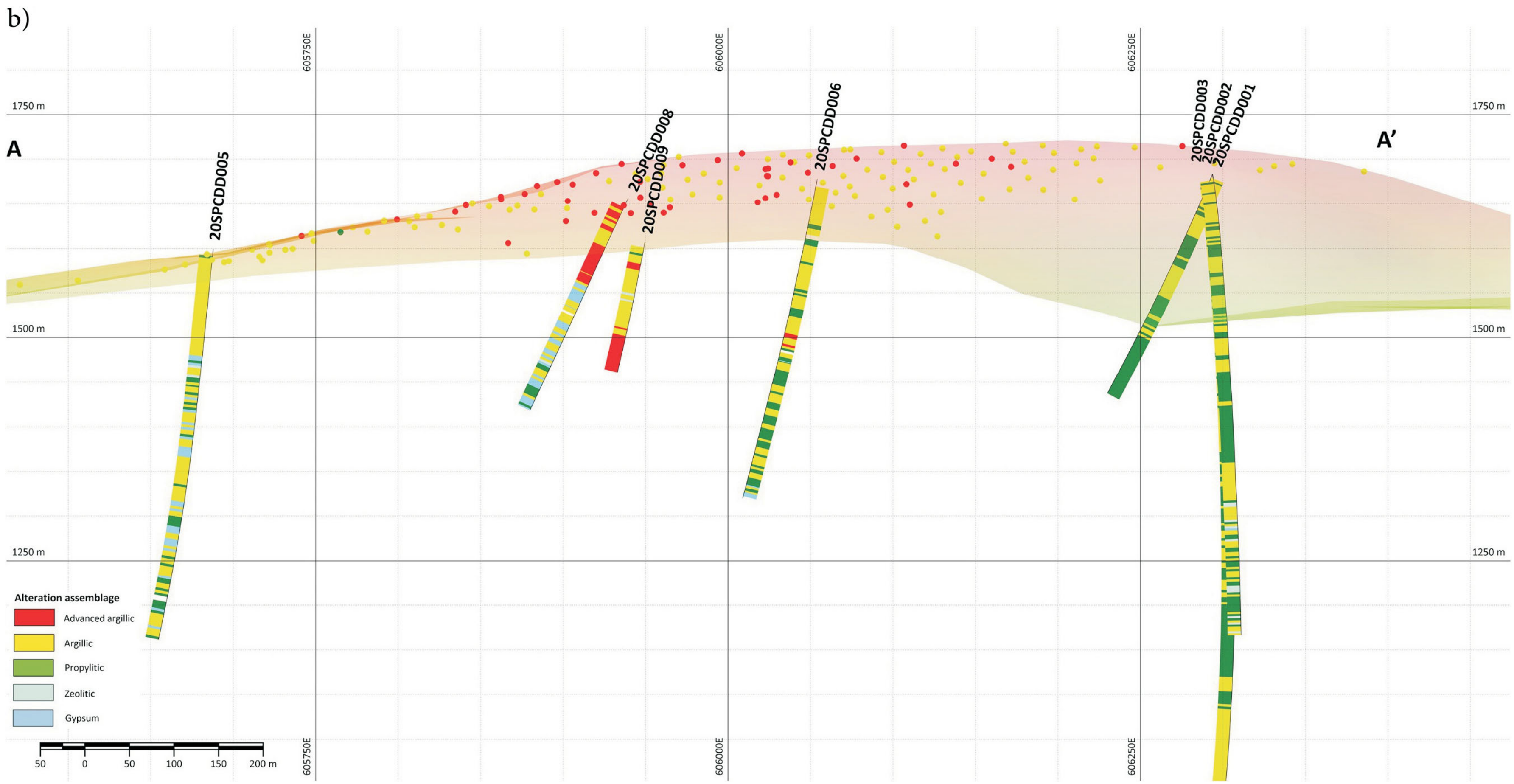

Figure 3 (continued). b) North-northwest cross-section A–A' (from Figure 3a; Silver Pond prospects and surrounding area) shows a high temperature advanced argillic-alteration core (red; drillholes 20SPCDD008, 20SPCDD009) surrounded by a broad argillic-alteration zone (yellow). All co-ordinates are in UTM Zone 9, NAD 83, and elevation is in metres (m) above sea level.

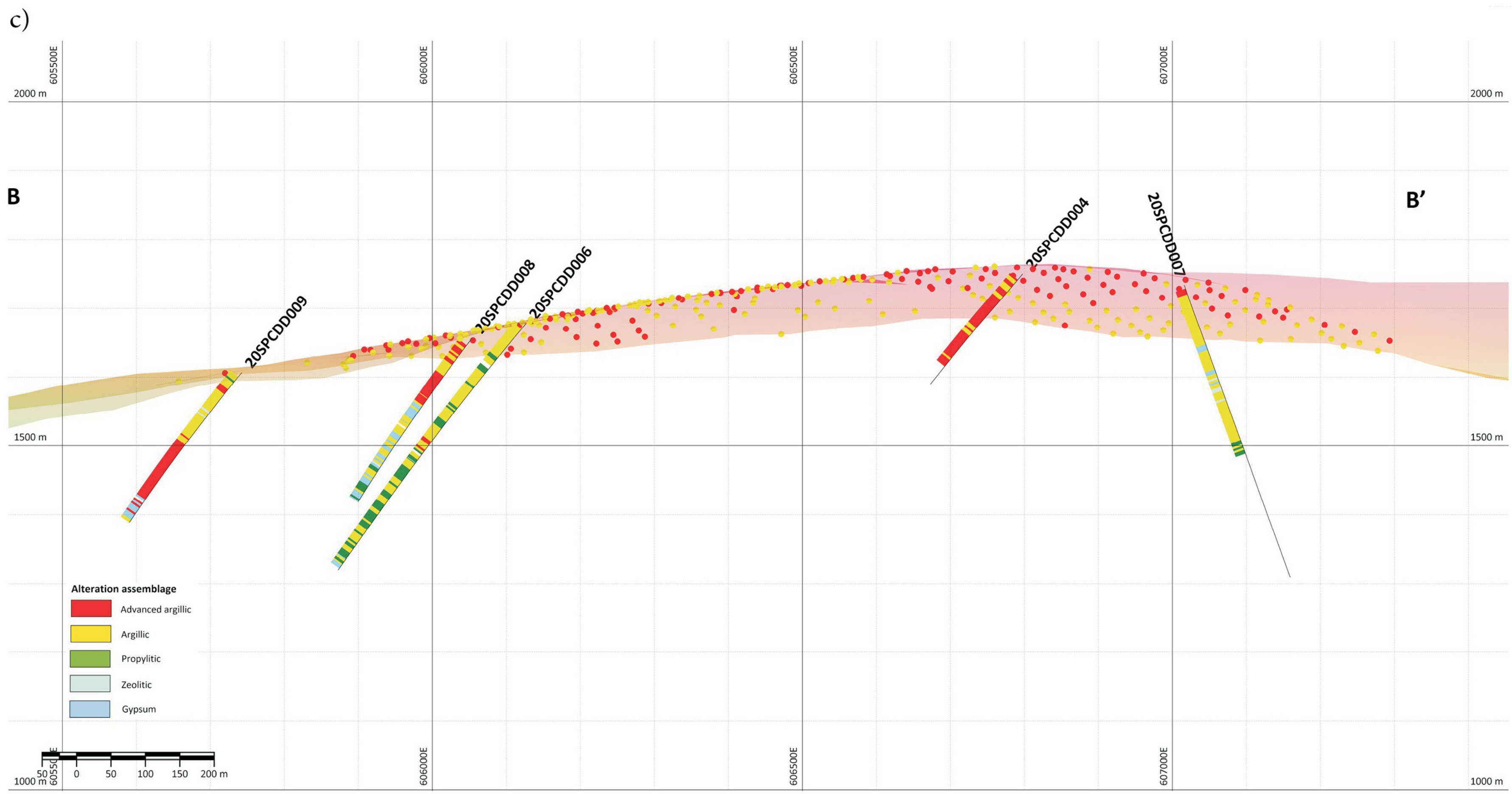

Figure 3 (continued). c) South-southwest cross-section B–B’ (from Figure 3a; Silver Pond prospects and surrounding area) shows the lateral extent of the advanced argillic-alteration core zone and confirms that the surface expression of the advanced argillic-alteration zone is vertically extensive and continues into deeper high temperature clay assemblages in the subsurface. Drillhole locations indicated by 20SPCDD00X. All co-ordinates are in UTM Zone 9, NAD 83, and elevation is in metres (m) above sea level.

a)

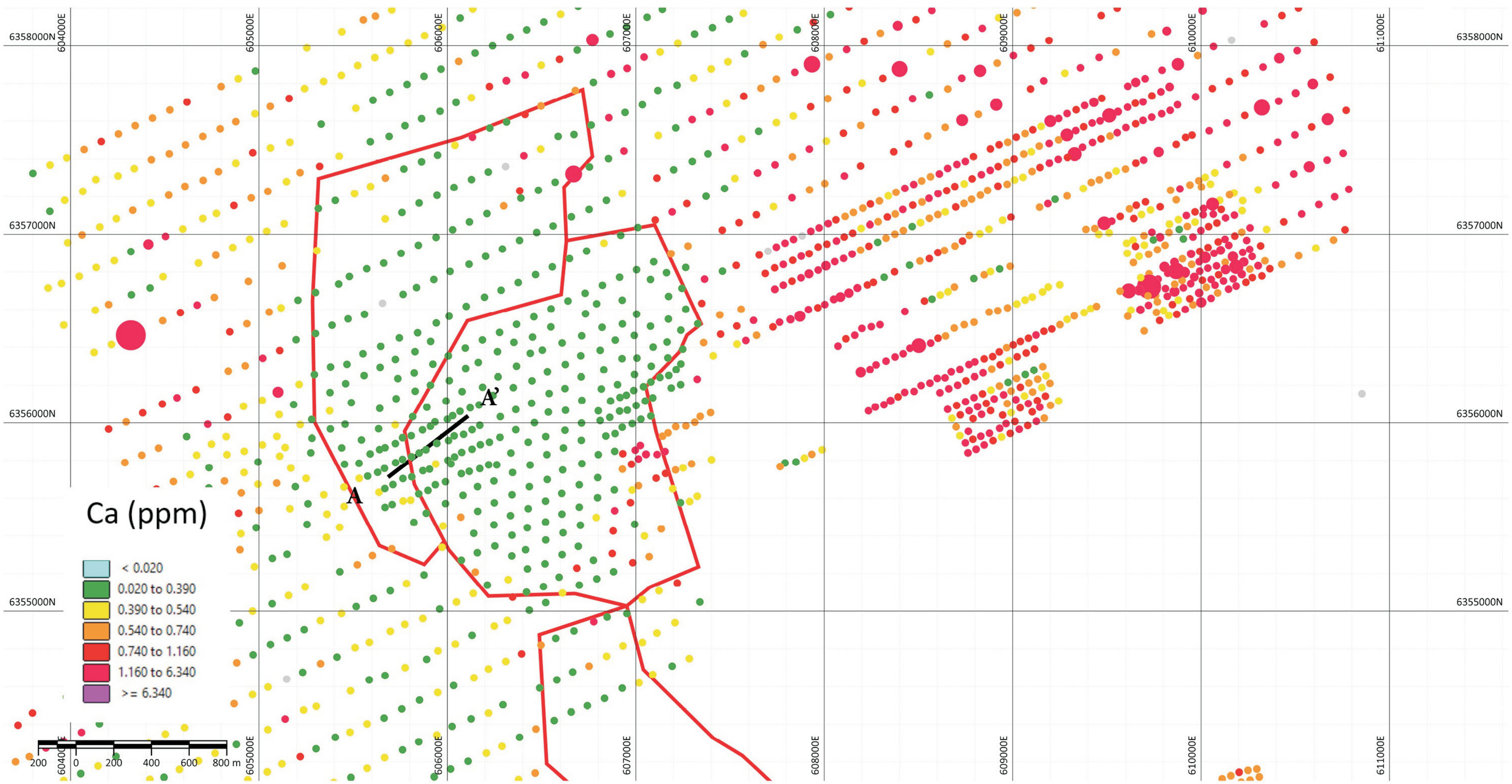

Figure 4. a) Plan view of Silver Pond prospects (outlined in red) and surrounding area displays a systematic depletion in rock-forming elements (i.e., Ca) at surface, which illustrates the leaching of the hostrock by high temperature, low pH, magmatic fluids. Relative concentrations of Ca are indicated using a colour scheme with a corresponding scale factor of the representative circles within each concentration range. See Figure 4c, d for cross-section A-A'. All co-ordinates are in UTM Zone 9, NAD 83.

b)

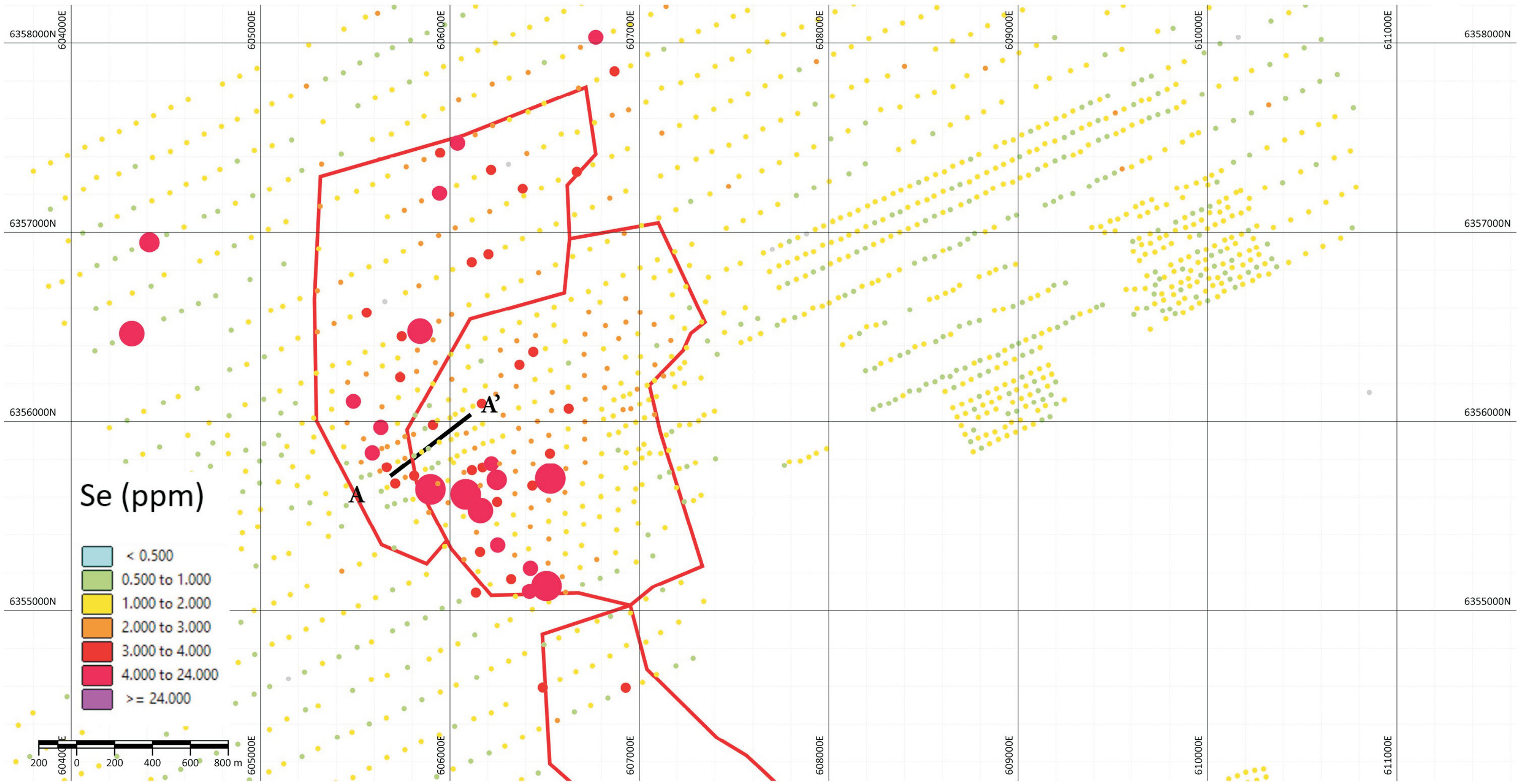

Figure 4 (continued). b) Plan view of Silver Pond prospects (outlined in red) and surrounding area shows high concentrations of Se, a pathfinder element commonly enriched in low or high sulphidation epithermal systems. Relative concentrations of Se are indicated using a colour scheme with a corresponding scale factor of the representative circles within each concentration range. See Figure 4c, d for cross-section A-A'. All co-ordinates are in UTM Zone 9, NAD 83.

c)

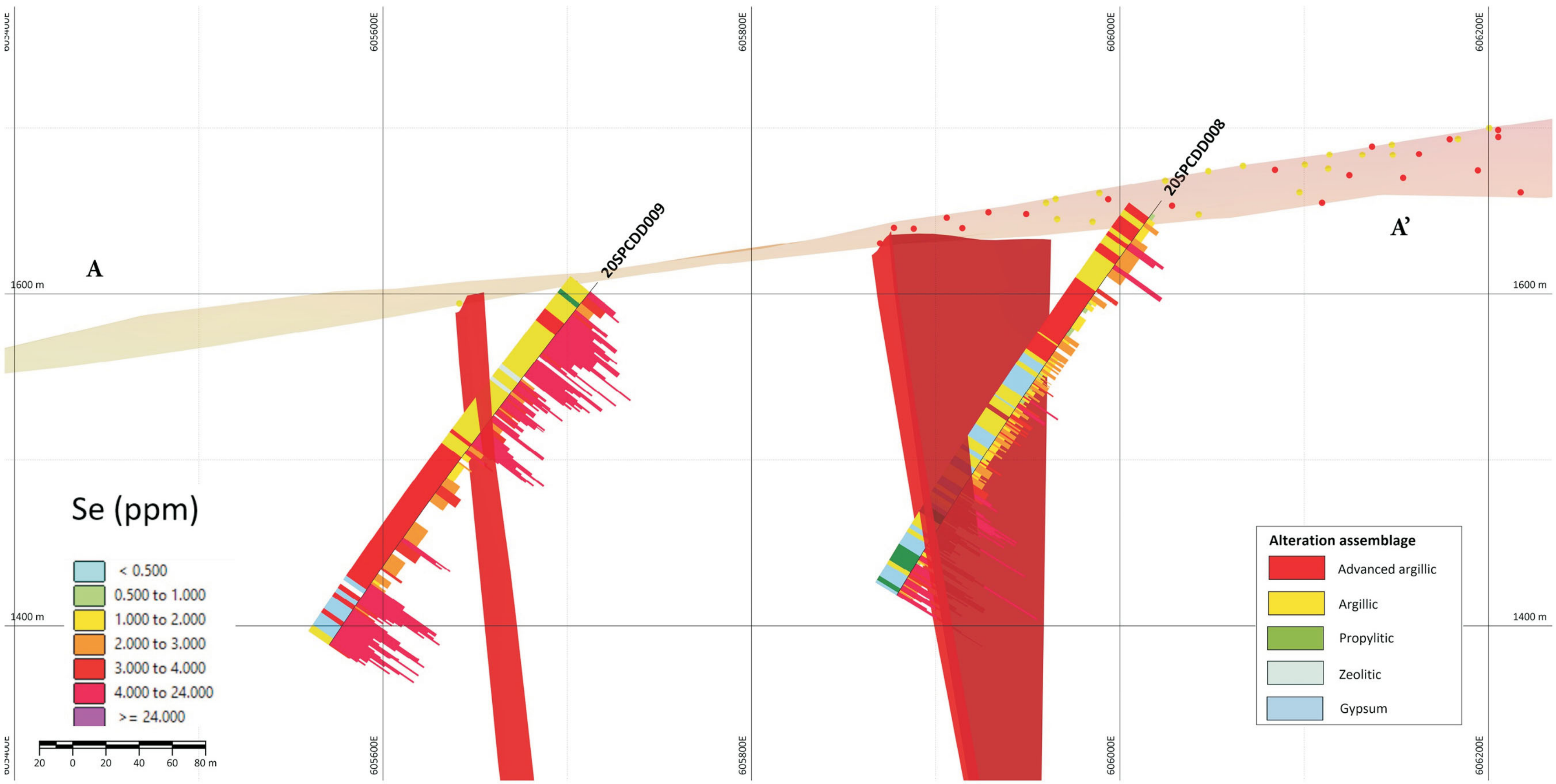

Figure 4 (continued). c) Cross-section A–A' (from Figure 4a, b) illustrates modelled fault surfaces (dark red) and indicates the correlation of anomalously high concentrations of the epithermal suite element of Se (shown to right of drillhole) with high temperature alteration assemblages (shown to left of drillhole) at depth. These high concentrations commonly occur along major fault surfaces indicating the faults likely acted as hydrothermal-magmatic fluid conduits. Drillhole locations indicated by 20SPCDD00X. All co-ordinates are in UTM Zone 9, NAD 83, and elevation is in metres (m) above sea level.

d)

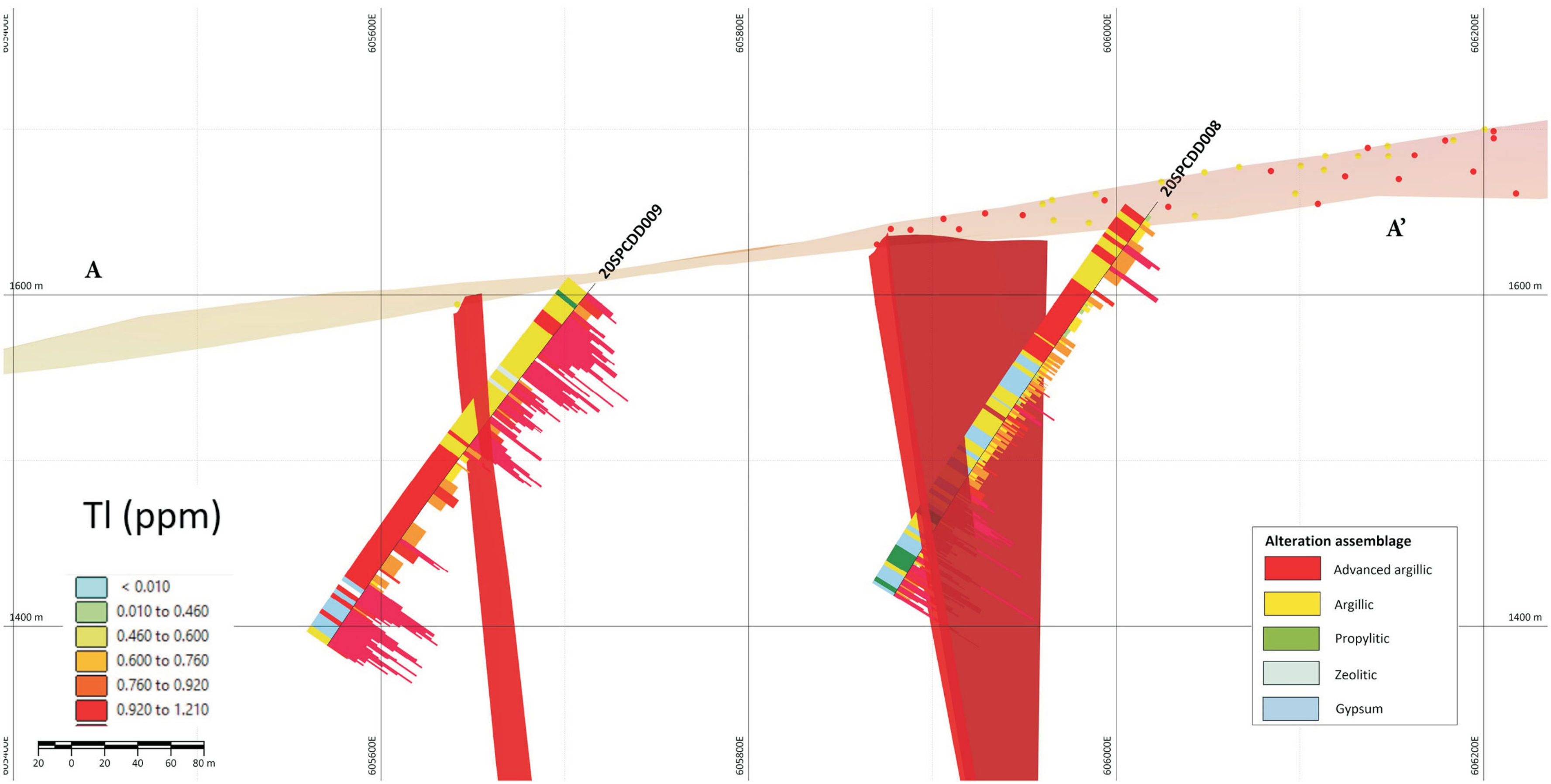

Figure 4 (continued). d) Cross-section A–A' (from Figure 4a, b) illustrates modelled fault surfaces (dark red) and indicates the correlation of anomalously high concentrations of the epithermal suite element of Tl (shown to right of drillhole) with high temperature alteration assemblages (shown to left of drillhole) at depth. These high concentrations commonly occur along major fault surfaces indicating the faults likely acted as hydrothermal-magmatic fluid conduits. Drillhole locations indicated by 20SPCDD00X. All co-ordinates are in UTM Zone 9, NAD 83, and elevation is in metres (m) above sea level.

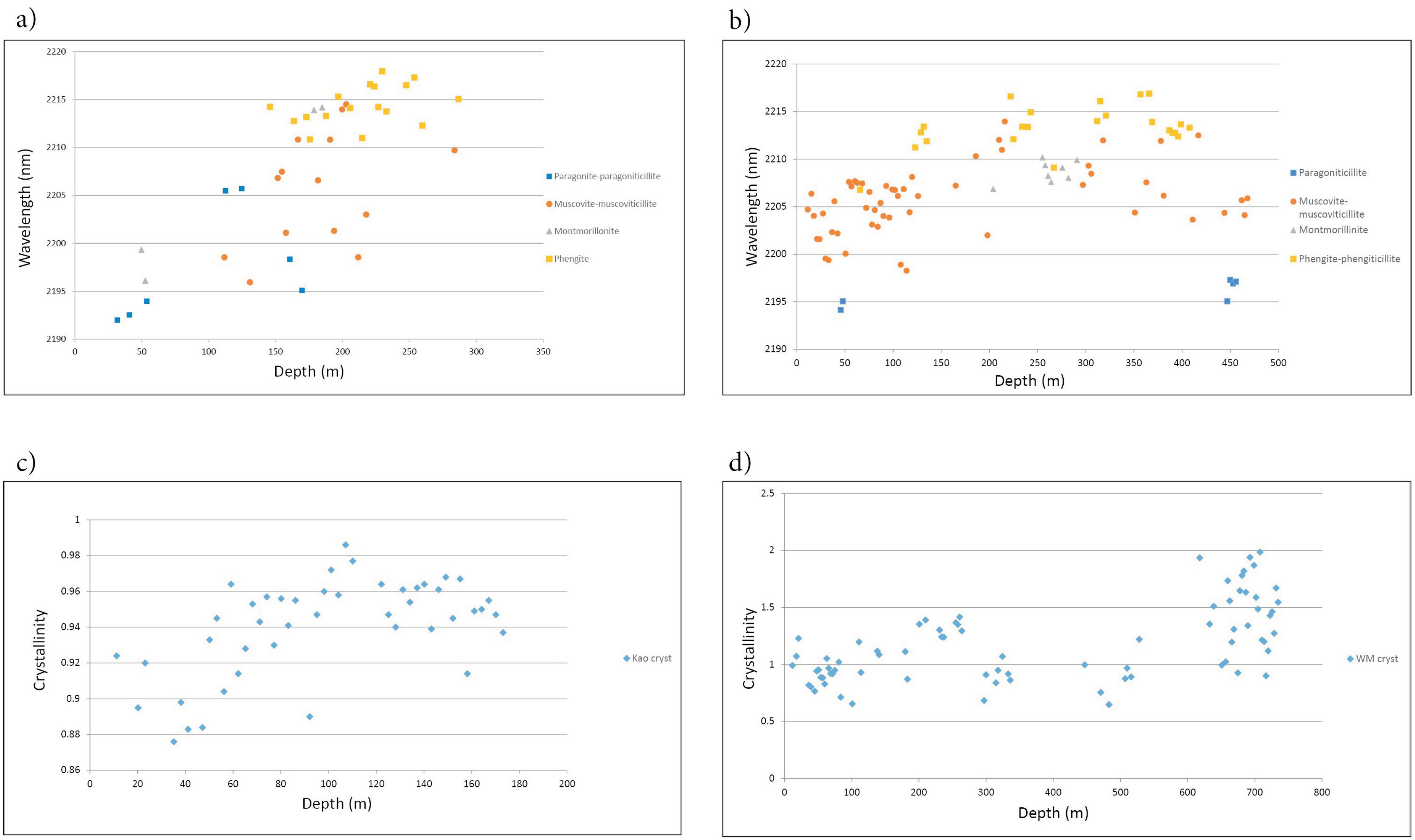

Figure 5. These scatter plots illustrate a general increasing trend in the 2200 nm wavelength feature in white mica from an advanced argillic-alteration zone in **a)** drillhole 20SPCDD008 and **b)** drillhole 20SPCDD005. The higher wavelength values indicate higher temperature conditions at depth. These scatter plots illustrate a trend toward increasing **c)** kaolinite crystallinity (Kao cryst; drillhole 20SPCDD004) and **d)** white mica crystallinity (WM cryst; drillhole 20SPCDD003) at depth, illustrating a transition to a higher temperature regime at depth. Drillhole locations shown on Figure 3.

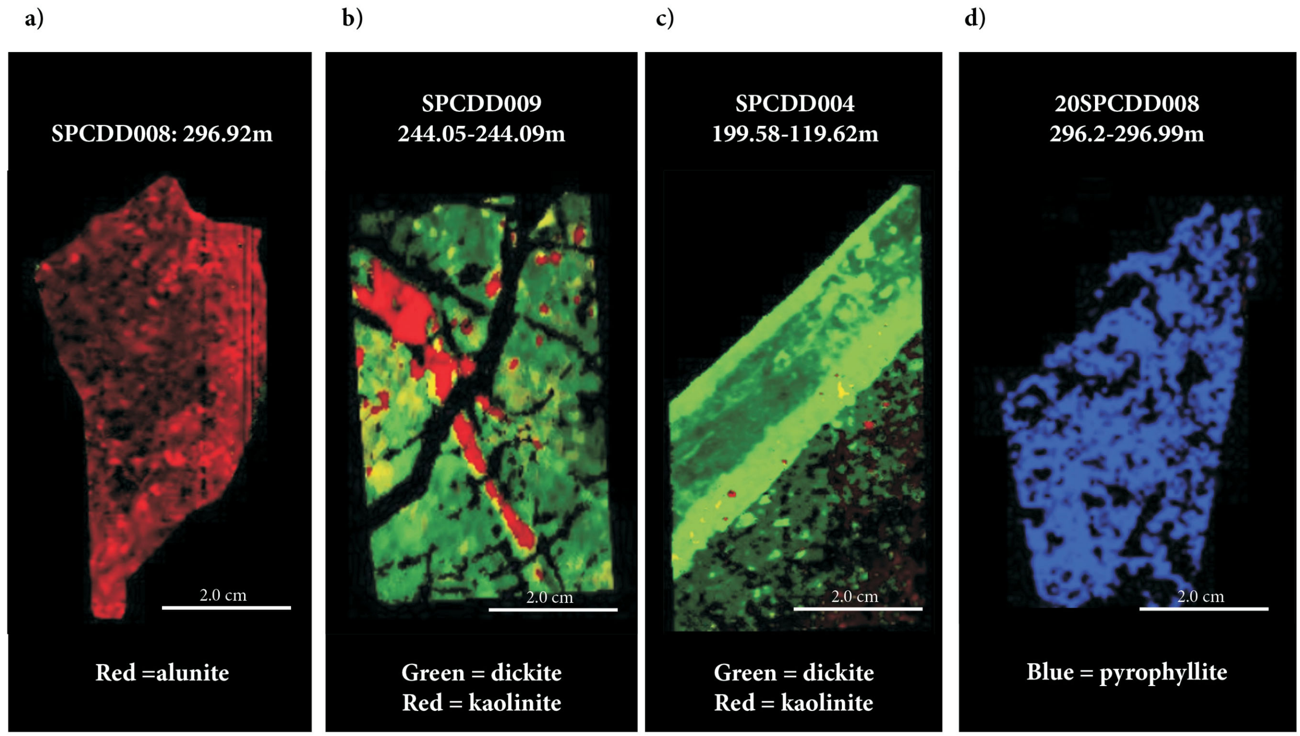

Figure 6. Hyperspectral core scans confirm the pervasive alteration of key indicator minerals used for constraining temperature and pH conditions within the categorized alteration zones, including **a)** alunite, **b, c)** dickite and kaolinite and **d)** pyrophyllite. Locations of drillholes (20SPCDD00X) shown on Figure 3.

Discussion

The SWIR techniques and results were used to help determine the mineralogy of the Silver Pond prospects with the aim of understanding 1) the type of alteration system and 2) what portion of a magmatic-hydrothermal system is present at the Silver Pond site, with the purpose of exploring the potential for economic mineralization. Previous research and exploration programs at the Silver Pond prospects generally describe the area as a lithocap, defined by a high degree of clay alteration caused by a downfaulted acid sulphate outflow, possibly representing the upper portion of the Lawyers property hydrothermal system (Diakow et al., 1991). The combined SWIR analysis of surface clay and drillcore samples confirmed the extent and depth of the lithocap, with the presence of key clay assemblages and mineralogical transitions suggesting that sections of the Silver Pond clay alteration zone formed in high temperature and low pH conditions typical of intermediate to high sulphidation–type settings (Arribas, 1995). The advanced argillic-alteration assemblages discussed have been known to commonly cap porphyry copper systems (Sillitoe, 1973), which is a plausible setting in the context of the regional stratigraphy of the Toodoggone district. This district hosts a series of low and high sulphidation systems some of which have demonstrable base-metal associations, indicative of a deeper hydrothermal system(s) that affected shallower mineralization and alteration domains.

The temperature and pH conditions and their associated alteration assemblages exhibited at the Silver Pond prospects indicate that this may be the site of the portion of the magmatic-hydrothermal system(s) that typically hosts Au-Ag mineralization in analogous deposit types. The system did not undergo complete erosion at the Silver Pond prospects, as the associated alteration zonation is expressed at surface and at depth. The type and distribution of clay assemblages that occur at the Silver Pond prospects are typically associated with hypogene hydrothermal-magmatic environments. Large alunite-kaolinite-dickite haloes with isolated sections of pyrophyllite correspond to intervals that display the highest degree of texturally destructive alteration and intense leaching of the hostrock and likely represent feeder zones. The narrow advanced argillic-alteration zones bounded by a broad argillic alteration zone (dominantly illite-smectite) are characteristic of intermediate to high sulphidation deposits as classified by John et al. (2018). To date, exploration efforts have intersected the main alteration envelopes (i.e., sericite-pyrophyllite, quartz-dickite/kaolinite, quartz-alunite, illite-smectite) but not a zone of residual quartz, which typically hosts Au-Ag mineralization in high sulphidation systems. The confirmed intersections of quartz-alunite, quartz-dickite/kaolinite and sericite-pyrophyllite zones are possible indicators of proximity to a residual or vuggy silica zone.

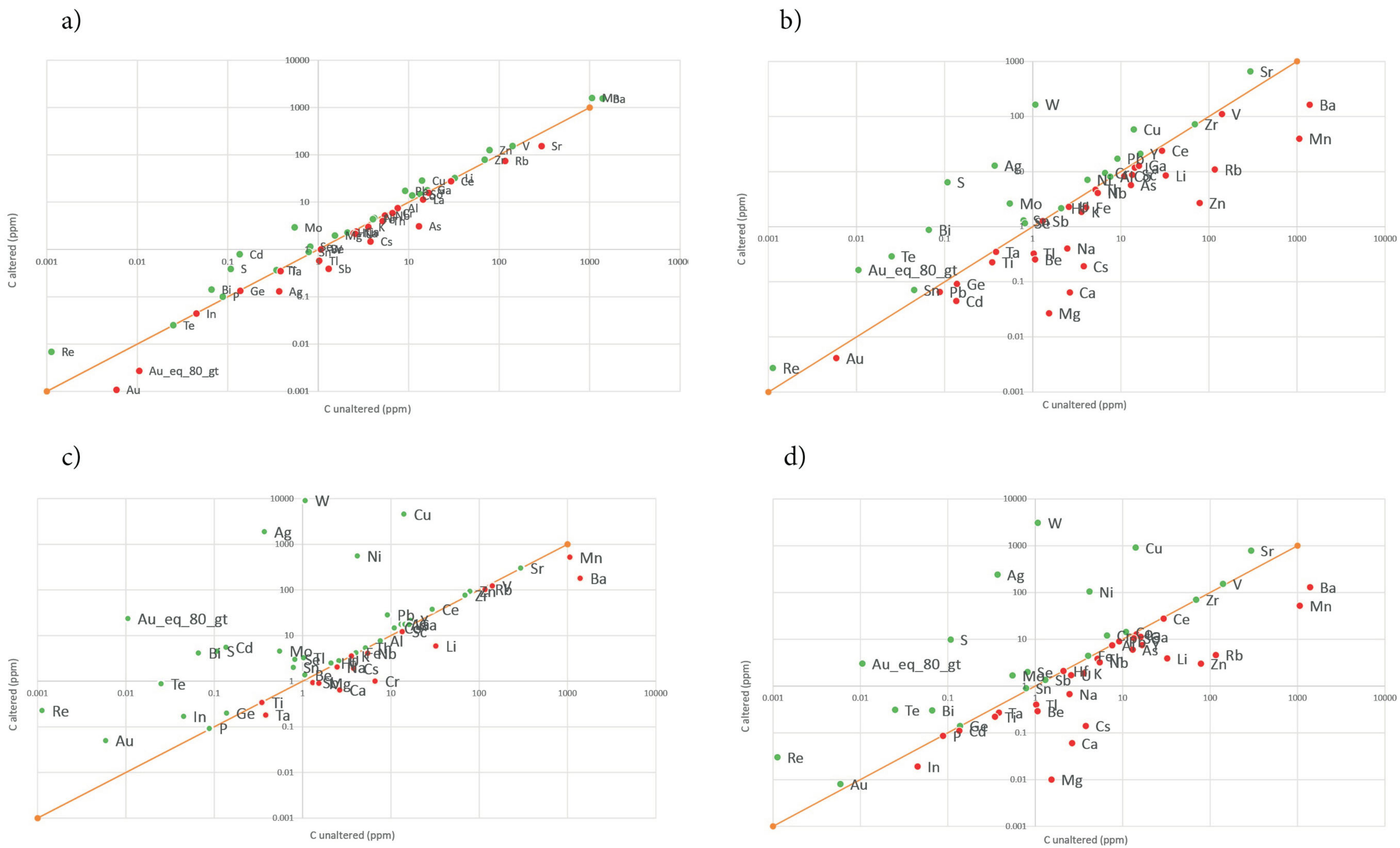

Figure 7. Isocon plots showing elemental relationships of alteration assemblages and mineralized zones plotted against reference unaltered hostrock, where C altered (vertical axis) represents the concentration of each assayed element in the altered/mineralized hostrock, and C unaltered (horizontal axis) represents the concentration of each assayed element in the unaltered hostrock. **a)** Isocon plot of the propylitic alteration zones shows minimal enrichment/depletion due to the occurrence of dominantly lower temperature hydration reactions (i.e., chlorite, epidote). **b)** Isocon plot of representative high temperature, advanced argillic-alteration zones shows a high degree of enrichment in epithermal suite elements (i.e., W, S, Ag, Se, Mo) and major depletion in rock-forming elements (i.e., Mg, Ca, Na). **c)** Isocon plot of elemental distribution in a 1 m drillcore interval (drillhole 20SPCDD009) with 23.6 ppm Au equivalent. **d)** Isocon plot of elemental distribution in 1 m drillcore interval (drillhole 20SPCDD005) with 3.05 ppm Au equivalent. The isocon plots of mineralized sections indicate a similar geochemical signature as the advanced argillic-alteration zones, indicating the identified enrichment trends can be used for targeting mineralization. Drillhole locations shown on Figure 3. Abbreviation: gt, grams per tonne.

The propylitic mineralogy in the north and south shoulders of the Silver Pond prospects are characteristic of low–moderate temperature (0–250°C) and neutral pH conditions. The mineralogy of the argillic–advanced argillic alteration assemblages in the core of the system indicates a temperature range of ~200–350°C in moderate to highly acidic conditions (pH <2–4). The mineralogy identified by SWIR analysis in the central zone of the prospects reveals a systematic shift to higher temperate and lower pH conditions, indicating that this zone is more proximal to focused fluid flow or a hydrothermal-magmatic source, which likely exploited deep-rooted north-northwest-trending faults as fluid conduits.

The results from the SWIR analysis were overlain with geochemistry, core logging and geophysical data and strong correlations were evident between enrichment in epithermal suite elements, magnetic signatures and key structural controls. The distribution of alteration assemblages appears to have a strong correlation with a series of north-northwest-trending faults, with increased alteration intensity, as well as the presence of advanced argillic alteration, occurring proximal to the fault system. The main north-northwest-trending faults have a similar orientation to the fault system that served as a key control for mineralization in the adjacent low sulphidation–style deposits in the property.

Analysis of relative crystallinity values for white mica and kaolinite group minerals were used as an additional proxy for the influence of hydrothermal fluids, which helped with understanding temperature regimes within the Silver Pond prospects. Higher crystallinity values indicate more ordered crystal structures, which occur in higher temperature environments. Shifts in the crystallinity index of kaolinite group minerals and white mica can therefore be used to indicate temperature regimes and aid in the vectoring of higher temperature alteration zones and assemblages. A general increase in crystallinity of both kaolinite and white mica correlates strongly with an increase in depth and/or proximity to high temperature assemblages (Figure 5c, d), indicating a broad-scale trend of increasing temperature regimes with proximity to fault surfaces at depth within the Silver Pond clay alteration zone.

The observed transition of muscovite to phengite with depth (Figure 5a, b) provides additional information on the pH conditions present in select areas of the Silver Pond prospects. This transition is demonstrated in drillhole 20SPCDD008 (Figure 3b, c), where a shallow, fault-bounded, advanced argillic-alteration zone correlates with an overlap of predominantly muscovitic white mica, which has a higher stability in lower pH conditions and when occurring in conjunction with pyrophyllite, likely formed in a moderate to high temperature regime of 280–400°C (Monier and Robert, 1986; Cohen, 2011).

Epithermal deposits are commonly enriched in elements such as As, Sb, Hg, Se, Te, Tl, Mo and/or W (White and Hedenquist, 1995; Saunders et al., 2014). The three types of epithermal deposits (low, intermediate and high sulphidation) also exhibit large variations in absolute and relative concentrations of elements (John et al., 2018) and commonly exhibit distinct zonation patterns. The geochemical fingerprint of the Silver Pond prospects, as illustrated in the isocon plots (Figure 7b–d), shows high levels of enrichment in key elements such as Mo, Se, Te, Pb, Bi, Th and Sn, which coincides with the signature of other known intermediate to high sulphidation epithermal systems (i.e., La Coipa, Chile; Summitville, United States; Pueblo Viejo, Dominican Republic), which are commonly enriched in Cu, Pb, Zn, Mo, Bi, Sn, Te, Th and Se (John et al., 2018).

Conclusions

The clay assemblages identified by shortwave infrared analysis as well as the geochemical signature of zones that experienced intense fluid flow indicate that the alteration zones and characteristics present at the Silver Pond prospects were likely formed as part of a hydrothermal-magmatic system within a high sulphidation–type epithermal setting. The shortwave infrared analysis as well as field observations have documented the presence of a low pH zone dominated by alunite, dickite, anhydrite±pyrophyllite assemblages with a broad illite-smectite, montmorillonite zone. To date, only very narrow (~5–30 cm) occurrences of the vuggy quartz zone, which typically hosts Au-Ag ore, have been encountered. The Silver Pond prospects remain largely underexplored and have strong discovery potential due to the presence of promising alteration assemblage and zonation relationships, geochemical indicators and the proven broad-scale resource potential of the hydrothermal-magmatic system in the greater Lawyers property.

Acknowledgments

This project was supported through scholarships to the lead author from Geoscience BC and Natural Sciences and Engineering Research Council of Canada (NSERC). Benchmark Metals Inc. provided samples and access to data. The authors would also like to thank V. Elongo for guidance and review of the presented research to date.

References

Arribas Jr., A. (1995): Characteristics of high-sulfidation epithermal deposits, and their relation to magmatic fluid; Mineralogical Association of Canada, Short Course 23, p. 419–454.

Benchmark Metals Inc. (2021): Benchmark delivers 2.1 million ounces of 1.62 g/T Au eq indicated and 821,000 ounces of 1.57 g/T Au eq inferred for its initial mineral resource estimate; Benchmark Metals Inc., press release, May 14, 2021, URL <https://www.benchmarkmetals.com/news/news-releases/benchmark-delivers-2-1-million-ounces-of-1-62-g-t-aueq-indicated-and-821000-ounces-of-1-57-g-t-aueq-in-

ferred-for-its-initial-mineral-resource-estimate/> [November 2021].

Bouzari, F., Bissig, T., Hart, C.J.R. and Leal-Meja, H. (2019): An exploration framework for porphyry to epithermal transitions in the Toodoggone mineral district (94E); Geoscience BC, Report 2019-08 and MDRU Publication 424, 101 p., URL <http://www.geosciencebc.com/wp-content/uploads/2019/11/Geoscience-BC-Report-2019-08.pdf> [November 2021].

Cohen, J.F. (2011): Compositional variations in hydrothermal white mica and chlorite from wall-rock alteration at the Ann-Mason porphyry copper deposit, Nevada; M.Sc. thesis, Oregon State University, 121 p.

Cooke, D.R., White, N.C., Zhang, L., Chang, Z. and Chen, H. (2017): Lithocaps – characteristics, origins and significance for porphyry and epithermal exploration; *in* Mineral Resources to Discover, Proceedings of the 14th SGA Biennial Meeting, v. 1, Society for Geology Applied to Mineral Deposits, August 20–23, 2017, Quebec City, Quebec, p. 291–294.

Diakow, L.J., Panteleyev, A. and Schroeter, T.G. (1991): Jurassic epithermal deposits in the Toodoggone River area, northern British Columbia; examples of well-preserved, volcanic-hosted, precious metal mineralization; Economic Geology, v. 86, no. 3, p. 529–554, URL <https://doi.org/10.2113/gsecongeo.86.3.529>.

Duuring, P., Rowins, S.M., McKinley, B.S.M., Dickinson, J.M., Diakow, L.J., Kim, Y.-S. and Creaser, R.A. (2009): Examining potential genetic links between Jurassic porphyry Cu-Au±Mo and epithermal Au±Ag mineralization in the Toodoggone district of north central British Columbia, Canada; Mineralium Deposita, v. 44, p. 463–496.

Grant, J.A. (2005): Isocon analysis: a brief review of the method and applications; Physics and Chemistry of the Earth, Parts A/B/C, v. 30, no. 17–18, p. 997–1004, URL <https://doi.org/10.1016/j.pce.2004.11.003>.

Guggenheim, S., Bain, D.C., Bergaya, F., Brigatti, M.F., Drits, V.A., Eberl, D.D., Formoso, M.L.L., Galán, E., Merriman, R.J., Peacor, D.R., Stanjek, H. and Watanabe, T. (2002): Report of the Association Internationale pour l'Etude des Argiles (AIPEA) Nomenclature Committee for 2001: order, disorder and crystallinity in phyllosilicates and the use of the 'Crystallinity Index'; Clay Minerals, v. 37, no. 2, p. 389–393.

Hauff, P.L., Kruse, F.A. and Thiry, M. (1990): Characterization of interstratified kaolinite/smectite clays using infrared reflectance spectroscopy (1.2–2.5 µm); Chemical Geology, v. 84, no. 1–4, p. 267–270, URL <https://doi.org/10.1016/0009-2541(90)90234-x>.

John, D.A., Vikre, P.G., du Bray, E.A., Blakely, R.J., Fey, D.L., Rockwell, B.W., Mauk, J.L., Anderson, E.D. and Graybeal, F.T. (2018): Descriptive models for epithermal gold-silver deposits; U.S. Geological Survey, Scientific Investigations Report 2010–5070–Q, 247 p., URL <https://doi.org/10.3133/sir20105070Q>.

MapPlace (2021): Claims data, regional geology, aeromagnetic data and MINFILE digital data for portions of NTS 094E; BC Ministry of Energy, Mines and Low Carbon Innovation, BC Geological Survey, MapPlace website, URL <http://apps.empr.gov.bc.ca/pub/mapplace/mp2/fusion/templates/mapguide/slate/index.html?ApplicationDefinition=Library://mp2.ApplicationDefinition&locale=en> [September 2021].

Monier, G. and Robert, J.-L. (1986): Muscovite solid solutions in the system K_2O-MgO-FeO-Al_2O_3-SiO_2-H_2O: an experimental study at 2 kbar P_{H2O} and comparison with natural Li-Free white micas; Mineralogical Magazine, v. 50, no. 356, p. 257–266, URL <https://doi.org/10.1180/minmag.1986.050.356.08>.

Saunders, J.A., Hofstra, A.H., Goldfarb, R.J. and Reed, M.H. (2014): Geochemistry of hydrothermal gold deposits; *in* Treatise on Geochemistry (2nd edition), v. 13, H.D. Holland and K.K. Turekian (ed.), Elsevier, Oxford, United Kingdom, p. 383–424.

Sillitoe, R.H. (1973): The tops and bottoms of porphyry copper deposits; Economic Geology, v. 68, p. 799–815.

Steven, T.A. and Ratte, J.C. (1960): Geology and ore deposits of the Summitville district, San Juan Mountains, Colorado; U.S. Geological Survey, Professional Paper 343, 70 p.

White, N.C. and Hedenquist, J.W. (1995): Epithermal gold deposits—styles, characteristics and exploration; Society of Economic Geologists, Newsletter 23, p. 1, 9–13.

Development of Rare-Earth Elements Database for the East Kootenay Coalfield of Southeastern British Columbia (NTS 082G/10, 15) Using Field-Collected Samples: Updated Results

V.K. Kuppusamy, NBK Institute of Mining Engineering, The University of British Columbia, Vancouver, British Columbia, vkk@student.ubc.ca

M.E. Holuszko, NBK Institute of Mining Engineering, The University of British Columbia, Vancouver, British Columbia

Kuppusamy, V.K. and Holuszko, M.E. (2022): Development of rare-earth elements database for the East Kootenay coalfield of southeastern British Columbia (NTS 082G/10, 15) using field-collected samples: updated results; *in* Geoscience BC Summary of Activities 2021: Minerals, Geoscience BC, Report 2022-01, p. 39–44.

Introduction

According of the International Union of Pure and Applied Chemistry (IUPAC), rare-earth elements (REEs) include 15 lanthanides plus Sc and Y (Connelly et al., 2005). They are grouped into two categories: light REEs (LREEs) and heavy REEs (HREEs). The elements La to Gd and Sc belong to the LREEs group and the HREEs group consists of Tb to Lu and Y (Moldoveanu and Papangelakis, 2013; Zhang et al., 2015). The REEs are used in the manufacturing of a wide variety of products and devices, such as light-emitting diodes, permanent magnets, catalytic converters, hybrid cars, wind turbines, fibre optics, super conductors and defence equipment (Balaram, 2019). China is one of the dominant suppliers of REEs globally and accounts for on average 86% of total rare-earth oxide production in the last 20 years (U.S. Geological Survey, 2021). The demand for REEs has increased significantly as the global transition to a low carbon economy has gained greater momentum in the recent years (Goodenough et al., 2018). The REEs are classified as critical elements in different studies due to increased supply risk to meet the future demand, considering various geopolitical, geological, environmental and market risks (U.S. Department of Energy, 2010; Deloitte Sustainability et al., 2017; Natural Resources Canada, 2020). To mitigate the supply risk, coal-related feedstocks are being evaluated as alternative sources of REEs for future exploitation (Seredin and Dai, 2012; Dai and Finkelman, 2018). The detailed review of REE occurrences and enrichment in coal deposits and geochemical analyses results are reported in the literature (Zhang et al., 2015; Dai et al., 2016). Using the U.S. Geological Survey's (USGS) coal database, the National Energy Technology Laboratory (NETL) in the United States has assessed coal deposits as source material for REE production (Bryan et al., 2015). As a result, NETL has funded a research and development program to demonstrate the techno-economic feasibility of developing domestic technologies to separate REEs from coal and/or its byproducts that contain a minimum of 300 ppm total REEs (U.S. Department of Energy, 2016).

Data indicating the presence of REEs in Canadian coal deposits scarcely exists, but some coal deposits have been studied for trace elements (Goodarzi, 1988; Birk and White, 1991; Goodarzi et al., 2009). There have been no efforts made to specifically quantify and characterize the REEs in British Columbia (BC) coal deposits or other coal deposits in Canada for subsequent extraction. The main objective of this study is to create a REE database for the East Kootenay coalfield (Figure 1) using field-collected samples to identify the best potential source material in the study area. A few samples in the database were also evaluated for extraction of REEs, using processes such as magnetic-, density- and gravity-based methods, flotation, ion-exchange and leaching. Preliminary results on the REE database were reported previously (Kuppusamy and Holuszko, 2021), and this database is now updated with additional field-collected samples and presented in this paper.

Materials and Methods

In 2020 and 2021, samples were collected by coal geologists from their respective mines to develop the database. Sample preparation in the lab was conducted in accordance with ASTM standards for coal sample preparation. A lithium-borate fusion was used in the REE analysis and four-acid digestion in the analysis for other minor elements. For a few reactive samples, aqua-regia digestion was adopted for minor element analyses. The digested solutions were analyzed by inductively coupled plasma–mass spectrometry (ICP-MS). All the chemical analyses reported in this study were conducted by ALS-Geochemistry (Vancouver, British Columbia). In this study, REEs in samples are expressed as follows: on a whole coal basis (REE concentra-

This publication is also available, free of charge, as colour digital files in Adobe Acrobat® PDF format from the Geoscience BC website: http://geosciencebc.com/updates/summary-of-activities/.

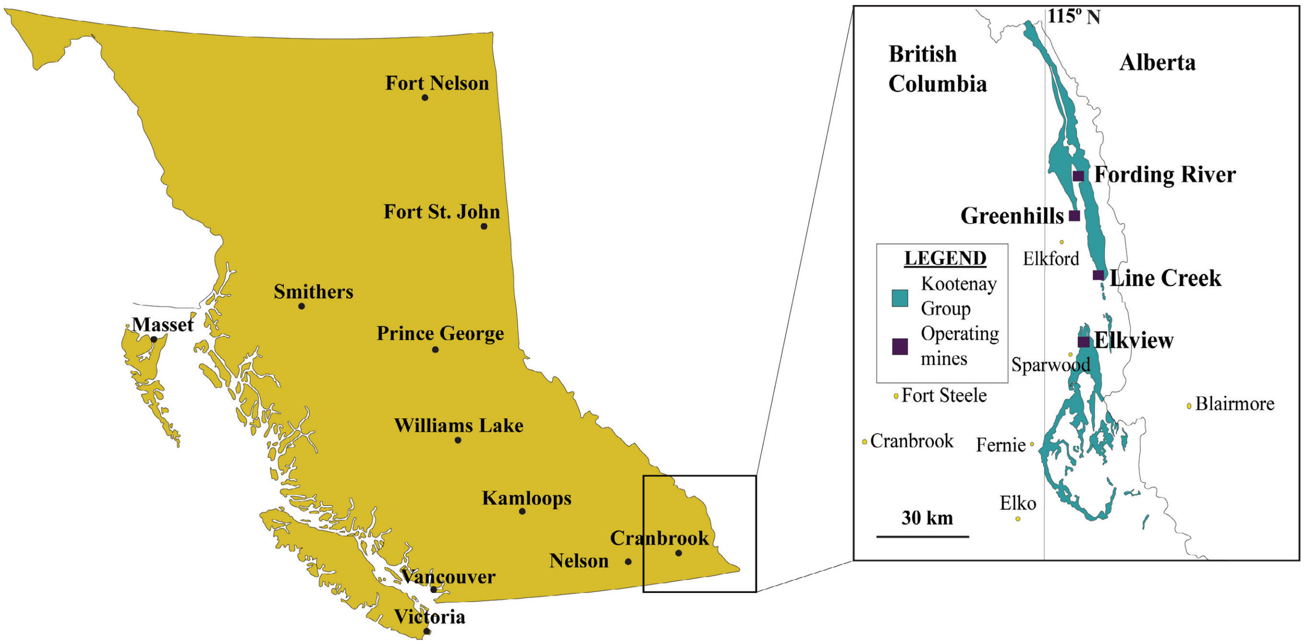

Figure 1. Location of East Kootenay coalfield and operating coal mines in southeastern British Columbia (adapted from BC Geological Survey, 2019).

tion in the coal sample) and on an ash basis (REE concentration in the ash of the coal sample). The procedure followed for sampling, preparation and chemical analyses is detailed in Kuppusamy and Holuszko (2021).

Results and Discussion

The preliminary results of 49 samples were reported previously (Kuppusamy and Holuszko, 2021). In this paper, the data is updated with an additional 55 samples collected from the study area. Results of the proximate analysis of 37 coal samples are shown in Table 1. According to ASTM D388-17 (2017), all the coal samples can be classified as low-to-medium volatile bituminous coal, which is of a metallurgical quality. For the database, more than 60 parameters were collected for each sample, including type, rank and major-, minor- and trace-elements concentrations. Once the study is completed, the comprehensive dataset will be released in future reports. Seam identification and the specific locations of the individual samples are not disclosed to uphold a confidentiality agreement.

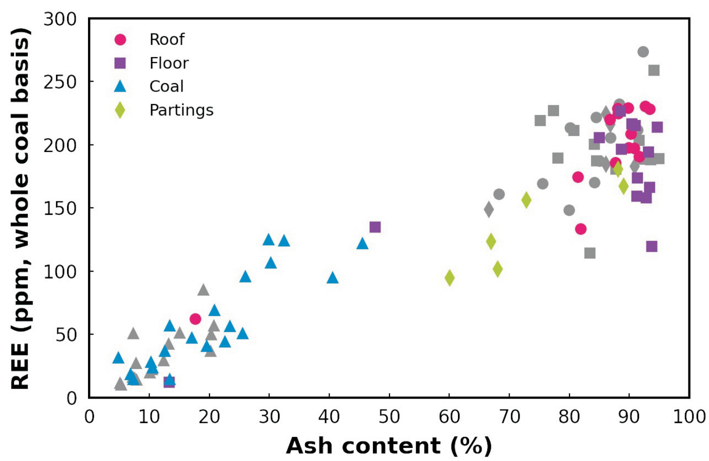

Figure 2. Rare-earth element (REE) concentration (on whole coal basis; ppm) versus ash content (%) for the roof, floor, coal and partings samples from the East Kootenay coalfield, southeastern British Columbia. Grey colour markers indicate data points reported last year.

The REE concentration in the samples varied from 91 to 686 ppm on ash basis and more than 77% of total REEs was accounted for by five elements (Ce, La, Nd, Y, Sc). The maximum, minimum and average REE concentrations on ash basis for different geological material collected, including roof, floor, coal and partings, are listed in Table 2. It can be observed that coal showed an enhanced concentration of REEs when compared to the other material types. As shown in Figure 2, the concentration of REEs increases with ash content of the material on a whole coal basis indicating the preferred REEs association with mineral matter, which is comparable with previously published results (Kuppusamy and Holuszko, 2021). On Figure 2, grey colour markers indicate data points reported last year. During the coal beneficiation process, the REEs associated with mineral matter are generally concentrated into waste tailings streams. The flotation of East Kootenay coal samples showed that most of the REEs by weight were reported to the middlings and tailings streams (Kuppusamy and Holuszko, 2019), which confirms the trend shown in Figure 2.

Table 1. Proximate analysis results for coal samples (as-determined basis) from the East Kootenay coalfield, southeastern British Columbia. Abbreviation: ID, identification.

Sample ID	Type	Moisture content (%)	Ash content (%)	Volatile matter (%)	Fixed carbon (%)
10	Coal	2.41	7.24	22.85	67.5
11	Coal	2.81	10.12	21.92	65.14
12	Coal	2.39	7.66	23	66.95
13	Coal	2.41	7.52	22.92	67.14
14	Coal	2.43	7.93	23.02	66.62
15	Coal	2.5	10.46	22.3	64.74
16	Coal	2.62	5.1	24.08	68.2
17	Coal	2.1	5.29	23.69	68.93
18	Coal	2.09	20.24	27.29	50.38
19	Coal	2.75	7.37	25.68	64.2
20	Coal	1.36	12.39	24.67	61.59
22	Coal	0.85	19.05	19.39	60.71
26	Coal	1.25	7.84	22.73	68.19
27	Coal	1.24	13.19	19.32	66.26
41	Coal	1.31	20.74	23.11	54.84
48	Coal	0.66	20.34	20.15	58.85
49	Coal	0.87	15.06	22.16	61.91
53	Coal	1.03	10.57	24.32	64.08
54	Coal	1.36	6.87	28.70	63.07
60	Coal	1.39	10.32	30.69	57.61
61	Coal	1.00	30.27	22.78	45.94
69	Coal	0.77	32.47	20.68	46.08
73	Coal	0.62	12.58	22.80	64.00
74	Coal	0.60	20.89	24.46	54.05
76	Coal	0.62	25.98	21.75	51.65
78	Coal	0.46	7.36	22.29	69.89
81	Coal	1.97	29.88	19.68	48.46
83	Coal	1.51	45.55	18.00	34.94
87	Coal	1.21	4.86	5.57	88.35
89	Coal	1.07	13.37	14.18	71.38
96	Coal	1.03	40.52	15.51	42.94
98	Coal	0.74	13.40	18.39	67.47
99	Coal	0.86	23.48	18.40	57.26
100	Coal	0.75	22.64	22.12	54.50
102	Coal	0.55	19.53	22.57	57.35
103	Coal	0.97	25.60	24.66	48.77
104	Coal	0.94	17.10	26.21	55.75

The preliminary economic evaluation of samples was conducted using the evaluation plot proposed by Dai et al. (2017). In the plot, REE concentration was plotted against outlook coefficient (C_{outl}), which signifies the quality of REEs present in the sample. Using the plot, samples were grouped into three categories. An explanation of the REE cut-off grades and calculation of outlook coefficient can be found in Kuppusamy and Holuszko (2021). The evaluation plot was adopted to accommodate the resource cut-off suggested in U.S. Department of Energy (2016), which classifies the samples into five categories: unpromising source (REE <300 ppm on ash basis or C_{outl} <0.7); promising resource (300<REE<720 ppm on ash basis and 0.7<C_{outl}<2.4); highly promising resource (300<REE<720 ppm on ash basis and C_{outl}>2.4); promising source (REE >720 ppm on ash basis and 0.7<C_{outl}<2.4); and highly promising source (REE >720 ppm on ash basis and C_{outl} >2.4). All the samples in the REE database were plotted in the modified plot and are shown in Figure 3. The updated data points are shown in different colours, whereas last year's data points are shown in grey.

Table 2. Maximum, minimum and average rare-earth element (REE) concentrations (on ash basis; ppm) in the roof, floor, coal and partings samples from the East Kootenay coalfield, southeastern British Columbia.

Type	Maximum	Minimum	Average
Roof	351.3	163.1	238.4
Floor	293.3	90.8	216.2
Coal	685.9	105.1	284.3
Partings	260.4	149.5	204.3

Table 3. Maximum, minimum and average heavy rare-earth elements (HREEs) to light rare-earth elements (LREEs) ratio and outlook coefficient in the different coal sample types from East Kootenay coalfield, southeastern British Columbia.

Type	HREEs-LREEs			Outlook coefficient		
	Maximum	Minimum	Average	Maximum	Minimum	Average
Roof	0.37	0.17	0.28	1.41	0.77	1.11
Floor	0.38	0.18	0.27	1.42	0.85	1.06
Coal	0.58	0.22	0.34	1.72	0.73	1.19
Partings	1.03	0.21	0.35	2.93	0.82	1.27

The C_{outl} values for most of the samples are >1, implying that the critical REE concentration is significant and accounts for, on average, 36% of the total REEs. Further, it can be noticed from Table 3 that HREE concentrations are generally more significantly concentrated in coal compared to roof, partings and floor samples, in some cases they consist of more than 50% of total LREEs, which contributes to the better C_{outl} values. The average C_{outl} for the coal samples is found to be 1.2, which is consistent with results from Kuppusamy and Holuszko (2021). Additionally, certain partings samples also showed enriched HREE concentrations, which resulted in the highest outlook coefficient observed among the tested samples. Because of HREE enrichment in some samples, the general statistics of partings were improved and comparable to that of coal values in terms of HREE-LREE ratio and outlook coefficient. Since the reported C_{outl} for world coal is 0.64 (Zhang et al., 2015; Dai et al., 2017), these results show that BC coals may become a viable source of REEs if extraction processes are further refined.

Correlation analysis also shows a strong correlation between coal ash and REE content (except Sc) when calcu-

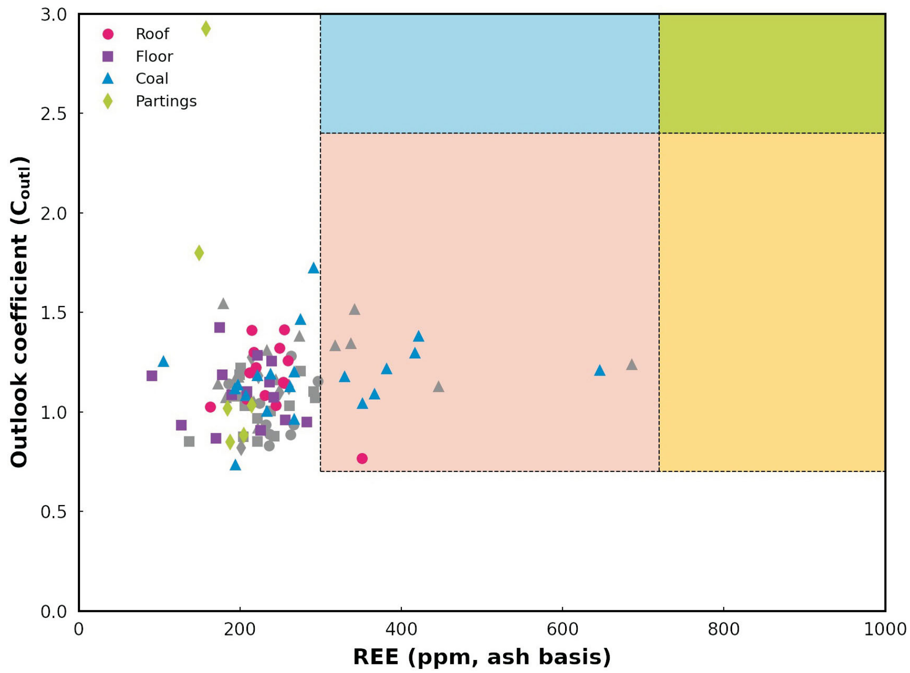

Figure 3. Outlook coefficient (C_{outl}) versus rare-earth element (REE) concentration for various types of coal samples from the East Kootenay coalfield, southeastern British Columbia. The REE resource categories for coal sources: green, highly promising source; yellow, promising source; blue, highly promising resource; light salmon, promising resource. Grey colour markers indicate data points reported last year.

lated on a whole coal basis (r = +0.86 to 0.93). This indicates the presence of various mineral phases containing REEs in the coal samples. One of the REE carriers in these types of metalliferous coal is zircon, which can originate from volcanic ash or authigenic minerals and it can be identified by enrichment of Hf, Th, U and HREEs (Finkelman, 1981; Seredin, 2004). A compelling correlation between Hf, Th, U, Y and other REEs implies that zircon could be one of the source minerals of REEs and indicates an input of volcanic ash containing REEs into these coals. Elemental analysis by ICP-MS indicated the presence of zirconium in these samples. Also, volcanic ash is believed to be the source of tonsteins associated with the coal beds in the Mist Mountain Formation in the East Kootenay coalfield (Grieve, 1993), which further validates the inference made in this study.

No correlation was observed between ash and REE content when calculated on an ash basis (r = –0.07 to 0.44). This implies that only a small amount of REEs is associated with organic matter in the studied samples. To confirm this, the next step would be to look for a strong correlation between REEs and W, which is believed to be organically fixed in coal. However, a very weak correlation was shown between REE and W in the studied samples (r = +0.14 to 0.37) indicating inorganically associated REEs.

In the samples, on the whole coal basis, REEs strongly correlated with U (r >+0.84) and Th (r >+0.80). This suggests that one of the REE mineral phases could be monazite, but a more detailed mineralogical study is required to confirm its presence in the sample.

The modified evaluation plot was used to select a few samples with a high potential for use as REE feedstock. These select few samples are currently being investigated to understand the mode of occurrence and REE mineralogy. Further, REE extraction potential from these samples is also being assessed using bench-scale test works. The final report containing the entire database, characterization and extraction study results will be published in the near future.

Conclusions

In this study, more than 100 samples were collected from the East Kootenay coalfield to develop a rare-earth element (REE) database for the study area. The results from the first 49 samples were reported previously and the database is now being updated with an additional 55 samples. It was found that total REE concentrations on ash basis varied from 91 to 686 ppm. Considering different geological material types, the tested coal samples showed enriched REE concentrations. Further, the concentrations of heavy rare-earth elements (HREEs) were generally higher in coal and partings samples. In certain partings samples, the HREE–light rare-earth element (LREE) ratio was >1 meaning the concentration of HREEs was greater than the LREEs, which was reflected in the significantly higher outlook coefficient value, showing increased economic potential.

Further, correlation analysis revealed a significant domination of inorganic association of REEs in the samples.

The extraction of REEs from alternative source material is currently being developed for successful exploitation of these resources. Even though REE concentration in coal sources are considerably lower than conventional REE deposits, the extraction of REEs from coal-based feedstocks has numerous advantages compared to traditional REE mining, including reduced cost, environmental footprint and waste management. Further, coal-based source material was also shown to contain other valuable elements such as Ge, Ga, Li, V, Nb Au, Ag, Al and platinum group elements, which can also be co-extracted with REEs paving the way for more sustainable resource usage.

Acknowledgments

Financial support for the project from Geoscience BC is greatly appreciated. The authors gratefully acknowledge the scholarship received from Geoscience BC in 2017–2018. Sincere gratitude is extended to the industrial partner Teck Coal Limited and Mitacs for an Accelerate Program grant. The authors would also like to thank M. Mastalerz, Indiana University, for her valuable comments and suggestions to improve this manuscript.

References

ASTM D388-17 (2017): Standard classification of coals by rank; ASTM International, West Conshohocken, Pennsylvania, 2017, URL <https://doi.org/10.1520/D0388-17>.

Balaram, V. (2019): Rare earth elements: a review of applications, occurrence, exploration, analysis, recycling, and environmental impact; Geoscience Frontiers, v. 10, p. 1285–1303.

BC Geological Survey (2019): British Columbia coal industry overview 2018; BC Ministry of Energy, Mines and Low Carbon Innovation, Information Circular 2019-2, 13 p., URL <http://cmscontent.nrs.gov.bc.ca/geoscience/PublicationCatalogue/InformationCircular/BCGS_IC2019-02.pdf> [September 2019].

Birk, D. and White, J.C. (1991): Rare earth elements in bituminous coals and underclays of the Sydney Basin, Nova Scotia: element sites, distribution, mineralogy; International Journal of Coal Geology, v. 19, p. 219–251.

Bryan, R.C., Richers, D., Andersen, H.T. and Gray, T. (2015): Assessment of rare earth elemental contents in select United States coal basins; U.S. Department of Energy, National Energy Technology Laboratory, 47 p., URL <https://edx.netl.doe.gov/dataset/ae5aa8e1-77f9-45fb-a2bc-aa361505706c/resource/137a0880-7c47-40d1-bc23-80b07264ab13> [November 2020].

Connelly, N.G., Damhus, T., Hartshorn, R.M. and Hutton, A.T. (2005): Nomenclature of Inorganic Chemistry – IUPAC Recommendations 2005; RSC Publishing, 377 p., URL <https://old.iupac.org/publications/books/rbook/Red_Book_2005.pdf> [September 2021].

Dai, S. and Finkelman, R.B. (2018): Coal as a promising source of critical elements: progress and future prospects; International Journal of Coal Geology, v. 186, p. 155–164.

Dai, S., Graham, I.T. and Ward, C.R. (2016): A review of anomalous rare earth elements and yttrium in coal; International Journal of Coal Geology, v. 159, p. 82–95.

Dai, S., Xie, P., Jia, S., Ward, C.R., Hower, J.C., Xiaoyun, Y. and French, D. (2017): Enrichment of U-Re-V-Cr-Se and rare earth elements in the Late Permian coals of the Moxinpo coalfield, Chongqing, China: genetic implications from geochemical and mineralogical data; Ore Geology Reviews, v. 80, p. 1–17.

Deloitte Sustainability, British Geological Survey, Bureau de Recherches Géologiques et Minières and Netherlands Organisation for Applied Scientific Research (2017): Study on review of the list of critical raw materials; European Commission, 92 p., URL <https://publications.europa.eu/en/publication-detail/-/publication/08fdab5f-9766-11e7-b92d-01aa75ed71a1/language-en> [September 2017].

Finkelman, R.B. (1981): Modes of occurrence of trace elements in coal; U.S. Geological Survey, Open File Report 81-99, 301 p., URL <https://pubs.usgs.gov/of/1981/0099/report.pdf> [September 2017].

Goodarzi, F. (1988): Elemental distribution in coal seams at the Fording coal mine, British Columbia, Canada; Chemical Geology, v. 68, issue 1–2, p. 129–154, URL <https://doi.org/10.1016/0009-2541(88)90092-7>.

Goodarzi, N.N., Goodarzi, F., Grieve, D.A., Sanei, H. and Gentzis, T. (2009): Geochemistry of coals from the Elk Valley coalfield, British Columbia, Canada; International Journal of Coal Geology, v. 77, p. 246–259.

Goodenough, K.M., Wall, F. and Merriman, D. (2018): The rare earth elements: demand, global resources, and challenges for resourcing future generations; Natural Resources Research, v. 27, p. 201–216.

Grieve, D.A. (1993): Geology and rank distribution of the Elk Valley coalfield, southeastern BC (82G/15, 82J/2, 6, 7, 10, 11); BC Ministry of Energy, Mines and Low Carbon Innovation, Bulletin 82, 188 p., URL <http://cmscontent.nrs.gov.bc.ca/geoscience/PublicationCatalogue/Bulletin/BCGS_B082.pdf> [September 2017].

Kuppusamy, V.K. and Holuszko, M.E. (2019): Characterization and extraction of rare-earth elements from East Kootenay coalfield samples, southeastern British Columbia; *in* Geoscience BC Summary of Activities 2018: Minerals and Mining, Geoscience BC, Report 2019-01, p. 33–44, URL <http://cdn.geosciencebc.com/pdf/SummaryofActivities2018/MM/Schol_SoA2018_MM_Kuppusamy.pdf> [October 2019].

Kuppusamy, V.K. and Holuszko, M.E. (2021): Development of rare-earth elements database for the East Kootenay coalfield of southeastern British Columbia (NTS 082G/10, 15) using field collected samples: preliminary results; *in* Geoscience BC Summary of Activities 2020: Minerals, Geoscience BC, Report 2021-01, p. 67–74, URL <http://www.geosciencebc.com/i/pdf/SummaryofActivities2020/Minerals/Project%202018-002_MineralsSOA2020.pdf> [October 2021].

Moldoveanu, G. and Papangelakis, V. (2013): Recovery of rare earth elements adsorbed on clay minerals: II. leaching with ammonium sulfate; Hydrometallurgy, v. 131, p. 158–166.

National Resources Canada (2020): Canada's critical minerals list; Natural Resources Canada, 1 p., URL <https://www.nrcan.gc.ca/sites/nrcan/files/mineralsmetals/pdf/Critical_Minerals_List_2021-EN.pdf> [September 2021].

Seredin, V.V. (2004): Metalliferous coals: formation conditions and outlooks for development; Coal Resources of Russia, v. 6, p. 452–519.

Seredin, V.V. and Dai, S. (2012): Coal deposits as potential alternative sources for lanthanides and yttrium; International Journal of Coal Geology, v. 94, p. 67–93.

U.S. Department of Energy (2010): Critical materials strategy; U.S. Department of Energy, 165 p., URL <https://www.energy.gov/sites/prod/files/edg/news/documents/criticalmaterialsstrategy.pdf> [November 2021].

U.S. Department of Energy (2016): Rare earth elements program; U.S. Department of Energy, National Energy Technology Laboratory, 19 p., URL <https://www.netl.doe.gov/File Library/Research/Coal/Rare Earth Elements/REE-Project-Portfolio-2016.pdf> [September 2017].

U.S. Geological Survey (2021): Rare earth statistics and information; U.S. Geological Survey, URL <https://www.usgs.gov/centers/nmic/rare-earths-statistics-and-information> [September 2021].

Zhang, W., Rezaee, M., Bhagavatula, A., Li, Y., Groppo, J. and Honaker, R. (2015): A review of the occurrence and promising recovery methods of rare earth elements from coal and coal by-products; International Journal of Coal Preparation and Utilization, v. 35, p. 295–330.

Microbial Sensing of Sulphide Mineralization, Southern British Columbia and Vancouver Island (NTS 092F/14, 092I/06, 093A/06)

B.P. Iulianella Phillips[1], Department of Earth, Ocean, and Atmospheric Sciences, The University of British Columbia, Vancouver, British Columbia, bphillips@eoas.ubc.ca

R.L. Simister, Department of Microbiology and Immunology, The University of British Columbia, Vancouver, British Columbia

P.M. Luck, Department of Earth, Ocean, and Atmospheric Sciences, The University of British Columbia and Galore Creek Mining Corporation, Vancouver, British Columbia

C.J.R. Hart, (formerly) Department of Earth, Ocean, and Atmospheric Sciences, The University of British Columbia, Vancouver, British Columbia

S.A. Crowe, Departments of Earth, Ocean, and Atmospheric Sciences, and Microbiology and Immunology, The University of British Columbia, Vancouver, British Columbia

Iulianella Phillips, B.P., Simister, R.L., Luck, P.M., Hart, C.J.R. and Crowe, S.A. (2022): Microbial sensing of sulphide mineralization, southern British Columbia and Vancouver Island (NTS 092F/14, 092I/06, 093A/06); *in* Geoscience BC Summary of Activities 2021: Minerals, Geoscience BC, Report 2022-01, p. 45–52.

Introduction

Mineral exploration in Canada is becoming increasingly difficult because the majority of deposits exposed at the surface have already been discovered, leaving undiscovered commodities buried beneath appreciable glacial overburden and/or bedrock. The effectiveness of many existing exploration tools is diminished and therefore the development of innovative exploration approaches is vital for continued success in the discovery of new resources (Winterburn, 2017). One such technique, microbial-community fingerprinting, shows great potential when exploring for mineral targets that are hidden by thick (>2 m), complex and transported surficial materials. With continued development, it may transform how exploration is carried out for buried natural resources (Iulianella Phillips, 2020; Simister et al., 2020).

Micro-organisms kinetically enhance geochemical reactions, including the dissolution and formation of diverse minerals, and harness energy from these reactions to support their metabolism and growth in nearly every low-temperature geological setting (Newman and Banfield, 2002; Falkowski et al., 2008). They are acutely sensitive, often responding rapidly to the dynamics of chemical and physical properties in their surrounding environments. Subtle changes in mineral bioavailability, for example, can be reflected in dramatic shifts in the composition and activity of microbial communities (Reith and Rogers, 2008; Wakelin et al., 2012; Leslie et al., 2014; Fierer, 2017). Analyses of microbial-community composition and structure thus have a strong potential to resolve chemical and physical differences between environments that are not readily discernible through conventional geochemical and geophysical surveys.

The advent of high-throughput sequencing platforms over the last decade has transformed the capacity to interrogate complex microbial communities across a wide range of environmental matrices (Binladen et al., 2007; Zhou et al., 2015). The application of these technologies enables high-throughput profiling of the taxonomic compositions and metabolic potential of soil-microbial communities across defined survey areas. Given that every individual soil sample contains thousands of microbial taxa, each containing hundreds to thousands of genes sensing and interacting with the surrounding soil environment (Fierer, 2017), the statistical power of this approach to identify anomalies is unprecedented.

Rationale for Microbial-Community Fingerprinting

Two British Columbia (BC) porphyry-copper deposits, the Highland Valley Highmont South Cu-Mo deposit (HVC) of Teck Resources Ltd. (NTS 092I/06) and the Consolidated Woodjam Copper Corp. Deerhorn Cu-Au deposit (NTS 093A/06), were used to evaluate microbiological techniques for sulphide exploration in BC (Figure 1). B-horizon soil samples were analyzed for inorganic geochemistry (aqua-regia digestion with inductively coupled plasma–mass spectrometry [ICP-MS] finish) and microbial DNA

[1]*The lead author is a 2021 Geoscience BC Scholarship recipient.*

This publication is also available, free of charge, as colour digital files in Adobe Acrobat® PDF format from the Geoscience BC website: http://geosciencebc.com/updates/summary-of-activities/.

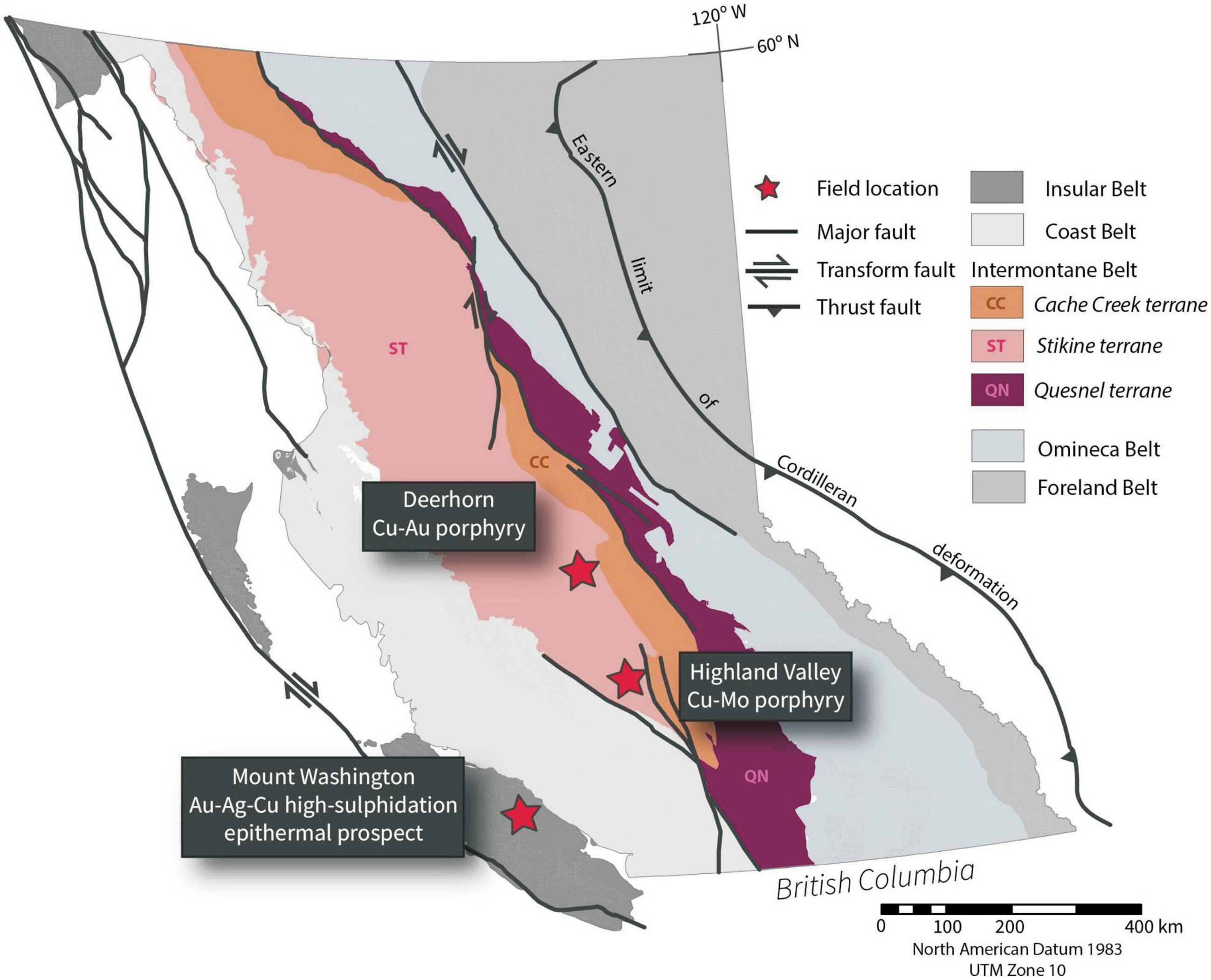

Figure 1. Locations of porphyry-Cu research sites (Highland Valley Highmont South Cu-Mo deposit and Deerhorn Cu-Au deposit) and the Mount Washington high-sulphidation Au-Ag-Cu epithermal prospect. Thick black lines indicate major faults. Terranes and geological belts are characterized based on bedrock mapping carried out by the British Columbia Geological Survey (BCGS; Cui et al., 2017).

sequencing (16S rRNA marker gene; Iulianella Phillips, 2020; Simister et al., 2020). In both cases, mineralization is covered by transported glacial overburden (2–10 m at HVC and 25–60 m at Deerhorn), with compositional variation in surface materials (e.g., till blanket, organic deposits, glaciolacustrine sediments; Iulianella Phillips, 2020).

The authors have shown that microbial-community fingerprinting can detect anomalies in bacterial populations in the surface environment that correlate with the surface projection of sulphide mineralization (Iulianella Phillips, 2020; Simister et al., 2020). Deposit-scale investigations of HVC and Deerhorn revealed suites of micro-organisms that have statistically significant (p <0.05) shifts in relative abundance occurring directly above the surface projection of mineralization (0.1% Cu equivalent and 0.2% Au equivalent at HVC and Deerhorn, respectively; Figures 2, 3). Specifically, microbial anomalies at Deerhorn discriminate mineralization at the surface where no detectable geochemical signal has been generated (Figure 3). These results signify the efficacy of using modern DNA sequencing to elucidate buried mineralization and provide the support for further investigations into the use of microbial communities to sense chemical and physical changes in their environment, with respect to mineralization.

Mount Washington Au-Ag-Cu Epithermal System

In October 2018, the Mount Washington high-sulphidation, epithermal Au-Ag-Cu prospect (NTS 092F/14) was sampled for microbial-community fingerprinting and inorganic and organic soil geochemistry. The Mount Washington prospect is located on Vancouver Island (Figure 1). The area is underlain by the Mesozoic Karmutsen Group basalts and hosted in the Nanaimo Group sedimentary rocks and intrusive rocks of the Paleogene Mount Washington Plutonic Suite. Several north- and northwest-trending

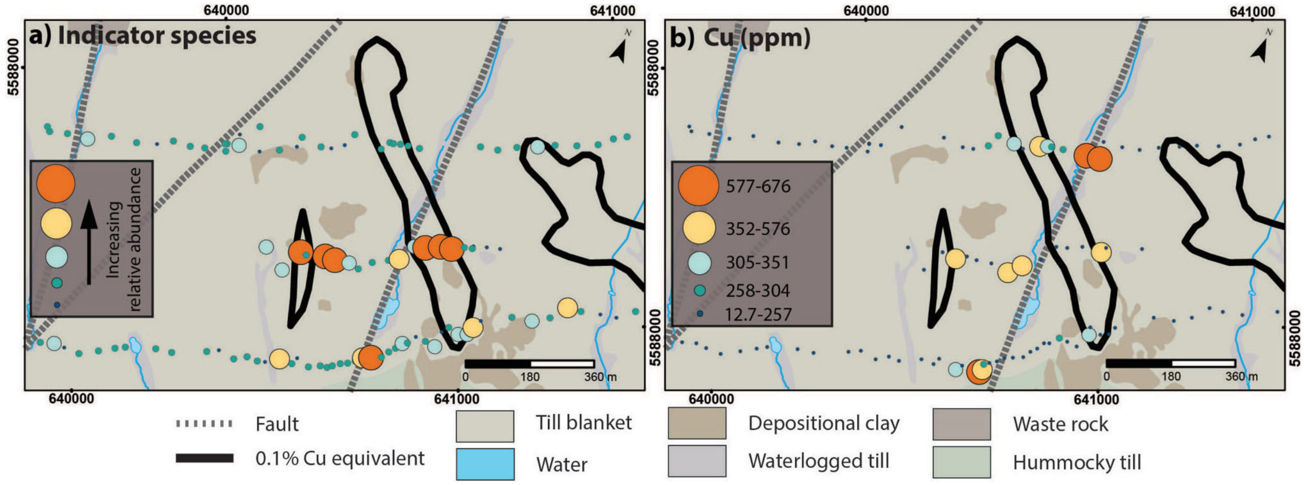

Figure 2. Example of an indicator micro-organism **(a)** and the Cu-anomaly map of the same area **(b)** from the Highland Valley Highmont South Cu-Mo deposit. Geochemical data derived from aqua-regia digestion of B-horizon soils with ICP-MS finish. Microbiological data derived from 16S rRNA gene DNA sequencing. Co-ordinates in UTM Zone 10, NAD 83.

extensional faults crosscut the area and appear to localize mineralization (Muller, 1989; Massey et al., 2005; Figure 4b). Mineralization is characterized by polymetallic sulphide minerals in a breccia zone and the Domineer vein, which together make up the Lakeview-Domineer resource (Houle, 2013). Surficial materials are dominated by colluvium, glacial till and organic deposits (Figure 4a), with the direction of ice flow at 058° (Fyles, 1960).

The survey was carried out in conjunction with a hydrocarbon survey (Luck, 2021) and comprised five survey lines with a total of 64 samples taken at 50 m spacing perpendicular to the strike of the mineralized breccia (Figure 4b). Soils for microbial-community analysis were sampled with sterilized equipment and without field screening to preserve the microbial community as much as possible. Descriptions were documented for in situ physicochemical

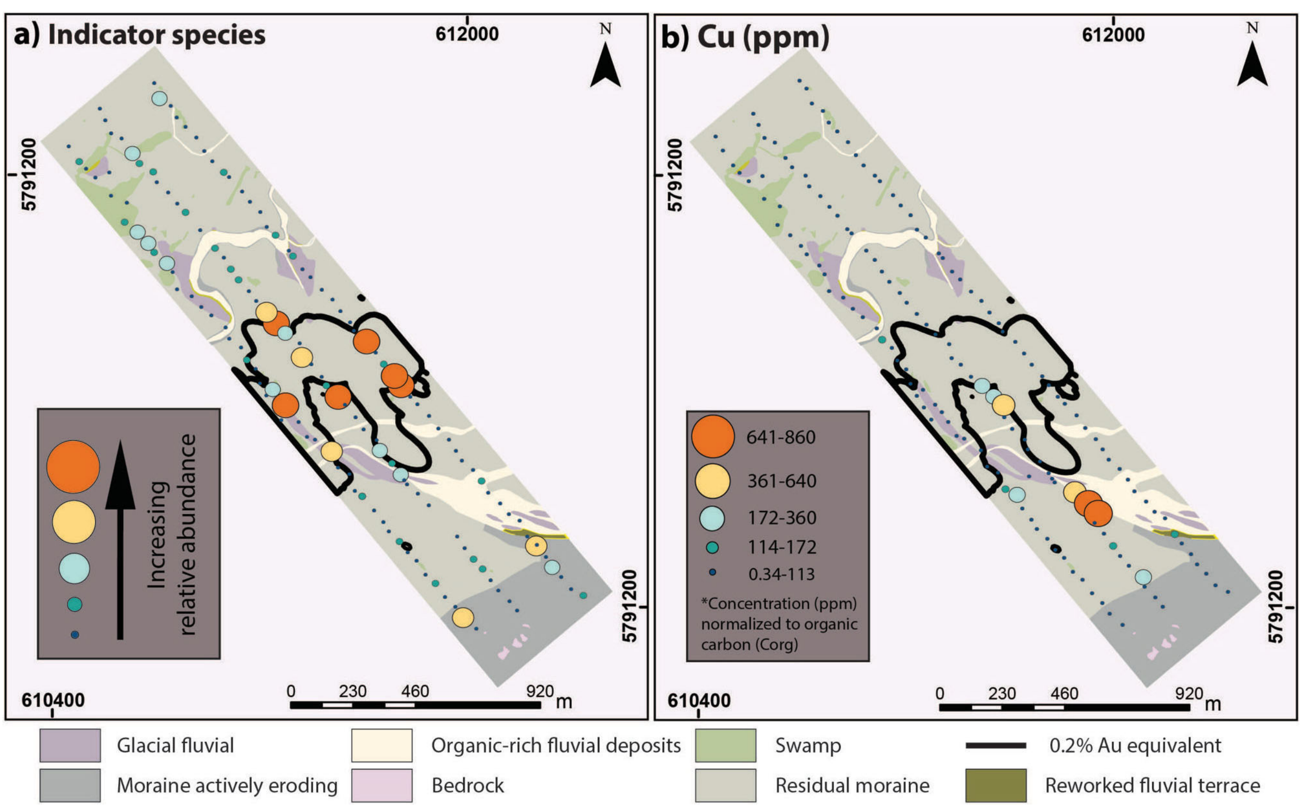

Figure 3. Example of an indicator micro-organism **(a)** and the Cu-anomaly map (normalized to organic carbon) of the same area **(b)** from the Deerhorn Cu-Au deposit. Geochemical data derived from aqua-regia digestion of B-horizon soils with ICP-MS finish. Microbiological data derived from 16S rRNA gene DNA sequencing. Co-ordinates in UTM Zone 10, NAD 83.

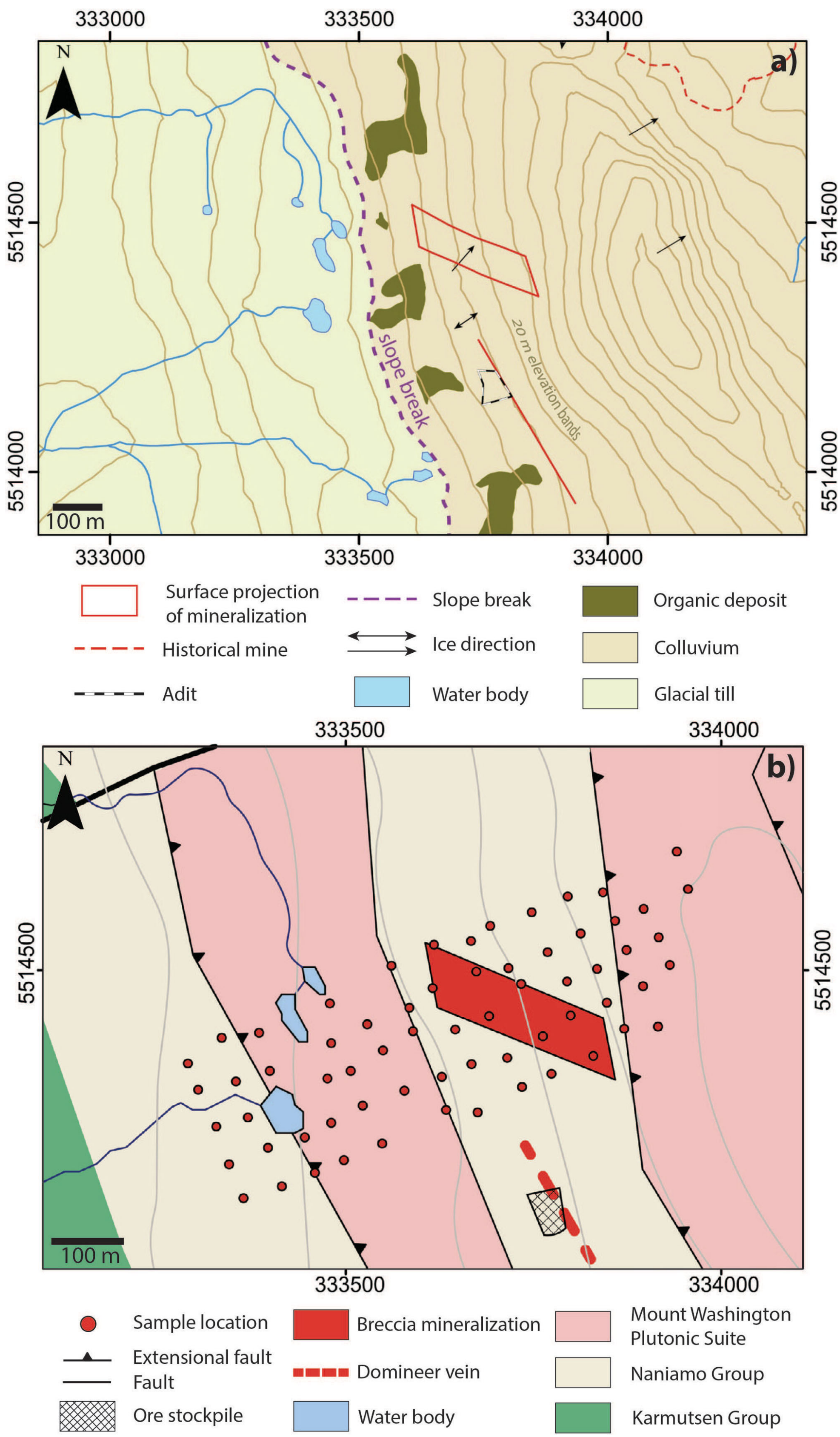

Figure 4. Mount Washington prospect **a)** surficial materials with field-survey transects (Luck, 2021), and **b)** bedrock geology (Luck, 2021; after Muller [1989] and Massey et al. [2005]). Mineralization denoted on both maps from McDougall (1987), Houle (2014) and Heberlein and Dunn (2017).

variables at each sample site for every observed soil horizon in the profile. The B-horizon soils were targeted for microbial-soil samples, although multiple horizons (including O, Ah, Ae and C) were taken where possible. Soil samples were also collected for geochemical analysis. Field measurements consisted of slurry tests for pH and oxidation-reduction potential (ORP) after field sieving through a 6 mm screen. Geochemical samples for each site were sent to ALS Chemex (Vancouver, BC) for fire assay and four-acid digestion, and subsequent analysis by ICP-MS (results can be found in Luck, 2021). The microbial samples were frozen at –4ºC upon return to the laboratory at The University of British Columbia (UBC) prior to DNA extraction. A subset of the Mount Washington microbial samples has been preserved to perform a cell-count analysis. A small amount of each soil sample was transferred with aseptic instruments into smaller vials containing an RNA preservative.

DNA extractions have been carried out for the Mount Washington soil samples and results are pending. Once data are received, they will be investigated for microbiological anomalies associated with the epithermal mineralization. Results from Mount Washington will be the first step in incorporating high-sulphidation, epithermal-style mineral systems into the project databases of indicator micro-organisms for use in future mineral exploration.

Bog Wetlands

A substantial challenge in the mineral-exploration industry is the lack of geochemical methodologies when exploring in saturated surficial environments (i.e., bog wetlands). The surface can be inconsistent in these environments, and traditional acid-digestion methods coupled with ICP-MS are not always possible because the dominant surface materials are composed of waterlogged organic matter. High degrees of saturation change the oxidation-reduction potential (ORP) of the local environment, thus exerting a control on the mobility of Eh-sensitive elements (e.g., Fe, Mn, S) that may obscure geochemical signals derived from subsurface mineralization. Furthermore, a high abundance of organic matter in soils may attenuate indicator and/or pathfinder elements (e.g., Mo) and generate false anomalies. One of the very few techniques marketed for application in these environments is the Spatiotemporal Geochemical Hydrocarbons (SGH) analysis of Activation Laboratories Ltd. However, a drawback to this technique is that the compound class or compound concentrations themselves are not released to the client, so the interpreted anomaly heat map is the only data product provided. Clearly, new tools are required to meet industry demand when exploring in complex low-relief and saturated terrains.

Bog wetlands also provide a unique opportunity to study the feedback relationships between land/soil type and microbial communities. Not only does this generate knowledge about microbial-community composition and function in saturated surface environments to support microbial-community fingerprinting as an exploration tool, but it informs the role micro-organisms play in biogeochemical cycling and the fate of carbon in the environment. Peatlands are extremely important carbon sinks globally (Dise, 2009). With changing temperatures, the investigation into microbial-community controls on carbon cycling of greenhouse gases such as CO_2 and CH_4 in these environments is vital (Belyea et al., 2008; Limpens et al., 2008; Dise, 2009).

Burns bog, located in Delta, BC, is a field location for studying microbial communities: their composition, structure and function across different land types (Figure 5). It is a raised-bog ecosystem with acidic, nutrient-poor waters and maintains a reducing environment due to its low oxygenation (Hebda et al., 2000). Plans are being made to sample across different land types in the bog along saturation gradients; characterize the composition of soil-microbial communities and its functional potential; and measure rates of microbial population turnover. The accessibility of Burns Bog also provides seasonal opportunities for sampling should it become relevant. Outcomes from these efforts may inform the applicability of microbial-community fingerprinting in saturated surface materials and shed light on the functional relationship between micro-organisms and peatland carbon storage.

Soil Preservation

Little is known about the stability of soil-microbial communities during transport and prolonged storage. It is widely accepted that soils should be frozen as soon as possible post sampling to preserve DNA (Delavaux et al., 2020). However, it is unknown how fluctuations in temperature and moisture over reasonable transport and storage time scales impact the preservation of soil-microbial communities, specifically in the microbial anomalies generated above mineral deposits and the relative abundance of indicator micro-organisms. To test this, a soil-preservation experiment has been designed that utilizes readily accessible soil material.

The UBC Totem Plant Science Field Station provides an excellent on-campus soil environment to conduct, and collect materials, for soil-related experiments. A bulk soil from the field station was sampled and the initial microbial-community composition characterized with 16S sequencing (Figure 6). The current phase of the experiment involves exposing the soil (within Poly Ore sample bags) to a range of temperature and moisture perturbations. These perturbations include freezing samples at –20°C, leaving samples at room temperature, and allowing the samples to dry out. The soil-microbial communities will be assessed at weeks- to

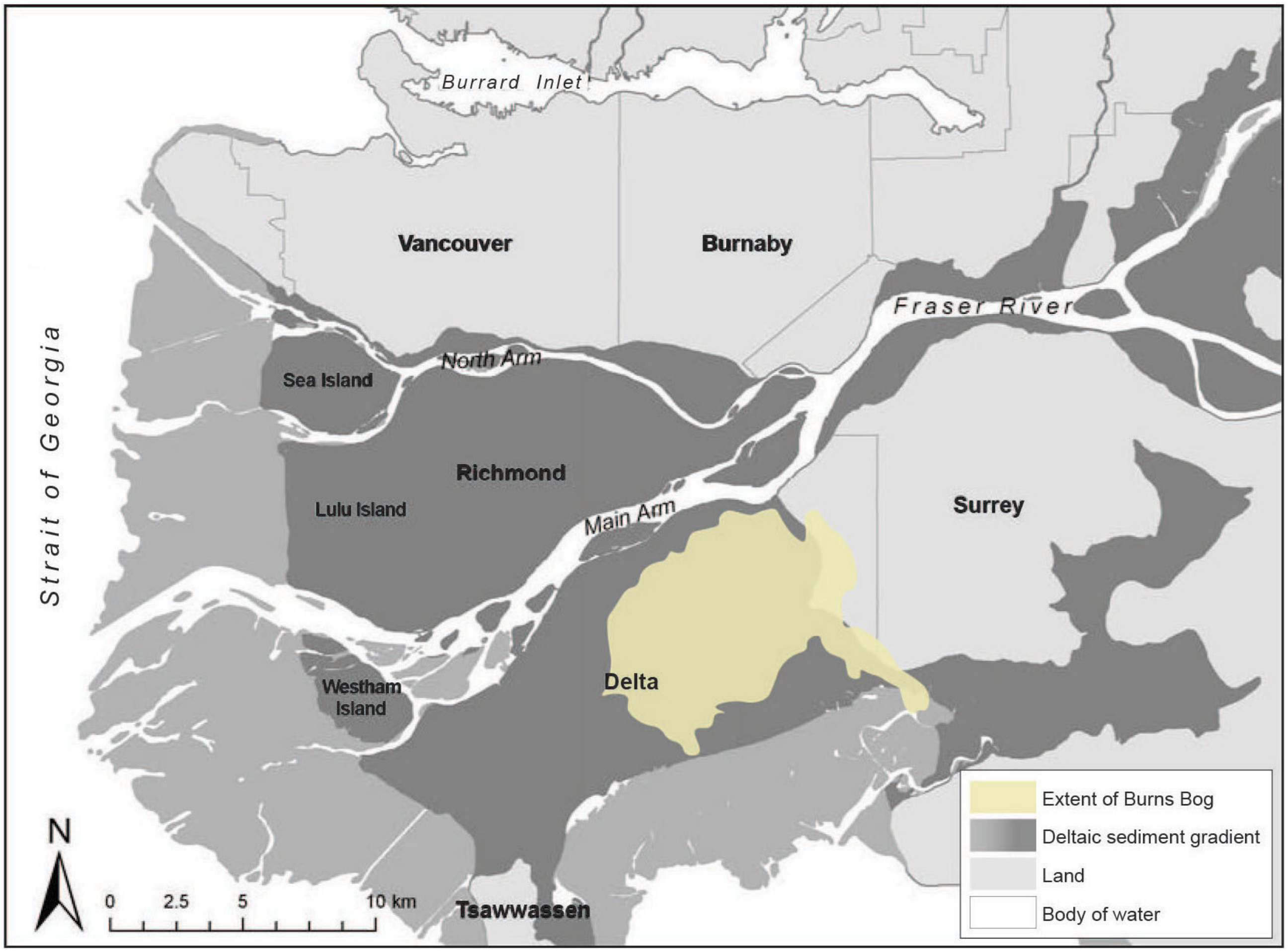

Figure 5. Burns Bog location (indicated by yellow shading) in the context of the Metro Vancouver deltaic system. Modified after Clague (1998).

months-long time intervals for at least one year and sampled in triplicate to examine the effects of temperature and moisture fluctuations on the microbial-community composition, diversity, structure and metabolic activity. This experiment will inform the development of robust sampling protocols for the mineral-exploration industry and serve as a laboratory test of the relationships between warming and drying soil conditions and microbial populations.

Conclusions

Outcomes from these deposit-scale orientation studies have highlighted the potential for geomicrobiological tools and techniques for successful application to through-cover mineral exploration. Current research directions focus specifically on reducing fundamental unknowns about the behaviour and variation of microbial communities in response to chemical and physical changes in the environment. This focus includes assessing DNA sequencing and microbial-community fingerprinting in a colluvium-dominated, Au-Ag-Cu, high-sulphidation, epithermal mineral system; exploring the relationships between micro-organism function and variation in land type; and assessing the impact of transport and storage on the persistence of microbial-community anomalies in soils. Each of these activities serves on a different level to support the use of microbiology-based mineral exploration in different mineral systems, in various terrains and climates, and to develop practical and informed transport and storage protocols for use by industry.

Acknowledgments

This research is derived from the Exploration Geochemistry Initiative at the Mineral Deposit Research Unit run by the late Dr. Peter Winterburn, and the Crowe Lab at The University of British Columbia. The author thanks the funding partners for the initial stages of this research, Natural Sciences and Engineering Research Council, Bureau Veritas and Geoscience BC, as well as the Northwest Territories Geological Survey for their ongoing support. Field sampling for this work would not have been possible without the efforts of R. Chouinard (Highland Valley), S. Rich (Deerhorn), and P.M. Luck, A.P. Wickham, R.C. Shaw and R.L. Simister (Mount Washington). Credit is also given to

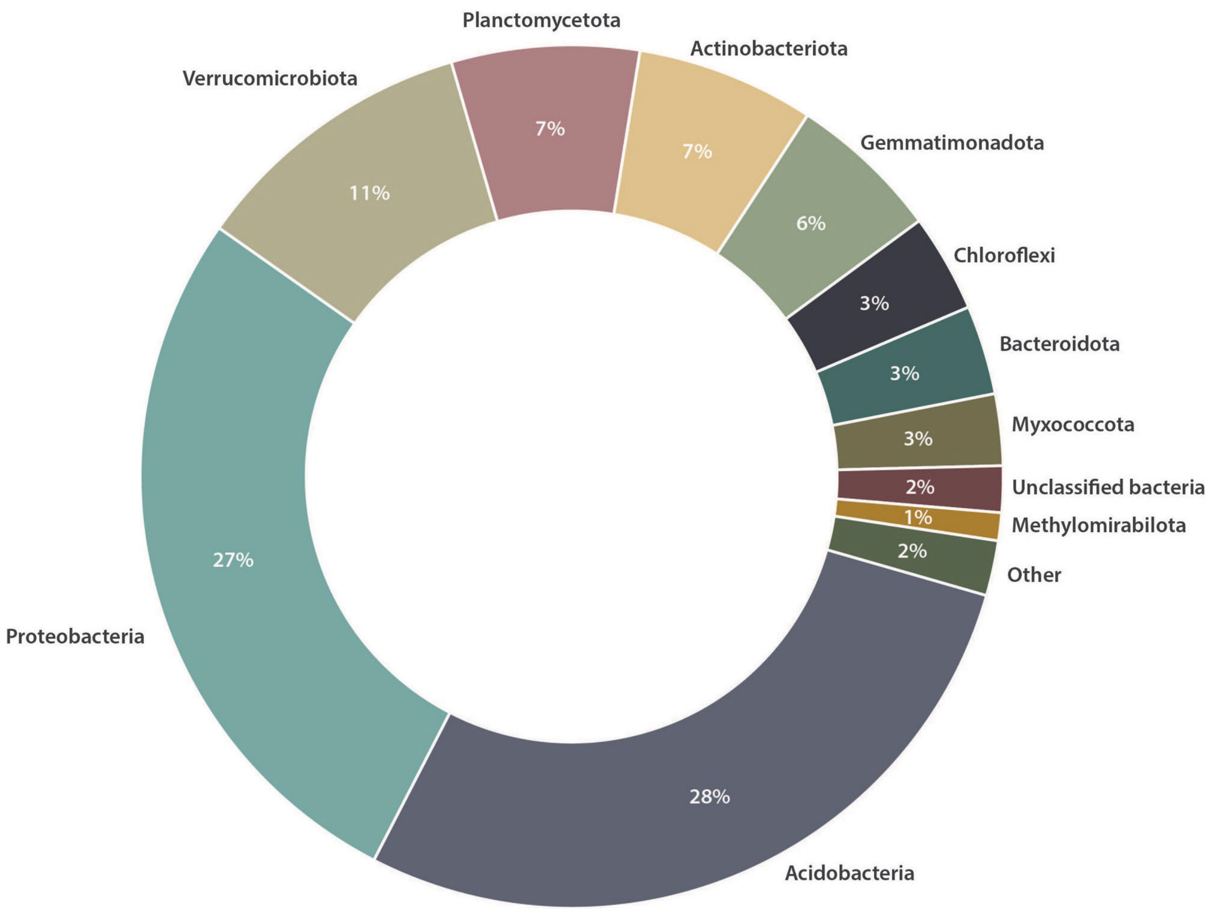

Figure 6. Phyla-level microbial-community composition of the initial soil derived from the UBC Totem Plant Science Research Station, expressed as the distribution of 16S rRNA reads per phylum. The number of reads per phylum is calculated as a percentage of the total reads for the sample. 'Other' is the sum of any phyla with less than 1% representation.

M. Friend for improving earlier versions of this manuscript.

References

Belyea, L.R. and Malmer, N. (2008): Carbon sequestration in peatland: patterns and mechanisms of response to climate change; Global Change Biology, v. 10, no. 7, p. 1043–1052, URL <https://onlinelibrary.wiley.com/doi/10.1111/j.1529-8817.2003.00783.x> [October 2021].

Binladen, J., Gilbert, M.T.P., Bollback, J.P., Panitz, F., Bendixen, C., Nielsen, R. and Willerslev, E. (2007): The use of coded PCR primers enables high-throughput sequencing of multiple homolog amplification products by 454 parallel sequencing; PLoS ONE, v. 2, no. 2, p. 1–9, URL <https://journals.plos.org/plosone/article?id=10.1371/journal.pone.0000197> [October 2021].

Clague, J.J. (1998): Geological setting of the Fraser River delta; *in* Geology and Natural Hazards of the Fraser River Delta, British Columbia, J.J. Clague, J.L. Luternauer and D.C. Mosher (ed.), Geological Survey of Canada, Bulletin 525, p. 7–16, URL <https://geoscan.nrcan.gc.ca/starweb/geoscan/servlet.starweb?path=geoscan/fulle.web&search1=R=210033> [October 2021].

Cui, Y., Miller, D., Schiarizza, P. and Diakow, L. (2017): British Columbia digital geology; British Columbia Ministry of Energy, Mines, and Low Carbon Innovation, British Columbia Geological Survey, Open File 2017-8, 9 p., URL <https://www2.gov.bc.ca/gov/content/industry/mineral-exploration-mining/british-columbia-geological-survey/geology/bcdigitalgeology> [October 2021].

Delavaux, C.S., Dever, J.D., Karppinin, E.M. and Bainard, L.D. (2020): Keeping it cool: soil sample cold pack storage and DNA shipment up to 1 month does not impact metabarcoding results; Ecology and Evolution, v. 10, p. 4652–4664, URL <https://onlinelibrary.wiley.com/doi/full/10.1002/ece3.6219> [October 2021].

Dise, N.B. (2009): Peatland response to global change; Science, v. 326, p. 810–811, URL <https://www.science.org/doi/full/10.1126/science.1174268> [October 2021].

Falkowski, P.G., Fenchel, T. and Delong, E.F. (2008): The microbial engines that drive Earth's biogeochemical cycles; Science, v. 320, p. 1034–1040, URL <https://www.science.org/doi/10.1126/science.1153213> [October 2021].

Fierer, N. (2017): Embracing the unknown: disentangling the complexities of the soil microbiome; Nature Reviews Microbiology, v. 15, no. 10, p. 579–590, URL <https://www.nature.com/articles/nrmicro.2017.87> [October 2021].

Fyles, J.G. (1960): Surficial geology, Oyster River, Comox, Nanaimo and Sayward districts, British Columbia; Geological Survey of Canada, Preliminary Map 49-1959, URL <https://

geoscan.nrcan.gc.ca/starweb/geoscan/servlet.starweb?path=geoscan/fulle.web&search1=R=108639> [October 2021].

Hebda, R.J., Gustavson, K., Golinski, K. and Calder, A.M. (2000): Burns Bog ecosystem review synthesis report for Burns Bog, Fraser River delta, south-western British Columbia, Canada; Environmental Assessment Office, Victoria, BC, URL <https://www.osti.gov/etdeweb/biblio/20205111> [October 2021].

Heberlein, D.R. and Dunn, C.E. (2017): Halogens and other volatile compounds in surface sample media as indicators of mineralization, part 2: Mount Washington epithermal Au-Cu-Ag prospect, Vancouver Island, BC (NTS 092F/14); *in* Geoscience BC Summary of Activities 2016, Geoscience BC, Report 2017-1, p. 151–158, URL <http://www.geosciencebc.com/i/pdf/SummaryofActivities2016/SoA2016_Heberlein-MtWashington.pdf> [October 2021].

Houle, J. (2013): Geochemical and prospecting technical assessment report on the Mount Washington property for North Bay Resources Inc., Nanaimo Mining Division, BC; BC Ministry of Energy, Mines and Low Carbon Innovation, Assessment Report 34200, 206 p., URL <https://aris.empr.gov.bc.ca/ArisReports/34200.PDF> [October 2021].

Houle, J. (2014): NI 43-101 technical report on the Mount Washington property, Vancouver Island, British Columbia; NI 43-101 technical report prepared for North Bay Resources Inc., 92 p., URL <http://www.northbayresources.com/2014mw43101.pdf> [November 2021].

Iulianella Phillips, B.P. (2020): Microorganisms as sensors for concealed mineral deposits: application and development of microbiological mineral exploration in the Northwest Territories and British Columbia, Canada; M.Sc. thesis, The University of British Columbia, 211 p., URL <https://open.library.ubc.ca/soa/cIRcle/collections/ubctheses/24/items/1.0390297> [October 2021].

Leslie, K., Oates, C.J., Kyser, K.T. and Fowle, D. A. (2014): Biogeochemical controls on metal mobility: modeling a Cu-Zn VMS deposit in column flow-through studies; Geochemistry: Exploration, Environment, Analysis, v. 14, p. 59–70, URL <https://geea.lyellcollection.org/content/14/1/59/tab-figures-data> [October 2021].

Limpens, J., Berendse, F., Bloudau, C., Canadell, J.G., Freeman, C., Holden, J., Roulet, N., Rydin, H. and Schaepman-Strub, G. (2008): Peatlands and the carbon cycle: from local processes to global implications – a synthesis; Biogeosciences, v. 5, p. 1475–1491, URL <https://bg.copernicus.org/articles/5/1475/2008/> [October 2021].

Luck, P. (2021): Hydrocarbons in soil as pathfinders for base and precious metal exploration: an orientation study at the Mt. Washington epithermal Au-Ag-Cu prospect, British Columbia, Canada; M.Sc. thesis, The University of British Columbia, 271 p., URL <https://open.library.ubc.ca/soa/cIRcle/collections/ubctheses/24/items/1.0397404> [October 2021].

Massey, N.W.D., MacIntyre, D.G., Desjardins, P.J. and Cooney, R.T. (2005): Geology of British Columbia; BC Ministry of Energy, Mines and Low Carbon Innovation, Geoscience Map 2005-3, (3 sheets), scale 1:1 000 000, URL <https://www2.gov.bc.ca/gov/content/industry/mineral-exploration-mining/british-columbia-geological-survey/geology/bcdigitalgeology> [October 2021].

McDougall, J.J. (1987): Summary report on the Mt. Washington gold property; Better Resources Limited, February 1987.

Muller, J.E. (1989): Tertiary low angle faulting and related gold and copper mineralization on Mount Washington, Vancouver Island (92F/11, 14); *in* Geological Fieldwork 1988, BC Ministry of Energy, Mines and Low Carbon Innovation, BC Geological Survey, Paper 1989-1, p. 81–91, URL <https://www.semanticscholar.org/paper/TERTIARY-LOW-ANGLE-FAULTING-AND-RELATED-GOLD-AND-ON-Muller/53774dc7d9230f510d8e9e33b91e3800ad47c975?p2df> [October 2021].

Newman, D.K. and Banfield, J.F. (2002): Geomicrobiology: how molecular-scale interactions underpin biogeochemical systems; Science, v. 296, no. 5570, p. 1071–1077, URL <https://www.science.org/doi/abs/10.1126/science.1010716?keytype2=tf_ipsecsha&ijkey=3b7fbf439b72ef152968ec5b99e05a350dd73007> [October 2021].

Reith, F. and Rogers, S.L. (2008): Assessment of bacterial communities in auriferous and non-auriferous soils using genetic and functional fingerprinting; Geomicrobiology Journal, v. 25, no. 34, p. 203–215, URL <https://www.tandfonline.com/doi/abs/10.1080/01490450802081846> [October 2021].

Simister, R.L., Iulianella Phillips, B.P., Winterburn, P.A. and Crowe, S.A. (2020): Microbial-community fingerprints as indicators for buried mineralization, Geoscience BC Report 2020-03 and MDRU Publication 446, 31 p., URL <http://www.geosciencebc.com/i/project_data/GBC%20Report2020-03/GBC%20Report%202020-03%20Microbial-Community%20Fingerprints%20as%20Indicators%20for%20Buried%20Mineralization%20in%20British%20Columbia_revised_BIP.pdf> [October 2021].

Wakelin, S., Anand, R.R., Macfarlane, C., Reith, F., Noble, R. and Rogers, S. (2012): Assessing microbiological surface expression over an overburden-covered VMS deposit; Journal of Geochemical Exploration, v. 112, p. 262–271, URL <https://www.sciencedirect.com/science/article/abs/pii/S0375674211001853?via%3Dihub> [October 2021].

Winterburn, P., Noble, R. and Lawie, D. (2017): Advances in exploration geochemistry, 2007 to 2017 and beyond; Geochemistry: Exploration, Environment, Analysis, v. 20, p. 157–166, URL <https://www.mdru.ubc.ca/wp-content/uploads/2019/01/WinterburnExplore17.34.pdf> [October 2021].

Zhou, J., He, Z., Yang, Y., Deng, Y., Tringe, S. and Alvarez-Cohen, L. (2015): High-throughput metagenomic technologies for complex microbial community analysis: open and closed formats; mBio, v. 6, no. 1, p. 106–113, URL <https://pubmed.ncbi.nlm.nih.gov/25626903/> [October 2021].

Using Traditional Indigenous Knowledge of Prescribed Burning as a Tool to Shift a Reclaimed Tailings Storage Facility in Southern British Columbia Dominated by Agronomic Grass to a Native Plant Community

B.J. Williams[1], Department of Natural Resource Sciences, Thompson Rivers University, Kamloops, British Columbia, brandonwilliams@protonmail.com

W.C. Gardner, Department of Natural Resource Sciences, Thompson Rivers University, Kamloops, British Columbia

C.W. Mason, Department of Natural Resource Sciences and Department of Tourism Management, Thompson Rivers University, Kamloops, British Columbia

L.H. Fraser, Department of Natural Resource Sciences, Thompson Rivers University, Kamloops, British Columbia

Williams, B.J., Gardner, W.C., Mason, C.W. and Fraser, L.H. (2022): Using traditional Indigenous knowledge of prescribed burning as a tool to shift a reclaimed tailings storage facility in southern British Columbia dominated by agronomic grass to a native plant community; *in* Geoscience BC Summary of Activities 2021: Minerals, Geoscience BC, Report 2022-01, p. 53–66.

Introduction

With a growing global population and increasing consumption, urbanization and industrial expansion, maintaining healthy ecosystems that support access to tangible and intangible assets is a major challenge. As the use of land to yield materials for processing and creating goods and services represents some of the most substantial changes to Earth's ecosystems, we must properly manage both our impacted and natural landscapes to ensure a positive net balance is maintained with respect to ecosystem function (Vitousek et al., 1997). Additionally, a growing public demand for both socially responsible and ecologically viable industrial practices has forced industries to respond with advancing sustainable practices in their operations (Fonseca et al., 2014). Historically, Canadian mining operations often resulted in some combination of environmental degradation, Indigenous community disruption, and displacement of Indigenous peoples from traditional lands (Melosi, 2017). This was due to a lack of industry policy, regulation, and checks and balances with respect to restorative or reclamation practices, combined with little forethought given to the impact occurring to ecosystem services, human livelihoods and health (Virgone et al., 2018).

Because of this legacy, there currently exists a vast heritage of degraded lands and displaced communities from historical mining efforts that require restoration, reclamation and reconciliation (Bradshaw, 1997). Restoration and reclamation research has emerged within the last two decades as a relatively new scientific discipline to address and counteract the issues of worldwide loss of biodiversity and ecosystem services (Hölzel et al., 2012). Additionally, as mining industries faced significant amounts of scrutiny with respect to land use management, sustainability issues and other adverse socio-environmental issues, this stimulated a response from industry to place components like sustainability reporting, and social and environmental assessments at the forefront of operations, to prove due diligence is being met in order to secure a social licence to operate (Azapagic, 2004; Melosi, 2017; Virgone et al., 2018). Today, beyond addressing environmental impacts, reclamation and restoration efforts within the industry have begun to encapsulate building and maintaining strong, resilient and beneficial relationships with Indigenous peoples and local communities to reconcile past inequities. The gold standard moving forward for industries should be to move beyond a 'social licence to operate' and into dynamic, trusted and mutual management of the landscape with communities and rightful landowners.

The research presented in this paper is based on examination of a unique project partnership between management at Teck Resources Limited's (Teck) Highland Valley Copper (HVC) mine in the Thompson Okanagan Region of the southern interior of British Columbia (BC) and the Nlaka'pamux peoples, where part of the building of this relationship rests on the intent to collaborate on the goal of reclaiming and restoring ecosystem function and traditional land uses to a pre-mined landscape to the extent possible given the impacts the HVC mine has created. This work becomes especially important in reclaiming mined lands to more desirable native grasslands in a province where grass-

[1]The lead author is a 2020 Geoscience BC Scholarship recipient.

This publication is also available, free of charge, as colour digital files in Adobe Acrobat® PDF format from the Geoscience BC website: http://geosciencebc.com/updates/summary-of-activities/.

lands represent less than 1% of the total land base (Lee et al., 2014). This collaboration integrates and examines contemporary ecological theory with the traditional Indigenous knowledge of prescribed burning as a reclamation tool to enhance biodiversity and ecosystem reclamation, with the goal of reclaiming native grasslands on a tailings storage facility dominated by 25-year-old reclaimed, low diversity, agronomic species (Figure 1).

Figure 1. Landscape of the former site of Teck Resources Limited's Highmont tailings, Highland Valley Copper mine, in the Thompson Okanagan Region of the southern interior of British Columbia, is dominated by 25-year-old reclaimed vegetative cover crop represented by a monoculture of agronomic grass species.

Background and Theory

Traditional Ecological Knowledge, History of Indigenous Use of Fire and Changing Landscapes

The Thompson Okanagan Region comprises the traditional territory of numerous Indigenous peoples. The nations of particular interest with respect to the location of the HVC mine are the Nlaka'pamux (Thompson region) and Secwepemc (Shuswap region). The traditional territory of the Nlaka'pamux is centred around the Nicola valley, while farther north, encompassing the city of Kamloops and extending even farther north, is traditional Secwepemc territory (British Columbia Assembly of First Nations, 2021). For several thousand years the southern interior Indigenous peoples developed sustainable management practices that utilized what we understand today as fundamental ecological principles. For the Secwepemc and other Indigenous peoples, these practices are based on an intimate knowledge of their lived lands that facilitated a belief system that imposed social and spiritual sanctions on people who did not treat all living things sustainably and with respect. All interaction with the environment is grounded in respect for changing ecologies, and fine-tuning ways to sustainably harvest fish, plants and animals to ensure sustainable yield for the future (Turner et al., 2000; Ignace and Ignace, 2017). This type of natural resource management style and philosophy are becoming a focus of attention of many industries, professionals and researchers who seek ways to advocate for biodiversity and provide models for sustainable practices. Traditional ecological knowledge and wisdom has also received major recognition recently for being regarded as equivalent and complementary to western scientific knowledge, which has spurred western researchers into applying traditional ecological knowledge in various ways (Turner et al., 2000). Combining traditional ecological knowledge and western scientific knowledge to manage our landscapes can be used as a tool to help reconcile relationships and restore ecosystems.

The history of wildfire within BC presents a complicated and ever-changing path forward as we continue to modify our ecosystems and the way we manage our land. As the semi-arid grasslands of the interior receive typically less than 400 mm of rainfall on average, the low precipitation patterns paired with warm summer temperatures and moderate to high winds create a landscape that is naturally conducive to wildfire (Climatedata.ca, 2021). The most recent fire-regime study within the province places the southern interior of BC at a mixed-severity regime, with low-severity fires being most extensive and common (Heyerdahl et al., 2012). However, it is important to note that the semi-arid grasslands of BC present a prehistoric history of anthropogenic burning (called 'prescribed burning' from here on) by Indigenous peoples that ranges from roughly 7000 years before present (Blackstock and McAllister, 2004; Lewis et al., 2018) to shortly after European settlement in BC in the early 1900s, when prescribed burning by Indigenous communities was halted as European interest in the forest complex no longer permitted burning of any kind (Lewis et al., 2018).

The grasslands of BC, which now represent less than 1% of the provincial land base, provide habitat to over 30% of BC's threatened and endangered species, and is home to 42% of all vascular plant species that occur within the province (Wikeem and Wikeem, 2004). As the landscape of BC changes due to environmental and social factors, like the implementation of fire exclusion in the early 1900s, significant changes in the ecological and cultural conditions across the province have occurred and are readily visible upon inspection of our vulnerable grasslands ecosystems. Indigenous Elders from the Nlaka'pamux, Silx (Okanagan), Secwepemc, Stl'atl'imx (Lillooet) and Ts'ilquot'in (Chilcotin) nations from the interior of southern BC, have recalled and reminisced when "grasses were belly-high to a horse" and the grasslands were thriving (Blackstock and McAllister, 2004). Many bunchgrass biogeoclimatic zones that once naturally presented a high plant diversity to support ungulate species and foodstuffs for Indigenous communities have now been replaced with woody encroachment of sagebrush (*Artemisia tridentata*) and ponderosa pine (*Pinus ponderosa*) and these zones are at risk of shrinking in size and diversity (Fuhlendorf et al., 2008; Lewis et al., 2018). Cumulative effects of overgrazing by cattle and fire exclusion have strongly interacted to cause shifts in the plant community composition to be less productive and comprised of more ephemeral species. These changes also affect the habitat of grassland specialists and keystone species as these areas are slowly converted into shrublands and forests (Fuhlendorf et al., 2008; Symstad and Leis, 2017). Fire exclusion has also led to a shift in Indigenous community dynamics and the loss of important cultural use. Traditional prescribed burning, which was used to manage grasslands with ecological-based goals of selecting for desirable herbs and vegetation and maintaining important grazing habitat through managing woody encroachment, has now transitioned to understanding prescribed fire as a tool for fire safety only, within strict guidelines and only to be used when given government consent (Lewis et al., 2018). As the grasslands of BC have evolved naturally and anthropogenically in a fire-driven ecosystem, we must continue to push the boundaries of exploring how to move forward using traditional ecological knowledge to reclaim these shrinking landscapes.

Challenges in Reclaiming Mine Ecosystems and Disturbance Ecological Theory

In the pursuit to reclaim ecosystems within a mine setting there are many external factors that place limits on the reconstruction of a plant community. Restoration and reclamation following the mining process is both complex and challenging due to various biotic and abiotic factors (Turner et al., 2006; Gasch et al., 2014). One of the first steps in restoration or reclamation of these lands is typically revegetation. In addition to the semi-arid environment and climate conditions that exert the primary control on plant productivity and composition, many characteristics of mine wastes produce conditions unfavourable to successful vegetation establishment, notably the levels of residual heavy metals, low nutrient status, poor physical structure of soils, and extreme pH values (Tordoff et al., 2000; Sample and Barlow, 2013). The combination and interactive effects of unfavourable substrate paired with low annual precipitation can compound the challenges to restoration in semi-arid mine lands and poses a unique challenge. In the case of the HVC mine, as demonstrated by Figure 1, historical revegetation practices have used hearty, fast-growing, non-native species to achieve their goal of revegetating former mine and tailings sites. The problem ahead is the recovery of native grass communities into fields dominated by these fast-growing, exotic species, which is often impeded by the competitive advantages of the established plant community (Yahdjian et al., 2017). A mechanism to transition these exotic species to native species on mine lands may be prescribed burning and was brought to the attention of the HVC mine employees through consultation with the Nlaka'pamux community.

The contemporary ecological theory being used within this study to aid in biodiversity and successional advancement pertains to disturbance theory, and connects with the traditional Indigenous use of prescribed burning. It is important for both land managers and ecologists to understand various ecological theories that explore how ecosystems respond to limiting factors and disturbances that structure ecosystems and plant community assemblages. Grime's *C-S-R* triangle theory (Grime, 1977) has been discussed in plant ecology with respect to examining the role of competition, disturbance and stress tolerance, also known as environmental stressors to plant community dynamics. Generally, this theory states that species density or richness will increase as environmental stress increases along a bell curve, whereby disturbance acts to reduce competitive exclusion for species that can tolerate environmental stressors found on each side of the curve that limit the plant community (Grime, 1973; Fraser et al., 2015). Similarly, the intermediate disturbance hypothesis (IDH), which was initially proposed by Connell (1978), states that the greatest species diversity occurs in the middle range of disturbance severity. Both ecological theories have evidence to support predicting plant species diversity in response to disturbance and provide the ecological background for the basis of this study.

In natural ecosystems, disturbances, notably fire, have major positive and negative impacts as they can influence the abundance and diversity of species, nutrient cycling, biomass accumulation, primary production and other processes (Pulsford et al., 2016). In semi-arid grasslands, the relationship between prescribed burning and post-fire plant community response is not uniform. This is likely due to the highly variable nature of fire, as well as the lack of quantification of fire severity on the plant community and inherent environmental variance within each community.

Generally, fire can modify relationships among species on the landscape and change dominance in a community due to species-specific responses to changes in soil moisture, nitrogen cycling, and direct effects on meristem mortality (Ghermandi et al., 2004; Augustine et al., 2014). Fire in semi-arid and arid ecosystems has been shown to increase the availability of inorganic nitrogen in the first year post-burn, as well as for extended periods beyond the burn. This increase in plant-available nitrogen can influence regrowth, native species seedling establishment, invasion of annual plants and, ultimately, site recovery (Rau et al., 2007; Augustine et al., 2014), therefore making fire beneficial in reclamation of former mine sites where nitrogen is limited. Grasslands also benefit from fire in arid and semi-arid environments where microbes cannot readily break down accumulated plant litter (Brockway et al., 2002). Post-fire conditions often favour establishment of new species due to decreased soil moisture, removal of accumulated litter and subsequent release of nutrients immobilized within the dead plant tissue, increased solar radiation to the ground, and allowing a period of reduced competition (Brockway et al., 2002; Scheintaub et al., 2009). Additionally, in highly productive sites, litter accumulation that is left in a state without disturbance or some form of reduction may ultimately restrict above-ground net primary productivity (ANPP) and species richness, and favour tall species, reducing functional diversity in life form (Peco et al., 2012).

As described within the literature, plant community responses to prescribed burning with respect to community composition, amount and type of cover, and diversity of species, have been presented as net neutral, positive, or negative, depending on the study. Scheintaub et al. (2009) found that spring burning within a semi-arid shortgrass steppe community resulted in an overall decrease in ANPP by 20% in burned versus unburned control areas. However, as ANPP decreased, perennial grass and annual grass productivity decreased whereas perennial forb production and total vegetative cover increased with response to fire. Forb response to fire is most consistent with regard to increasing in total cover after fire, which is backed up by results presented within other literature, as compiled by Ruthven et al. (2000). This increase in cover is likely due to an interaction between death of the apical meristem during spring burning in select species, which removes growth inhibition and spurs formation of new shoots (Brown and Smith, 2000). In contrast to this, Augustine et al. (2014) found that annual burning significantly reduced cool-season (C_3) plant production and forb cover but did not affect warm-season (C_4) plant production. Positive plant community responses including increases in plant species richness and plant cover have been historically noted in semi-arid grasslands by Kirsch and Kruse (1973) with a steep increase in plant richness post-fire, from 38 to 69 species. More notably, McDonald and McPherson (2011) found that prescribed burning reduced the abundance of dominant non-native grasses and increased the abundance and diversity of native grasses and herbaceous dicotyledons.

Objectives

The aim of this study is to address three research questions that blend traditional Indigenous knowledge of prescribed burning with contemporary ecological theory pertaining to plant community dynamics and response to fire disturbance as a tool for enhancing ecosystem reclamation. Each research question is paired with an experimental procedure and associated methodology aimed at answering the specific question.

1) Can prescribed burning successfully act as a disturbance to transition low-diversity agronomic-driven vegetative communities to native grasslands?
2) What role does fire intensity play in the vegetative community when trying to establish native species under controlled conditions?
3) What level of involvement have the Nlaka'pamux peoples had in the prescribed burning project and what practices have industry professionals employed to connect with these communities?

Methodology

Field Study

In May of 2019, a total of 12 prescribed burns were conducted for this study at the Highland Valley Copper mine (UTM Zone 10, 638846E, 5594478N, NAD 83; Figure 2), located approximately 35 km from Logan Lake, BC. The prescribed burns were conducted at the Highmont tailings facility (UTM Zone 10, 647608E, 5588930N, NAD 83), a historic tailings storage facility that has been reclaimed to agronomic grasslands for approximately 24 years. The study site is located at an approximate elevation of 1500 m, within the Montane Spruce Msxk2 biogeoclimatic zone (Meidinger and Pojar, 1991). The Montane Spruce zone is characterized by cold winters and moderately short, warm summers. The mean annual temperature is 3–4.5°C, and mean annual precipitation ranges from 380 to 900 mm (Mahoney and Lee, 2021).

A total of 12 plots (each 20 by 20 m) were arranged in a completely randomized block design spaced a metre apart on each side and subjected to one of the following four treatments:

- burn (no amendments)
- burn (no woody debris added, seeded post-burn and trees planted)
- burn (woody debris added, seeded post-burn and trees planted)
- control (no amendments or burning)

This design involves three blocks of twelve plots each, resulting in each treatment being replicated three times. Treatments that indicate 'woody debris added' had lodgepole pine slash placed on the experimental site prior to burning, to assist in fire spread and provide a source of conifer seed. After burning, treatments that indicate 'seeded' were hand-broadcast with a native seed mix (Table 1) at a density of 20 kg/ha, or 0.8 kg per plot. Tree planting was completed with two species: aspen (*Populus tremuloides*) and lodgepole pine (*Pinus contorta*) at a density of 5000 stems per hectare, or 200 stems per plot.

Omegalaq™ temperature-sensitive paints ranging from 107 to 510°C were applied at gradations of approximately 30°C to each plot to quantify fire intensity and estimate the measure of fire severity (Figure 3).

Vegetation measurements were collected in each experimental plot prior to burning. Measurements included estimating absolute cover amounts in 1 by 1 m quadrants and the collection of biomass from subquadrants 0.5 by 0.5 m in

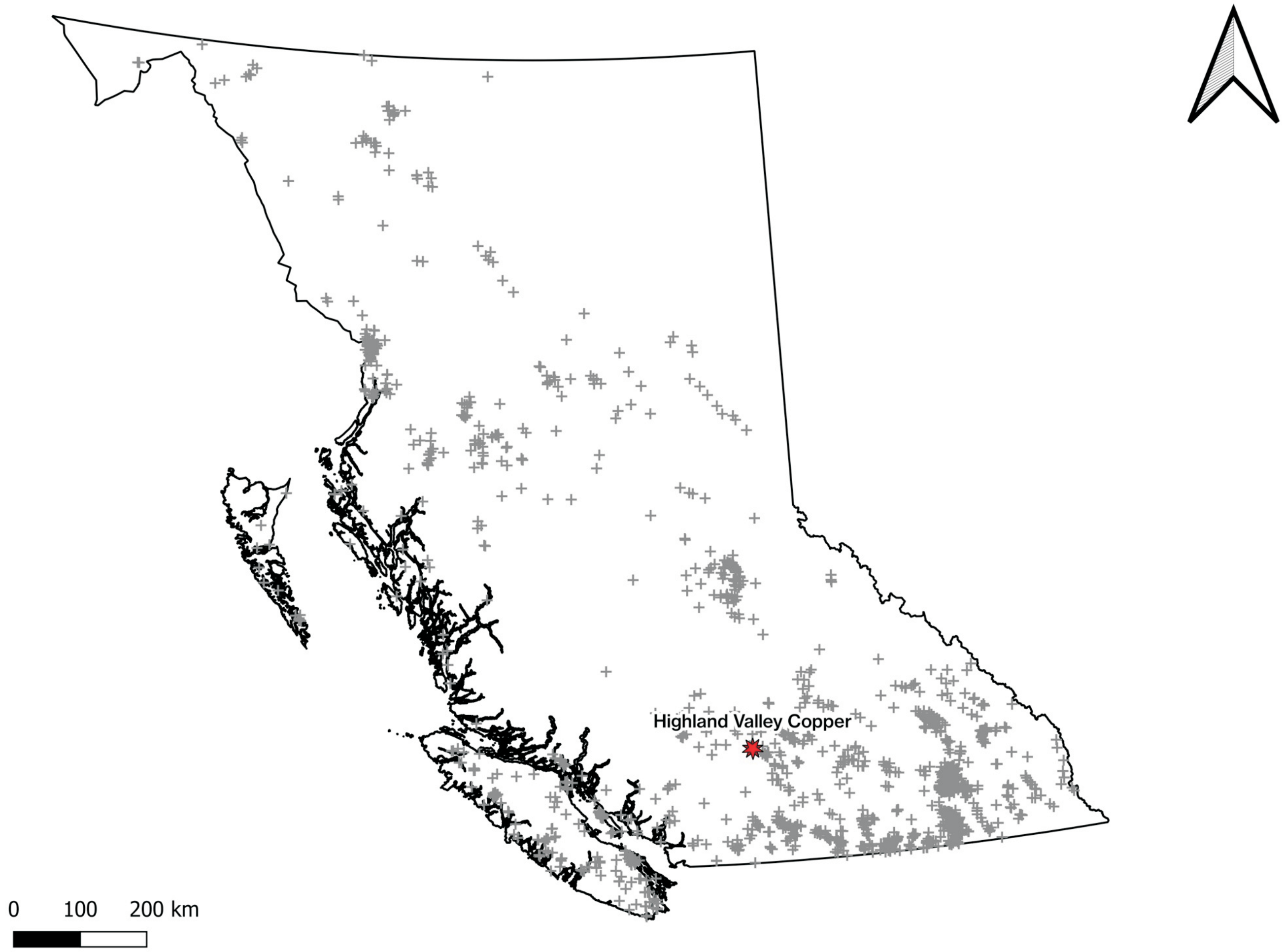

Figure 2. Map of British Columbia showing the location of the Highland Valley Copper mine, where experimental burns were conducted, and historical mines (grey crosses) that are classified as abandoned, closed, or in need of reclamation or restoration. This figure was created using QGIS version 3.18.0 using open-source data collected from the BC Data Catalogue (BC Geological Survey, 2021; BC Ministry of Energy, Mines and Low Carbon Innovation, 2021).

size (Figure 4), with a total of six biomass samples per plot, to quantify ANPP and fuel load. Biomass samples were clipped at ground level and sorted by species into live, litter and fine-fuel material, then dried in a regular oven at 65°C for 48 hours, or until a consistent dry weight was obtained. Sampling of vegetation to examine the post-burn plant community response will be conducted when standing crops are at their peak height, every year up until 2021.

Soil samples were collected at the following time intervals over the course of the research:

1) pre-burn
2) post-burn
3) 3 months post-burn
4) 12 months post-burn
5) 15 months post-burn

Table 1. Native plant species included in the seed mix hand-broadcast on the experimental plots, indicating plant successional status and plant functional group.

Group	Common name	Scientific name	Type	Succession
1	Western yarrow	*Achillea millefolium*	Native forb	Early
2	Arctic lupine	*Lupinus arcticus*	Native legume	Early
3	Rocky Mountain fescue	*Festuca saximontana*	Native grass	Early
4	Idaho fescue	*Festuca idahoensis*	Native grass	Late
5	Junegrass	*Koeleria macrantha*	Native grass	Early–Mid
6	Sandberg bluegrass	*Poa secunda*	Native grass	Early
7	Bluebunch Wheatgrass	*Pseudoroegneria spicata*	Native grass	Late

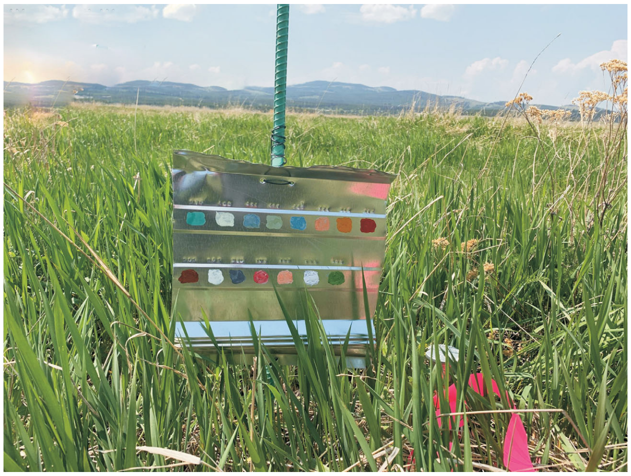

Figure 3. Omegalaq™ temperature-sensitive paints (painted sheet is approximately 30 by 45 cm), applied at gradations of approximately 30°C, used to quantify fire intensity for the prescribed burns conducted at the Highmont tailings facility of the Highland Valley Copper mine in 2019.

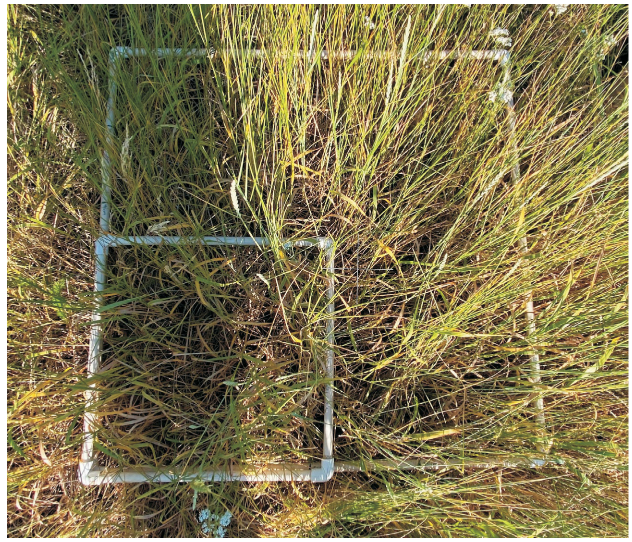

Figure 4. Example of a vegetation sampling quadrant (1 by 1 m) and biomass sampling subquadrant (0.5 by 0.5 m) used to examine the plant community pre- and post-burn, and measure above-ground net primary productivity.

The soil samples were extracted using a stainless-steel soil-sampling probe with a core diameter of 2 cm. A total of three 15 m transects were laid per experimental plot and three 15 cm cores were taken along each transect, resulting in a total of nine samples per experimental plot. Soil samples were then sieved down to 1 mm and will be analyzed for total carbon, nitrogen and hydrogen using a Thermo Scientific Flash*Smart*™ Elemental Analyzer, as well as other routine soils analyses, including soil pH.

Mesocosm Study

In August of 2019, a total of 30 grass turves were extracted from the ground around the Highmont tailings facility of Highland Valley Copper (UTM Zone 10, 647608E, 5588930N, NAD 83; Figure 5).

Each grass turf was extracted as a single unit and placed into a 102 L HDX Tough Storage Bin™ (0.56 m long by 0.46 m wide by 0.38 m high) that was modified by drilling holes for drainage through the bottom. These bins and turf sizes were selected to obtain an approximate area of 0.25 m^2 for vegetation analysis, and to ensure each grass turf contained intact root systems and soil profiles. The grass turves were then transported back to Thompson Rivers University. The mesocosm study was conducted under controlled conditions (natural and artificial light: 18 hours of daylight/6 hours of night; temperature: day and night, 21°C; humidity was between 50 and 60%) within a research greenhouse.

The 30 grass turves (each ~0.25 m^2) were arranged in a completely randomized block design, to examine four different disturbance treatments:

- high-severity burn (200 g litter applied, 20 s burn, seeded post-burn)

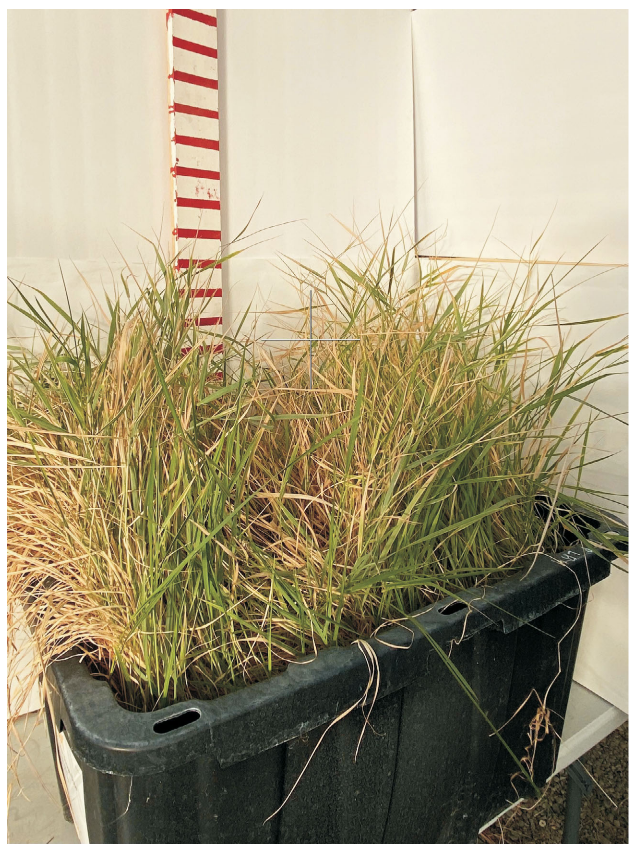

Figure 5. Example of grass turf extracted from the vicinity of Highland Valley Copper's Highmont tailings facility for this study. For reference, the scale in the back is 4 feet (~1.2 m) in height, with gradations every 1.5 inches (~3.8 cm).

- moderate-severity burn (150 g litter applied, 15 s burn, seeded post-burn)
- low-severity burn (50 g litter applied, 10 s burn, seeded post-burn)
- clip (litter and fines removed, clipped at ground height, not burned)
- control (seeded only)

This design involves three blocks, resulting in each treatment being replicated six times. Fire severity was determined by amending the weight of dried litter applied to each experimental unit, along with the length of time each grass turf was torched. After burning, all experimental units were seeded at a rate of 200 seeds/species/turf (~2400 seeds per m^2), with a total of six unique species applied (Table 2).

The composition of the native seed mix was guided by plant characteristic data that selected for species best fit to soil conditions at the site, pH tolerance and moisture regime for the ecosystem.

As for the field study, vegetation measurements that were collected in each experimental unit prior to burning included estimating the absolute cover on the entire grass turf as approximated by a 0.5 by 0.5 m quadrant. Biomass was collected from each unit, except the control units, to quantify ANPP. Biomass samples were clipped at ground level and sorted by species into live, litter and fine-fuel material, then dried in a regular oven at 65°C for 48 hours, or until a consistent dry weight was obtained.

Soil samples were extracted using a stainless-steel soil-sampling probe with a core diameter of 2 cm. A soil core was extracted from the complete depth of the grass turf and separated into the top 10 cm of soil and bottom 10 cm of soil (Figure 6), to be analyzed for total nitrogen, total carbon and total hydrogen, using a Thermo Scientific Flash-*Smart*™ Elemental Analyzer.

Sampling of vegetation and soil in the mesocosm study units will be conducted at the following time intervals over the course of the research:

1) pre-burn
2) post-burn
3) three months post-burn
4) six months post-burn
5) seven months post-burn

Semi-Structured Interviews

In August of 2020, a total of four, hour-long, semi-structured interviews were completed with non-Indigenous but

Table 2. Plant species selected for the mesocosm experiment, indicating plant successional status and plant functional group.

Group	Common name	Scientific name	Type	Succession
1	Common paintbrush	*Castilleja miniata*	Native forb	Late
2	Brown-eyed Susan	*Gaillardia aristata*	Native forb	Early-Mid
3	Rough fescue	*Festuca campestris*	Native grass	Mid-Late
4	Rocky Mountain fescue	*Festuca saximontana*	Native grass	Early
5	Field locoweed	*Oxytropis campestris*	Native legume	Early-Mid
6	Arctic lupine	*Lupinus arcticus*	Native legume	Early

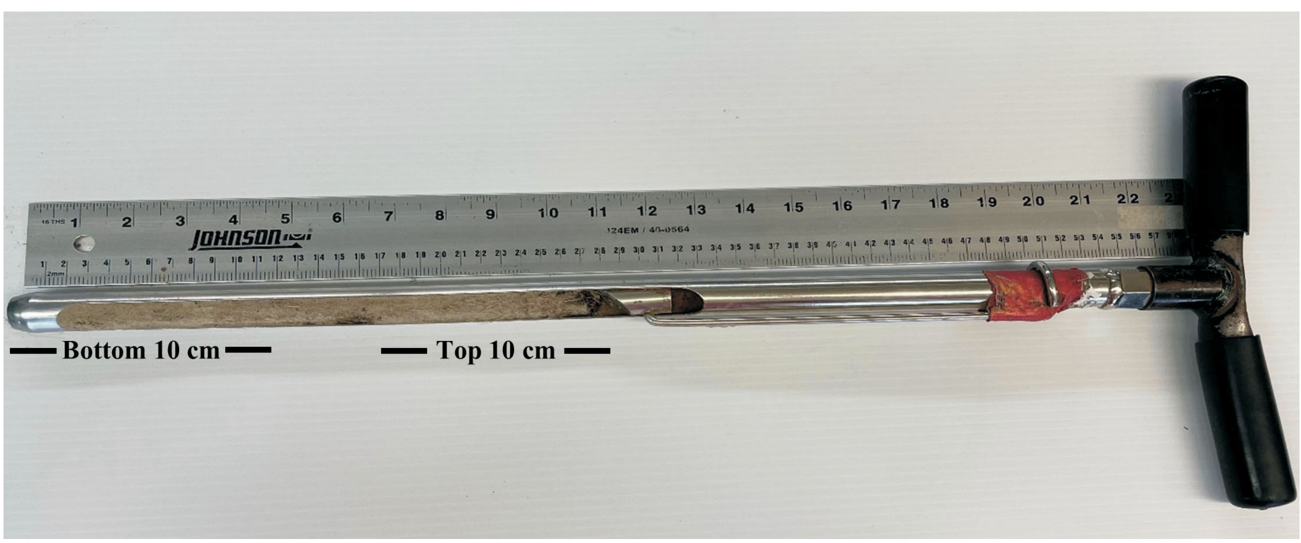

Figure 6. Intact soil core extracted from an experimental grass turf. The top 10 cm and bottom 10 cm of soil were separated and used for analysis.

key allied professionals who were instrumental in getting the project partnership between staff at Teck's Highland Valley Copper mine and the Nlaka'pamux peoples off the ground. Each interview was standardized in the sense that a predetermined list of 15 questions was prepared for each interviewee. However, questions were formulated to include open-ended and theoretically driven questions that aim to elicit data that is grounded in individuals' experience and guided by the constructs of the research scope. The statement of purpose for these interviews was to gain an understanding of how the project relationships came to fruition and understand the level of involvement the Nlaka'pamux have played in the project.

Each interview was recorded and transcribed verbatim and will be analyzed with coding software for keyword and phrase analysis.

Statistical Analysis

The data from the 2020 Highland Valley Copper mesocosm study was first analyzed descriptively by examining species richness relative to disturbance treatment over the duration of the study. All statistical analyses have not yet been completed, but linear mixed-effect models were used to spot differences between experimental treatments and analyze the variation within the data. Linear mixed modelling was used in this study to model the variation associated with the Shannon-Diversity index against treatments applied to the experimental units. Shannon-Diversity index considers species richness (the number of species present in an area) and evenness (the proportion that each species comprises of the whole) to determine a measure of biodiversity: the higher the number, the higher is the species diversity (Shannon 1948; Nolan and Callan 2006). An analysis of variance was used to examine the models, and Tukey-Kramer (Tukey, 1949) post-hoc analyses were used to determine where treatment effects were significant. In running the linear mixed-effect models, Shannon-Diversity was the dependent variable and disturbance treatment was used as the independent variable, with subject ID used as a random variable. The following models were analyzed:

1) Shannon-Diversity = disturbance treatment (fixed effect) + error (turf ID – within-subject error – random effect)
2) Shannon-Diversity = time span (fixed effect) + error (turf ID – within-subject error – random effect)

All statistical analyses were conducted in RStudio (R Core Team, 2021), a free, open-source integrated development environment for R software, a programming language for statistical computing.

Further statistical analyses will include examination of vegetation data with multivariate methods using the VEGAN package in R, to determine plant community response to fire disturbance, as well as examination of above-ground primary productivity.

Results

Examining species richness as a function of disturbance treatment across a time series reveals a significant and observable difference by simple descriptive statistics only (Figure 7).

The most significant trend shows an increase in overall diversity across all disturbance treatments in comparison to the control group. Additionally, species richness is found to be highest within the first month post-burn in all disturbance treatments except the clip and the moderate-severity treatment. Another significant trend observed is that during the last two months of the experiment (months six and seven) there is a drop in diversity.

The Shannon-Diversity index between disturbance treatments provides more information than species richness data alone (Figure 8). In running the linear mixed-effect model examining the interaction and all pairwise comparisons of the means between Shannon-Diversity and disturbance treatment the results show a significant difference between the control treatment and all other disturbance treatments (df = 4, F = 7.0378, p = <0.001; where df is degrees of freedom, F is a comparison of the variance between two statistical populations, and p is the probability that a result could have occurred by chance).

The comparison examining Shannon-Diversity index between time spans (Figure 9) highlights the distinct grouping examined in Figure 7. In running the linear mixed-effect model examining the interaction and comparison between Shannon-Diversity index and time span the results show three distinct groupings, a significant difference between the control treatment and all other time points, and a significant difference between the first and third time points and sixth and seventh time points (df = 4, F = 34.4417, p = <0.001).

Discussion

Fire Severity and the Plant Community in a Mesocosm

The effects of fire severity on post-mining reclamation within a mesocosm were examined for a semi-arid, historically reclaimed area of grassland in BC. The species richness data as presented in Figure 7 show a promising but slightly skewed vision of how the plant community responds to fire-severity treatments and fire in general, and only represents a small portion of what is occurring within the plant community. However, examining Figures 7 through 9 together, a more accurate depiction of the plant response to fire severity can be pieced together. In Figure 8, it can be

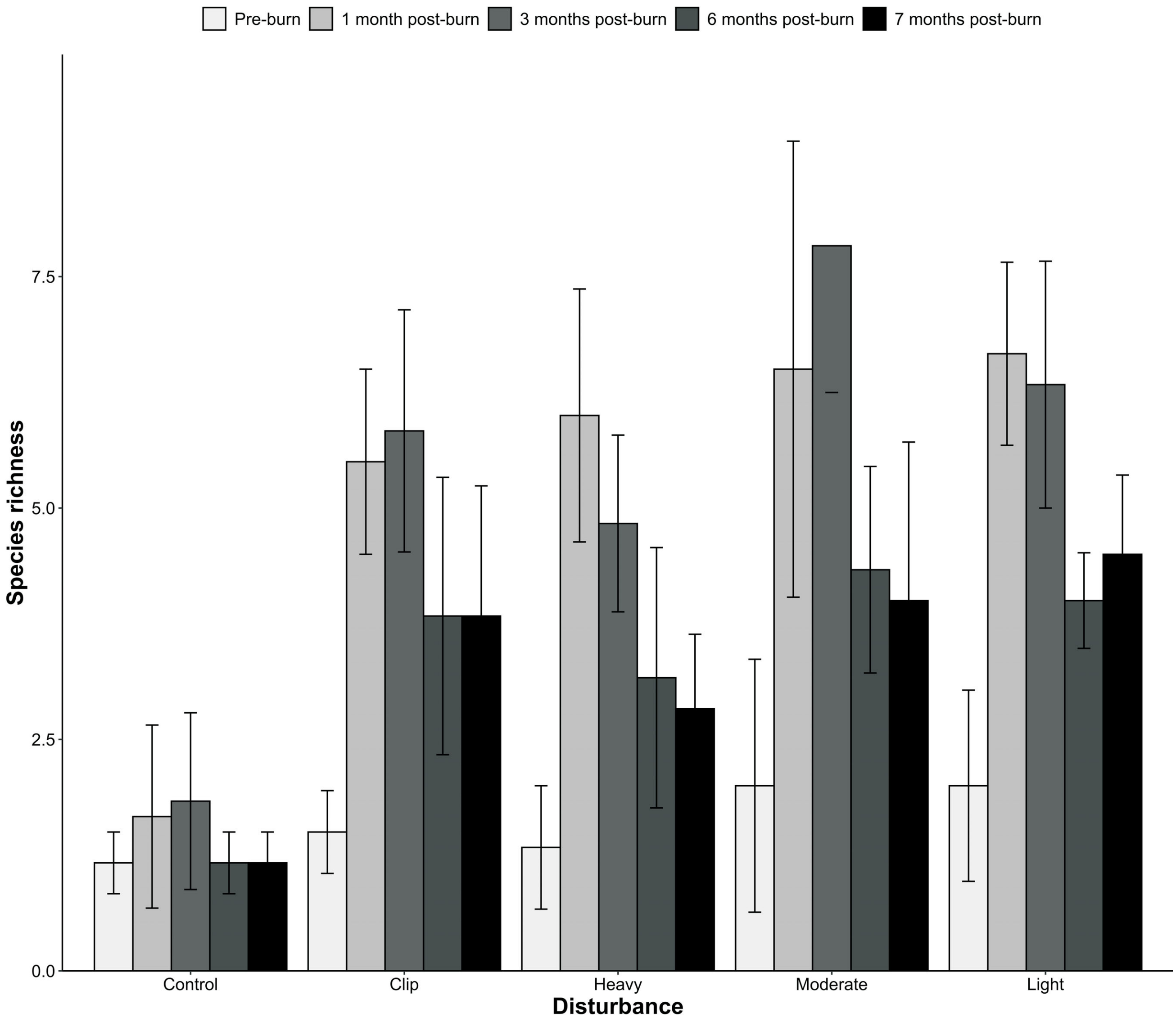

Figure 7. Time series distribution of species richness (number of unique species present in each sample) between disturbance treatments within the controlled mesocosm experiment (number of samples = 6, confidence interval = ±95%).

seen that all the disturbance treatments are causing a significant increase in Shannon-Diversity in comparison to the control unit, which is on par with the initial hypothesis that disturbance will increase diversity. In Figure 9 it can also be seen that timing is playing a significant role in species diversity, whereby the first and third months post-burn result in the highest Shannon-Diversity measurements, and the sixth and seventh months post-burn begin to reach a midpoint between the control unit and the maximum diversity obtained. This, in part, could be explained by competitive exclusion and competition dynamics that are occurring in the grass turves over the course of the seven months. Species richness, as noted in Figure 7, reaches its maximum value in disturbance treatments within the first month post-burn and begins to decrease as the seven-month mark approaches. Within the first month of post-burn conditions it would be expected that these conditions are most favourable for germination of the native seedlings. As the experiment proceeds, the agronomic, rhizomatous-dominant grasses begin to expand above and below ground while also depositing a dense layer of litter on the ground surface. This competition observably prevented many of the native species from germinating while select native species, notably the early successional forbs and grasses, in some cases, won the fight for space and persisted within the environment.

Conclusions and Ongoing Work

The above results and the conclusions reached to date are based upon data that was collected during 2020. Additional and more detailed analyses are underway as the remaining dataset and samples continue to be examined.

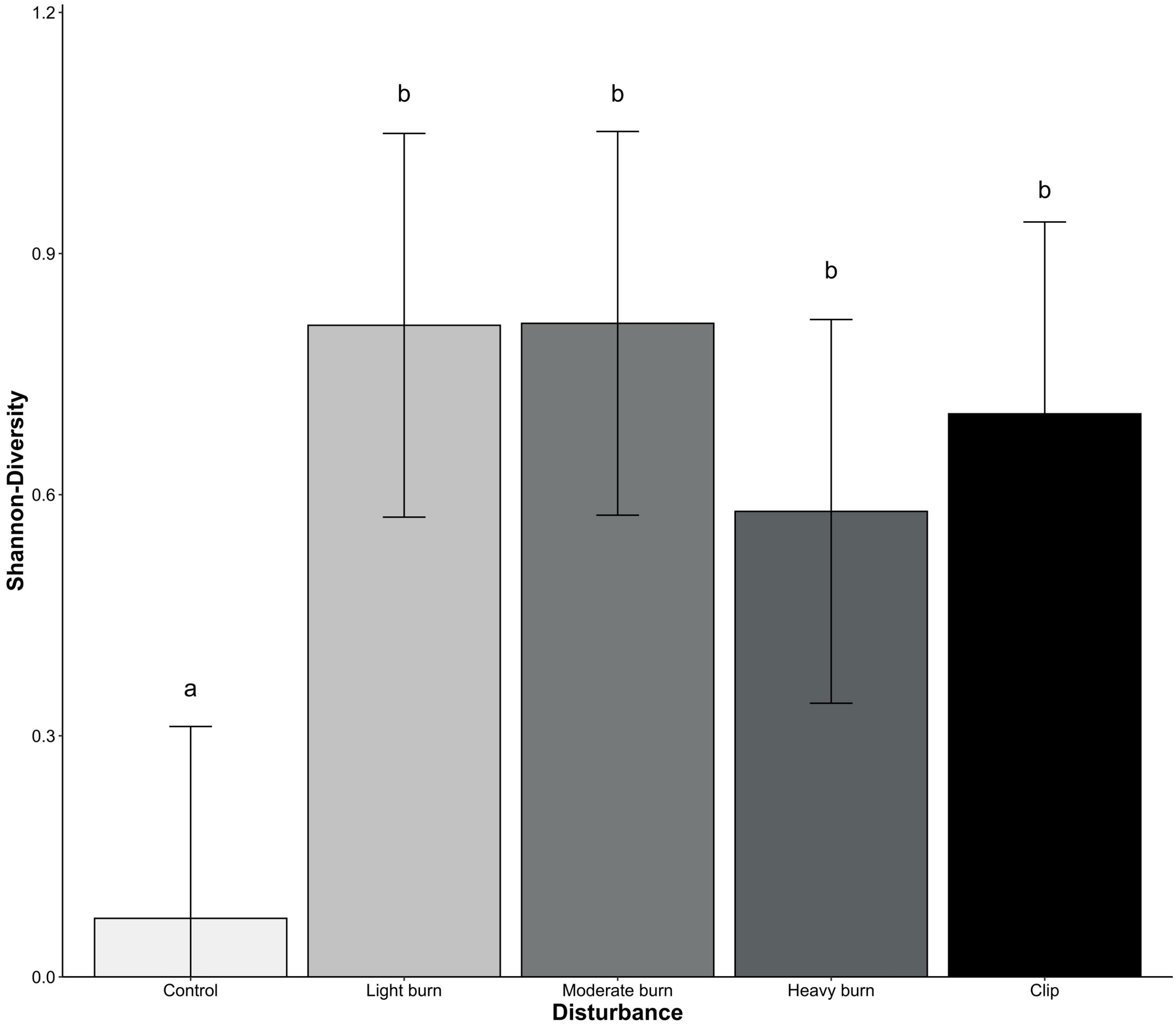

Figure 8. Examining the effect of fire-severity treatment on Shannon-Diversity index plotted as the least-squares mean (number of samples = 6, p = <0.001, confidence interval = ±95%, where p is the probability that a result could have occurred by chance). Bars with different letters indicate significant differences. Pairwise comparisons between the treatment levels were adjusted with false-detection-rate corrections.

This study will aid significantly in enhancing western scientific knowledge surrounding the novel idea of using prescribed burning as a tool for ecosystem reclamation and restoration. This work also bridges western scientific knowledge and traditional Indigenous knowledge to reclaim disturbed landscapes while reconciling past historical inequities between industry and Indigenous communities. This study also pioneers a mesocosm methodology to address the effects that fire severity has on plant community dynamics in a reclamation lens, and will aid others in determining and validating the role fire severity plays on the plant and soil communities. Future studies should continue to examine the role of fire severity in similar experiments but within non-disturbed study areas. Further development should also be taken to incorporate additional Indigenous methodologies and traditional ecological knowledge into restoration and reclamation practices.

Acknowledgments

Funding for this project was provided through the Natural Sciences and Engineering Research Council of Canada - Industrial Research Chair in Ecosystem Reclamation, with industry partners Geoscience BC, Genome British Columbia, Arrow Transportation Systems Inc., the Real Estate Foundation of BC, New Afton mine, Highland Valley Copper mine, Kinder Morgan Canada Limited, Metro Vancouver, and British Columbia Cattlemen's Association. Schol-

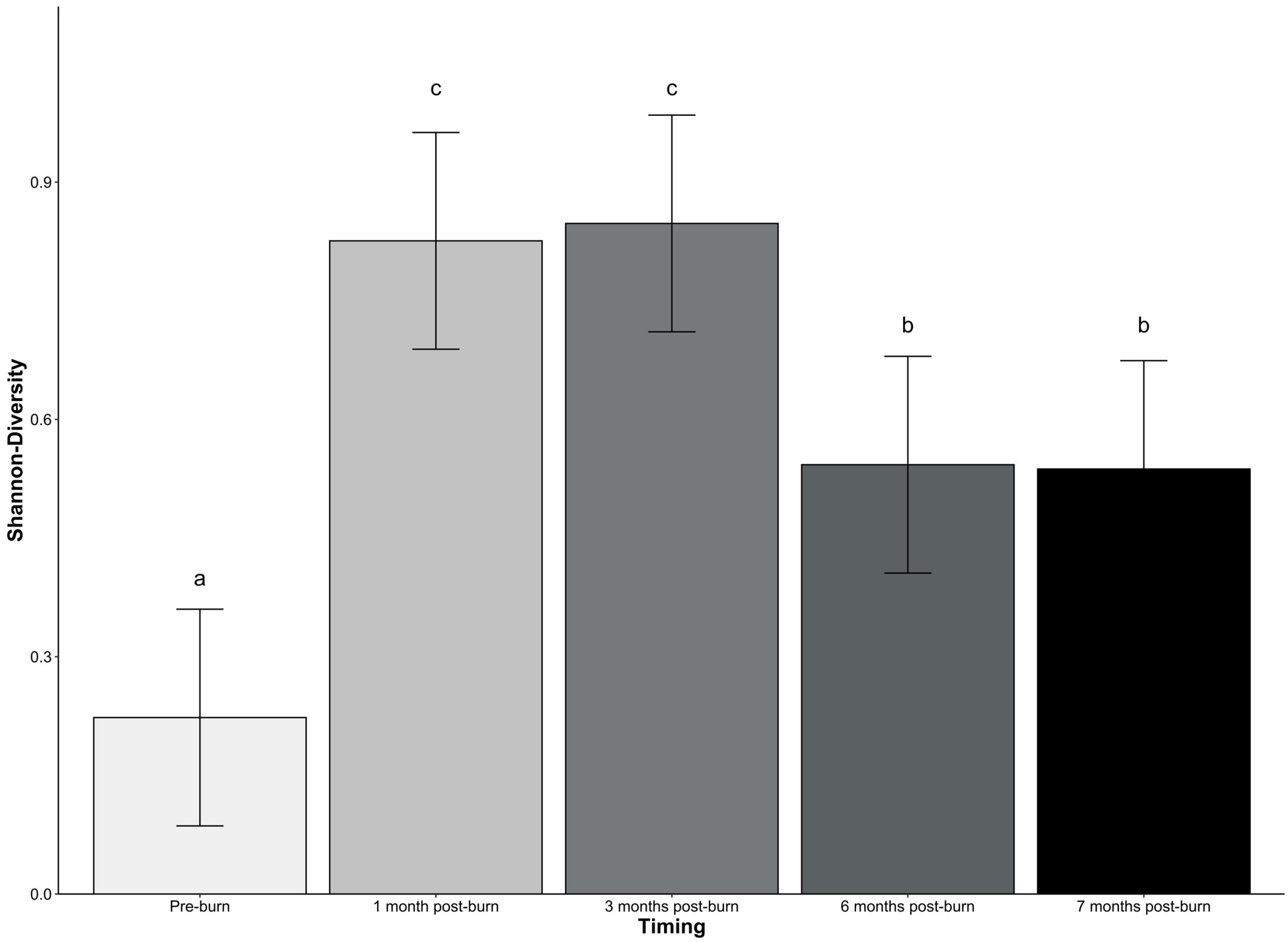

Figure 9. Examining the effect of timing on Shannon-Diversity index plotted as the least-squares mean (number of samples = 30, p = <0.001, confidence interval = ±95%, where p is the probability that a result could have occurred by chance). Bars with different letters indicate significant differences. Pairwise comparisons between the treatment levels were adjusted with false-detection-rate corrections.

arship funding was also provided in support of this project from Geoscience BC and the Society of Contaminated Sites Approved Professionals of British Columbia. Special thanks go to the student researchers and fellow graduate students who helped in the field and lab: S. Vogel, C. Stephens, M. Coghill, K. Gillich and K. Baker. Special thanks also go to peer reviewer S. Bayliff.

References

Augustine, D.J., Brewer, P., Blumenthal, D.M., Derner, J.D. and von Fischer, J.C. (2014): Prescribed fire, soil inorganic nitrogen dynamics, and plant responses in a semiarid grassland; Journal of Arid Environments, v. 104, p. 59–66, URL <https://dx.doi.org/10.1016/j.jaridenv.2014.01.022>.

Azapagic, A. (2004): Developing a framework for sustainable development indicators for the mining and minerals industry; Journal of Cleaner Production, v. 12, p. 639–662, URL <https://doi.org/10.1016/S0959-6526(03)00075-1>.

BC Geological Survey (2021): MINFILE inventory database; BC Ministry of Energy, Mines and Low Carbon Innovation, BC Geological Survey, URL <https://catalogue.data.gov.bc.ca/dataset/minfile-inventory-database> [February 2021].

BC Ministry of Energy, Mines and Low Carbon Innovation (2021): Permitted mine areas - major mine; BC Ministry of Energy, Mines and Low Carbon Innovation, Mines Health, Safety and Enforcement Division, URL <https://catalogue.data.gov.bc.ca/dataset/permitted-mine-areas-major-mine> [February 2021].

Blackstock, M. and McAllister, R. (2004): First Nations perspectives on the grasslands of the interior of British Columbia; Journal of Ecological Anthropology, v. 8, p. 24–46, URL <https://doi.org/10.5038/2162-4593.8.1.2>.

Bradshaw, A. (1997): Restoration of mined lands - using natural processes; Ecological Engineering, v. 8, p. 255–269, URL <https://doi.org/10.1023/A:1005177815154>.

British Columbia Assembly of First Nations (2021): First Nations in BC; British Columbia Assembly of First Nations, URL <https://www.bcafn.ca/first-nations-bc/interactive-map> [November 2021].

Brockway, D.G., Gatewood, R.G. and Paris, R.B. (2002): Restoring fire as an ecological process in shortgrass prairie ecosystems: initial effects of prescribed burning during the dormant and growing seasons; Journal of Environmental Management, v. 65, p. 135–152.

Brown, J.K. and Smith, J.K., editors (2000): Wildland fire in ecosystems: effects of fire on flora; United States Department of Agriculture, Forest Service, Rocky Mountain Research Station, General Technical Report RMRS-GTR-42-vol 2, 257 p., URL <http://www.fs.fed.us/rm> [November 2021].

Connell, J.H. (1978): Diversity in tropical rainforest and coral reefs; Science, v. 199, p. 1302–1310.

Climatedata.ca (2021): Kamloops, BC; Climatedata.ca, URL <https://climatedata.ca/explore/location/?loc=JAFNW&location-select-temperature=tx_max&location-select-precipitation=rx1day&location-select-other=frost_days>.

Fonseca, A., McAllister, M.L. and Fitzpatrick, P. (2014): Sustainability reporting among mining corporations: a constructive critique of the GRI approach; Journal of Cleaner Production, v. 84, p. 70–83, URL <https://dx.doi.org/10.1016/j.jclepro.2012.11.050>.

Fraser, L.H., Pither, J., Jentsch, A., Sternberg, M., Zobel, M., Askarizadeh, D., Bartha, S., Beierkuhnlein, C., Bennett, J.A., Bittel, A., Boldgiv, B., Boldrini, I.I., Bork, B., Brown, L., Cabido, M., Cahill, J., Carlyle, C.N., Campetella, G., Chelli, S., Cohen, O. et al. (2015): Worldwide evidence of a unimodal relationship between productivity and plant species richness; Science, v. 349, issue 6245, p. 302–305, URL <science.org/doi/10.1126/science.aab3916>.

Fuhlendorf, S.D., Archer, S.A., Smeins, F., Engle, D.M. and Taylor, C.A., Jr. (2008): The combined influence of grazing, fire, and herbaceous productivity on tree-grass interactions; Chapter 12 *in* Western North American *Juniperus* Communities: A Dynamic Vegetation Type, O.W. Van Auken (ed.), Springer, p. 219–238, URL <https://doi.org/10.1007/978-0-387-34003-6_12>.

Gasch, C., Huzurbazar, S. and Stahl, P. (2014): Measuring soil disturbance effects and assessing soil restoration success by examining distributions of soil properties; Applied Soil Ecology, v. 76, p. 102–111, URL <https://dx.doi.org/10.1016/j.apsoil.2013.12.012>.

Ghermandi, L., Guthmann, N. and Bran, D. (2004): Early post-fire succession in northwestern Patagonia grasslands; Journal of Vegetation Science, v. 15, p. 67–76, URL <https://doi.org/10.1111/j.1654-1103.2004.tb02238.x>.

Grime, J.P. (1973): Competitive exclusion in herbaceous vegetation; Nature, v. 242, p. 344–347.

Grime, J.P. (1977): Evidence for the existence of three primary strategies in plants and its relevance to ecological and evolutionary theory; American Naturalist, v. 111, p. 1169–1194, URL <https://doi.org/10.1086/283244>.

Heyerdahl, E.K., Lertzman, K. and Wong, C.M. (2012): Mixed-severity fire regimes in dry forests of southern interior British Columbia, Canada; Canadian Journal of Forest Research, v. 42, p. 88–98, URL <https://doi.org/10.1139/X11-160>.

Hölzel, N., Buisson, E. and Dutoit, T. (2012): Species introduction - a major topic in vegetation restoration (editorial); Applied Vegetation Science, v. 15, p. 161–165, URL <https://doi.org/10.1111/j1654-109X.2012.01189x>.

Ignace, M. and Ignace, R.E. (2017): Secwépemc People, Land, and Laws; McGill-Queen's University Press, 624 p.

Kirsch, L.M. and Kruse, A.D. (1973): Prairie fires and wildlife; *in* Proceedings, 12th Annual Tall Timbers Fire Ecology Conference, Lubbock, Texas, Tall Timbers Research Inc., Tallahassee, Florida, p. 289–303.

Lee, R.N., Bradfield, G.E., Krzic, M., Newman, R.F. and Cumming, W.F.P. (2014): Plant community – soil relationships in a topographically diverse grassland in southern interior British Columbia, Canada; Botany, v. 92, p. 837–845, URL <https://doi.org/10.1139/cjb-2014-0107>.

Lewis, M., Christianson, A. and Spinks, M. (2018): Return to flame: reasons for burning in Lytton First Nation, British Columbia; Journal of Forestry, v. 116, p. 143–150, URL <https://doi.org/10.1093/jofore/fvx007>.

Mahoney, C. and Lee, J. (2021): BC Climate Explorer; URL <http://www.bc-climate-explorer.org/> [February 2021].

McDonald, C.J. and McPherson, G.R. (2011): Absence of a grass/fire cycle in a semiarid grassland: response to prescribed fire and grazing; Rangeland Ecology and Management, v. 64, p. 384–393, URL <https://doi.org/10.2111/REM-D-10-00036.1>.

Meidinger, D. and Pojar, J., compilers and editors (1991): Ecosystems of British Columbia; BC Ministry of Forests, Special Report Series, No. 6, 330 p.

Melosi, M.V., reviewer (2017): *Transient Landscapes: Insights on a Changing Planet*, by E.E. Wohl; Environmental History, v. 22, p. 356–358, URL <https://doi.org/10.1093/envhis/emw116>.

Nolan, K. and Callan, J. (2006): Beachcomber biology: the Shannon-Weiner species diversity index; Association of Biology Laboratory Education (ABLE) Conference Proceedings, v. 27, p. 334–338.

Peco, B., Carmona, C.P., de Pablos, I. and Azcárate, F.M. (2012): Effects of grazing abandonment on functional and taxonomic diversity of Mediterranean grasslands; Agriculture, Ecosystems and Environment, v. 152, p. 27–32, URL <https://dx.doi.org/10.1016/j.agee.2012.02.009>.

Pulsford, S.A., Lindenmayer, D.B. and Driscoll, D.A. (2016): A succession of theories: purging redundancy from disturbance theory; Biological Reviews of the Cambridge Philosophical Society, v. 91, p. 148–167, URL <https://doi.org/10.1111/brv.12163>.

R Core Team (2021): R: a language and environment for statistical computing; *in* R Foundation for Statistical Computing (4.0.3), R Foundation, software manual, URL <https://www.r-project.org/> [November 2021].

Rau, B.M., Blank, R.R., Chambers, J.C. and Johnson, D.W. (2007): Prescribed fire in a Great Basin sagebrush ecosystem: dynamics of soil extractable nitrogen and phosphorus; Journal of Arid Environments, v. 71, p. 362–375, URL <https://doi.org/10.1016/j.jaridenv.2007.05.006>.

Ruthven, D.C., III, Gallagher, J.F. and Synatzske, D.R. (2000): Effect of fire and grazing on forbs in the western South Texas Plains; The Southwestern Naturalist, v. 45, p. 89–94.

Sample, D. and Barlow, S. (2013): Best management practice fact sheet 4: soil restoration; Virginia Cooperative Extension, publication 426-123, 4 p.

Scheintaub, M.R., Derner, J.D., Kelly, E.F. and Knapp, A.K. (2009): Response of the shortgrass steppe plant community to fire; Journal of Arid Environments, v. 73, p. 1136–1143, URL <https://dx.doi.org/10.1016/j.jaridenv.2009.05.011>.

Shannon, C. (1948): A mathematical theory of communication; The Bell System Technology Journal, v. 27, p. 519–520, URL <http://doi.org/10.1016/s0016-0032(23)90506-5>.

Symstad, A.J. and Leis, S.A. (2017): Woody encroachment in northern Great Plains grasslands: perceptions, actions, and needs; Natural Areas Journal, v. 37, p. 118–127, URL <https://doi.org/10.3375/043.037.0114>.

Tordoff, G.M., Baker, A.J.M. and Willis, A.J. (2000): Current approaches to the revegetation and reclamation of metalliferous mine wastes; Chemosphere, v. 41, p. 219–228, URL <https://doi.org/10.1016/S0045-6535(99)00414-2>.

Tukey, J.W. (1949): Comparing individual means in the analysis of variance; Biometrics, v. 5, p. 99–114.

Turner, N.J., Ignace, M.B. and Ignace, R. (2000): Traditional ecological knowledge and wisdom of aboriginal peoples in British Columbia; Ecological Applications, v. 10, p. 1275–1287, URL <https://doi.org/10.1890/1051-0761(2000)010[1275:TEKAWO]2.0.CO;2>.

Turner, S.R., Pearce, B., Rokich, D.P., Dunn, R.R., Merritt, D.J., Majer, J.D. and Dixon, K.W. (2006): Influence of polymer seed coatings, soil raking, and time of sowing on seedling performance in post-mining restoration; Restoration Ecology, v. 14, p. 267–277, URL <https://doi.org/10.1111/j.1526-100X.2006.00129.x>.

Virgone, K.M., Ramirez-Andreotta, M., Mainhagu, J. and Brusseau, M.L. (2018): Effective integrated frameworks for assessing mining sustainability; Environmental Geochemistry and Health, v. 40, p. 2635–2655, URL <https://doi.org/10.1007/s10653-018-0128-6>.

Vitousek, P.M., Mooney, H.A., Lubchenco, J. and Melillo, J.M. (1997): Human domination of Earth's ecosystems; Science, v. 277, p. 494–499, URL <https://science.org/doi/10.1126/science.277.5325.494>.

Wikeem, B. and Wikeem, S. (2004): The Grasslands of British Columbia; Grasslands Conservation Council of British Columbia, Kamloops, British Columbia, 479 p., URL <http://bcgrasslands.org/wp-content/uploads/2017/06/bcgrasslandsfinal2004ver3.pdf> [February 2021].

Yahdjian, L., Tognetti, P.M. and Chaneton, E.J. (2017): Plant functional composition affects soil processes in novel successional grasslands; Functional Ecology, v. 31, p. 1813–1823, URL <https://doi.org/10.1111/1365-2435.12885>.

Revisiting Rock Engineering Empirical Standards in the Era of Machine Learning to Benefit the Mineral Resources Sector in British Columbia

B. Yang[1], **Norman B. Keevil Institute of Mining Engineering, The University of British Columbia, Vancouver, British Columbia**

D. Elmo, Norman B. Keevil Institute of Mining Engineering, The University of British Columbia, Vancouver, British Columbia, delmo@mining.ubc.ca

D. Stead, Department of Earth Sciences, Simon Fraser University, Vancouver, British Columbia

Yang, B., Elmo, D. and Stead, D. (2022): Revisiting rock engineering empirical standards in the era of machine learning to benefit the mineral resources sector in British Columbia; *in* Geoscience BC Summary of Activities 2021: Minerals, Geoscience BC, Report 2022-01, p. 67–72.

Introduction

The past decade has seen an increased interest in the application of machine learning (ML) to mining and geotechnical engineering, especially in the mineral resources development sector. There are numerous benefits to ML, including increased efficiency through the ability to quickly sort and characterize large amounts of field data, and increased accuracy by being able to detect relationships and patterns in complex data, all with minimal human intervention (Morgenroth et al., 2019). Even though ML is a powerful tool, the success of ML algorithms depends on the quantity and quality of the data (Schmidt et al., 2019). For rock engineering, in particular, one of the main challenges is that it is difficult to obtain high quality, unbiased and objective data, and it is even more difficult to obtain high quality data in the large quantities needed for ML. These difficulties associated with rock engineering data can be attributed to the highly variable nature of geological materials as well as the qualitative nature of the data collection process and the empirical approach to design. A significant portion of the empirical design process in rock engineering involves the use of empirical industry standards developed from experiences several decades ago when the nature of rock engineering projects was significantly different to that of today. Key examples include rock mass classification systems used to quantify rock mass quality to aid engineering decision making, and rock mass characterization used to scale laboratory rock properties to field-scale properties required for numerical analyses. Even though these standards have become routine in rock engineering practice, they are not without their limitations. They include a relatively high degree of subjectivity due to various forms of bias, geological constraints and engineering constraints. However, rock engineers in both industry and academia often ignore these limitations and treat these empirical standards as standards. As rock engineering is increasingly integrating the design process with ML and other advanced computational techniques, a critical review of these empirical industry standards is needed to examine the feasibility of integrating them with ML. This study provides a critical review of commonly used rock mass classification systems with the goal of helping rock engineers integrate them with ML.

Background

The following section provides an overview of i) common empirical rock mass classification systems used in rock engineering and ii) ML.

Rock Mass Classification Systems

Rock mass classifications systems have become an industry standard and their use can be found in most rock engineering projects. They can be traced back to Terzaghi (1946), who created a system that linked rock mass characteristics to rock mass behaviour and failure mechanisms. Presently, the most common rock mass classification systems used in practice are the Rock Mass Rating (RMR; Bieniawski, 1973, 1976, 1989), the Q-system (Barton et al., 1974) and the Geological Strength Index (GSI; Hoek, 1994; Hoek and Marinos, 2000). Separate from these is the Rock Quality Designation (RQD), which was developed by D.U. Deere in 1964 (Deere et al., 1969) to define rock mass quality from borehole cores; this was subsequently adopted as an input parameter by the RMR and Q-system. It is defined as the summation of all sound core pieces greater than 10 cm (4 in.) in length divided by the total length of the core run and is expressed as a percentage (Deere et al., 1969).

The RMR was first introduced by Bieniawski (1973) based on experiences in South African tunnelling, with subsequent updates in 1976 and 1989. It is defined as the summa-

[1]*The lead author is a 2021 Geoscience BC Scholarship recipient.*

This publication is also available, free of charge, as colour digital files in Adobe Acrobat® PDF format from the Geoscience BC website: http://geosciencebc.com/updates/summary-of-activities/.

tion of the ratings assigned to five parameters deemed the most important for rock mass quality:

- strength of the intact rock material
- rock quality designation
- spacing of discontinuities
- condition of discontinuities
- groundwater flow

Once RMR is calculated, it can be used to determine the support needed for a tunnelling, mining or slope stability project based on experiences from projects with similar RMR values. The RMR has been modified over the years in order to be more relevant to specific applications (e.g., caving methods and slopes). Some commonly used modified RMRs include the Mining Rock Mass Rating developed by Laubscher (1977) for mining applications and the Slope Mass Rating introduced by Romana (1985) for slopes.

The Q-system was first introduced by Barton et al. (1974) based on experiences in Scandinavian tunnelling and consists of six parameters organized as quotients (the 'Q' system) as shown in the following equation:

$$Q = (RQD / J_n)(J_r / J_a)(J_w / SRF)$$

where RQD is the rock quality designation as previously defined, J_n is the number of joint sets, J_r is the joint roughness coefficient, J_a is the joint alteration coefficient, J_w is the water reduction factor and SRF is the stress reduction factor. The SRF distinguishes the Q-system from the RMR and speaks to the respective experience base from which the two systems were developed. Scandinavian tunnelling projects have to contend with high horizontal stresses related to the geological history of the Scandinavian shield and therefore this was seen to be an important influencing parameter on rock mass behaviour. This is not the case in South African tunnelling and thus there was no stress factor included with its rating system.

Once a Q value has been calculated, the support for a tunnel can be determined from a support chart, which is similarly based on experiences from projects with different Q values.

The GSI was introduced by Hoek (1994) to provide a visually based estimation of the rock mass quality. It has undergone numerous updates since its introduction, going from a simple equivalency with RMR to a chart that combines the blockiness of the rock mass and the condition of discontinuities (Yang et al., 2021b). Although it was based on the RMR system, it differs from the RMR and Q-system in that it is not intended to rate the rock mass for support design classes; rather, it is used as a scaling parameter in combination with the Hoek-Brown failure criterion (Hoek and Brown, 1980) to determine the strength of the rock mass.

It is important to keep in mind that even though RMR, Q-system and GSI result in a numeric value, they are still quantifications of qualitative descriptions and are subject to the limitations of nominal and ordinal scale measurements. Additionally, these rock mass classification systems are subjective, with engineering judgement playing an important role, and they suffer from a lack of standardization between individual or company practices despite being treated as industry standards. Notwithstanding, they are often (wrongly) perceived as unbiased and objective.

Machine Learning

Machine learning is a subset of artificial intelligence in which mathematical models are used to help a computer find relationships among data. It enables a computer system to learn without direct instruction and to continue learning and improving on its own (Azure, 2021). In other words, ML enables a computer system to build a predictive model from data and that model can then be used to make predictions from new data (Google Developers, 2021a). Machine learning is divided into classification (where a label is predicted) and regression (where a numeric value is predicted). As previously mentioned, the success of ML algorithms depends on both the quality and quantity of data. A common saying in ML is 'garbage in equals garbage out'; if the data used to train the model are of poor quality, the results of the model will also be of poor quality and unreliable (Google Developers, 2021b). Poor quality data come in many forms, including, but not limited to, wrong data (i.e., data input error), biased data and irrelevant data. Poor quality data, especially those that are biased, can have a significant impact on the results of a ML model. The importance of good quality data has long been recognized in the ML field (Sessions and Valtorta, 2006) and there has been significant research on how to mitigate biases (e.g., Dixon et al., 2018; Das et al., 2019); however, rock engineering has arguably yet to consider this sufficiently and biased data, such as rock mass classification values, are increasingly being incorporated in ML training. The other important aspect needed for a successful ML model is having enough relevant, good quality data so that the model is trained on a variety of scenarios and can find the relevant relationships between parameters (Google Developers, 2021b). Rock engineering often lacks the amount of relevant and good quality data needed to allow for a robust ML model.

Revisiting Rock Mass Classification Systems

The lead author's research into the use of ML in rock engineering began in 2020, and the following section highlights the published progress to date. As discussed in Yang et al. (2021b), the use of ML in rock engineering is made difficult by the lack of standardization and need to statistically analyze databases that have been created through a quantification of qualitative assessments, such as in the use of rock mass classification systems. In order for data compilation to progress in rock engineering, rock engineers need to address how to digitize rock engineering information effectively and uniquely and how to better consider failure mechanisms. To accomplish this, rock engineers need to consider the original definitions and development of commonly used rock mass classification systems, something that is often overlooked in practice. Palmstrom and Broch (2006) highlighted the importance of this by stating that the use of rock mass classification systems required a good knowledge of their basis, their structure and their limitations. Yang et al. (2020, 2021b) provided an in-depth discussion on the development and limitations of the most commonly used rock mass classification systems (RQD, RMR, Q-system and GSI), which is summarized below.

As discussed in Yang et al. (2020), the RQD was developed based on observations that poorer quality core resulted in a significantly higher number of smaller core pieces (Deere et al., 1969). The RQD has two main applications: i) it is a quantitative measure to compare geological conditions at different sites, and ii) it is a red flag indicator to bring attention to what factors cause low core recovery (Deere and Deere, 1989). Of note is the arbitrariness associated with the 10 cm threshold when calculating RQD and the acknowledgment by Deere and Deere (1989) that the weighted RQD (calculated by counting all the core pieces and squaring the lengths of the pieces shorter than 30 cm) would have been better but the 10 cm threshold remained in use because of its early adoption and familiarity gained over time. Additionally, the use of RQD has four main requirements that have been largely overlooked: i) the core run length should be no longer than 1.5 m, ii) the core diameter should ideally be 54.7 mm (but larger core diameters can be used), iii) the core pieces should be hard and sound, iv) the core logging should occur at the same time as drilling (especially in shale and claystone). The limitations of RQD have been widely discussed since its development; however, they have also been largely overlooked by rock engineers. These limitations include i) the subjectivity surrounding the 10 cm threshold, ii) the difficulty in differentiating between mechanical and natural fractures, iii) the subjectivity in determining if the core is hard and sound, iv) its sensitivity to the relative orientation of the fractures with respect to the orientation of the borehole or scanline (i.e., orientation bias), and v) the ignoring of the effects that incipient fractures and veins have on rock mass strength (Yang et al., 2020).

The development of RMR by Bieniawski (1973) involved 49 initial case histories in 1973, followed by an additional 62 cases in 1984 and another 78 cases in 1987. By 1989, RMR had been used in 351 case histories, which contributed to its development. Approximately 63% of the case histories used in its development are in sedimentary rocks, whereas only 19% are in igneous rocks and 16% in metamorphic rocks. The majority of the case histories are in shale (98 cases or 28% of the case histories), followed by mudstone (31 cases) and sandstone (27 cases; Bieniawski, 1989). In contrast, 212 case studies were used in the development of the Q-system by Barton et al. (1974); 48% of the case histories are in metamorphic rocks, whereas only 38% are in igneous rocks and 13% in sedimentary rocks. The majority of the case histories are in granite (46 cases or 22% of the case histories), followed by schist (17 cases) and gneiss (14 cases). These differences again highlight the empirical nature of the development of the RMR and Q-system, and specifically, the geology encountered in tunnelling projects in South Africa (primarily sedimentary) that shaped the RMR versus that encountered in the Scandinavian shield (primarily crystalline) that shaped the Q-system. Based on the case histories used in the development of RMR and Q-system, RMR might be considered more applicable for projects in sedimentary rocks, whereas the Q-system more applicable for projects in igneous and metamorphic rocks. However, as shown in Yang et al. (2021b), these geological constraints have been ignored and RMR and Q-system have been used to describe rock mass conditions for projects in various rock types. Even though rock mass classification systems can be expanded to scenarios outside those in their original databases, Barton (1988) noted that it should be done with caution and careful consideration of the geological setting. Despite this, current practices in rock engineering have seemingly created a geological equivalency between RMR and Q-system.

It is also important to note that the case histories used in the development of RMR and Q-system are from several decades ago when the scale of projects was much more limited compared to today's projects. For RMR, the majority of its case histories involved tunnelling and shallow mining projects; most of these case histories have a span of up to 10 m and are limited to depths of up to 250 m. Similarly, the case histories for Q-system show that most of the projects used in its development had spans of up to 15 m and were at depths of up to 250 m. These case histories show that RMR and Q-system were not developed for deeper projects. This raises the question: should rock engineers use RMR and Q-system for current projects that are not only bigger but deeper? An important consideration is the potential failure mechanism, which depends in part on the size and depth of the project, as well as the geology.

As previously mentioned, the development of GSI differs from that of RMR and Q-system in that it was introduced to better characterize poorer quality rock masses and thus assist in determining input values for the Hoek-Brown failure criterion. Specifically, Hoek wanted a new system that "would not include RQD, would place greater emphasis on basic geological observations of rock mass characteristics, and reflect the material, its structure and its geological history" (Marinos et al., 2005). Initially, GSI was taken as being equivalent to RMR76 with the rating for water set to 10 (dry). As a result, it can be assumed that GSI was born out of the same geology database as RMR.

The current method of using rock mass classification systems ignores the geological and engineering constraints associated with their development and homogenizes the different nature of the geological and structural processes at play, which may be unique for a given regional or tectonic setting. The current classification process treats rock like other engineering materials (e.g., concrete) and generalizes its response to engineering activities; however, it is important that rock engineers recognize the role geology, and in particular structural geology, has not only on rock mass strength but also ground performance. One method of recognizing the inherent geological variability in rock masses is by reporting a range of classification values rather than one value that is often misconstrued as being 'accurate' and 'precise'.

Another limitation of rock mass classification systems that is often overlooked is that the rating values are nonunique and on their own do not provide any information on the rock mass conditions. As shown in Yang et al. (2021a), there are many combinations of parameter ratings in RMR, Q-system and GSI that can lead to the same classification value. For example, according to the GSI chart from Hoek and Marinos (2000), a GSI of 50 is associated with a rock mass that has a blocky structure and fair joint surface conditions (e.g., due to weathering) as would a rock mass that is very blocky but has good joint surface conditions (e.g., if it was unweathered). Even though both rock masses have the same GSI, they have different rock mass conditions. Yang et al. (2021a) showed that the majority of combinations are in the 'Fair' rock mass class for RMR (RMR = 40–60) and the 'Very good' rock mass class for the Q-system (Q = 40–100). This means that there is more uncertainty surrounding the classification values in these ranges because of the variability in rock mass conditions. As a result, it is imperative that rock engineers report the parameter ratings they used to determine their classification values.

The Future of Rock Engineering Standards for Machine Learning

There has been increasing pressure to integrate rock mass classification systems with ML in recent years under the guise of providing more accurate and precise RQD, RMR, Q-system or GSI values. However, as shown in the previous section, the notion that classification values are accurate and precise does not reflect the inherent geological variability found in rock masses or the subjectivity in quantifying them. Even though it is possible to incorporate ML in rock mass classification systems, it is important to always keep in mind the aforementioned limitations of these systems (both geological and engineering constraints) and the original purpose behind their development. If rock engineering is to continue moving forward with the incorporation of ML into its design processes, then more objective and unbiased parameters need to be developed. Some examples of objective parameters currently under development are the Representative Elementary Length (REL) introduced by Elmo and Stead (2018) and the Network Connectivity Index (NCI) introduced by Elmo et al. (2021). The REL is a new rock mass quality indicator that is more objective, whereas NCI is a new rock mass classification system that is more objective and considers failure mechanisms. Both of these new parameters are not subject to the same limitations and subjectivity as their predecessors and, as a result, they can be more easily integrated with ML techniques. These parameters will benefit the mineral resources sector in British Columbia by improving the efficiency of the exploration and design process, as well as improving the accuracy of the design. Ultimately, this will result in improved sustainability during mineral exploration and mine design.

Future Work

The next steps include developing a set of guidelines for the use of ML in rock engineering as well as building on Elmo and Stead (2018) and Elmo et al. (2021) to refine the concepts of REL and NCI and incorporate them within ML algorithms. Both the development of the guidelines and refinement of REL are currently underway and are expected to be completed in the upcoming year. Additionally, the guidelines are expected to be published in a conference and journal paper in the upcoming year. It is anticipated that this research will be completed by 2024.

Conclusion

The rock engineering design process is highly empirical and dependent on empirical industry standards, such as the Rock Quality Designation, Rock Mass Rating, Q-system and Geological Strength Index. As rock engineering transitions into the era of digitalization and machine learning, it is essential that these empirical industry standards are revisited in order to better understand their development and limitations. The geological and engineering constraints of rock mass classification systems are not widely acknowledged by rock engineers, and subjectivity and bias make it difficult for them to be easily integrated with machine learning. If rock engineers want to continue using current rock mass classification systems, then they should ensure that their geological and engineering constraints are recognized. However, the development of more objective and unbiased rock mass classification systems can help rock engineering transition to successfully implementing machine learning by ensuring that the data is of good quality. In order for rock engineering industry standards to be the best available solution, they should undergo continuous revisions and improvements.

Acknowledgments

This project was supported through a scholarship from Geoscience BC. The authors would like to thank E. Eberhardt for their comments and assistance.

References

Azure (2021): Artificial intelligence (AI) vs machine learning (ML); Microsoft, URL <https://azure.microsoft.com/en-ca/overview/artificial-intelligence-ai-vs-machine-learning/#introduction> [October 2021].

Barton, N. (1988): Rock mass classification and tunnel reinforcement using the Q-system; *in* Rock Classification Systems for Engineering Purposes, L. Kirkaldie (ed.), ASTM International, STP984, p. 59–88.

Barton, N., Lien, R. and Lunde, J. (1974): Engineering classification of rock masses for the design of tunnel support; Rock Mechanics, v. 6, p. 189–236, URL <https://link.springer.com/article/10.1007/BF01239496> [September 2021].

Bieniawski, Z.T. (1973): Engineering classification of jointed rock masses; Transaction of the South African Institution of Civil Engineers, v. 15, p. 335–344.

Bieniawski, Z.T. (1976): Rock mass classification in rock engineering; Proceedings of the Symposium on Exploration for Rock Engineering, v. 1, p. 97–106.

Bieniawski, Z.T. (1989): Engineering Rock Mass Classification: A Complete Manual for Engineers and Geologists in Mining, Civil, and Petroleum Engineering; John Wiley & Sons, New York, 272 p.

Das, A., Dantcheva, A. and Bremond, F. (2019): Mitigating bias in gender, age and ethnicity classification: a multi-task convolutional neural network approach; *in* Computer Vision – ECCV 2018 Workshops, Proceedings, Part 1, L. Leal-Taixé and S. Roth (ed.), September 8–14, 2018, Munich, Germany, 13 p., URL <https://openaccess.thecvf.com/content_eccv_2018_workshops/w5/html/Das_Mitigating_Bias_in_Gender_Age_and_Ethnicity_Classification_a_Multi-Task_ECCVW_2018_paper.html> [October 2021].

Deere, D.U. and Deere, D.W. (1989): Rock quality designation (RQD) after twenty years; US Army Corps of Engineers, 100 p., URL <https://www.nrc.gov/docs/ml0037/ML003749192.pdf> [September 2021].

Deere, D.U., Merritt, A.H. and Coon, R.F. (1969): Engineering classification of in-situ rock; Air Force Weapons Laboratory, Technical Report No. AFWL-TR-67-144, 272 p., URL <https://apps.dtic.mil/sti/pdfs/AD0848798.pdf> [September 2021].

Dixon, L., Li, J., Sorensen, J., Thain, N. and Vasserman, L. (2018): Measuring and mitigating unintended bias in text classification; *in* Proceedings of the 2018 AAAI/ACM Conference on AI, Ethics, and Society, Association for Computing Machinery, February 2–3, 2018, New Orleans, Louisiana, p. 67–73, URL <https://dl.acm.org/doi/abs/10.1145/3278721.3278729> [October 2021].

Elmo, D. and Stead, D. (2018): The concept of representative elementary length (REL) as an effective tool to study scale effects in rock engineering problems; Boletín Geológico y Minero, v. 131, no. 3, p. 355–362, URL <http://revistas.igme.es/Boletin/2020/131_3/BGM_131-3_Art-1.pdf> [September 2021].

Elmo, D., Yang, B., Stead, D. and Rogers, S. (2021): A new discrete fracture network approach to rock mass classification; *in* Challenges and Innovations in Geomechanics, Proceedings of the 16th International Conference of IACMAG – Volume 1, M. Barla, A. Di Donna and D. Sterpi (ed.), International Association for Computer Methods and Advances in Geomechanics, May 5–8, 2021, virtual, p. 854–861, URL <https://link.springer.com/chapter/10.1007%2F978-3-030-64514-4_92> [September 2021].

Google Developers (2021a): Machine learning glossary; *in* Machine Learning, Google, URL <https://developers.google.com/machine-learning/glossary#machine_learning> [October 2021].

Google Developers (2021b): The size and quality of a data set; *in* Data Preparation and Feature Engineering for Machine Learning, Google, URL <https://developers.google.com/machine-learning/data-prep/construct/collect/data-size-quality> [October 2021].

Hoek, E. (1994): Strength of rock and rock masses; International Society of Rock Mechanics News Journal, v. 2, no. 2, p. 4–16, URL <https://isrm.net/download/media.file.afcfaa77c2928214.31333323136393339396973726d5f6e6577736a6f75726e616c5f2d5f313939342c5f766f6c756d655f322c5f6e756d.pdf> [September 2021].

Hoek, E. and Brown, E.T. (1980): Empirical strength criterion for rock masses; Journal of the Geotechnical Engineering Division, v. 106, no. GT9, p. 1013–1035, URL <https://www.rocscience.com/assets/resources/learning/hoek/1980-Empirical-Strength-Cruiterion-for-Rock-Masses.pdf> [November 2021].

Hoek, E. and Marinos, P. (2000): Predicting tunnel squeezing problems in weak heterogeneous rock masses; Tunnels and Tunnelling International, 22 p., URL <https://www.rocscience.com/assets/resources/learning/hoek/Predicting-Tunnel-Squeezing-Problems-in-Weak-Heterogeneous-Rock-Masses-2000.pdf> [September 2021].

Laubscher, D.H. (1977): Geomechanics classification of jointed rock masses – mining applications; Transactions of the Institution of Mining and Metallurgy, v. 86, p. 1–8.

Marinos, V., Marinos, P. and Evert, H. (2005): The geological strength index: applications and limitations; Bulletin of Engineering Geology and the Environment, v. 64, p. 55–65, URL <https://www.rocscience.com/assets/resources/learning/hoek/2005-The-GSI-Applications-and-Limitations.pdf> [September 2021].

Morgenroth, J., Usman, T.K. and Perras, M.A. (2019): An overview of opportunities for machine learning in underground rock engineering design; Geosciences, v. 9, no. 12, art. 504, 23 p., URL <https://www.researchgate.net/publication/337711656_An_Overview_of_Opportunities_for_Machine_Learning_Methods_in_Underground_Rock_Engineering_Design> [September 2021].

Palmstrom, A. and Broch, E. (2006): Use and misuse of rock mass classification systems with particular reference to the Q-system; Tunnels and Underground Space Technology, v. 21, p. 575–593, URL <https://doi.org/10.1016/j.tust.2005.10.005>.

Romana, M. (1985): New adjustment ratings for application of Bieniawski classification slopes; *in* Proceedings of the International Symposium on the Role of Rock Mechanics in Excavations for Mining and Civil Works, International Society for Rock Mechanics, September 2–4, 1985, Zacatecas, Mexico, p. 49–53.

Schmidt, J., Marques, M.R.G., Botti, S. and Marques, M.A.L. (2019): Recent advances and applications of machine learning in solid-state materials science; npj Computational Materials, v. 5, art. 83, 36 p., URL <https://www.nature.com/articles/s41524-019-0221-0> [October 2021].

Sessions, V. and Valtorta, M. (2006): The effects of data quality on machine learning algorithms; *in* Proceedings of the 11th International Conference on Information Quality, Massachusetts Institute of Technology, November 10–12, 2006, Cambridge, Massachusetts, 14 p., URL <http://mitiq.mit.edu/ICIQ/Documents/IQ%20Conference%202006/papers/The%20Effects%20of%20Data%20Quality%20on%20Machine%20Learning%20Algorithms.pdf> [October 2021].

Terzaghi, K. (1946): Rock defects and loads on tunnel supports; Rock Tunneling with Steel Supports, v. 1, p. 17–99.

Yang, B., Elmo, D. and Stead, D. (2020): Questioning the use of RQD in rock engineering and its implications for future rock slope design; *in* Proceedings of the 54th International Symposium on Rock Mechanics, American Rock Mechanics Association, June 28–July 1, 2020, virtual, 9 p.

Yang, B., Elmo, D. and Stead, D. (2021a): Applications of information theory in rock engineering; *in* Proceedings of EUROCK 2021, ISRM International Society of Rock Mechanics, September 21–24, 2021, virtual, 8 p.

Yang, B., Mitelman, A., Elmo, D. and Stead, D. (2021b): Why the use of rock mass classification systems requires revisiting their empirical past; Quarterly Journal of Engineering Geology and Hydrogeology, art. qjegh2021-039, URL <https://www.researchgate.net/publication/352382585_Why_the_future_of_rock_mass_classification_systems_requires_revisiting_their_empirical_past> [September 2021].

Investigating the Effect of Contributory Factors on the Response of Fibre Optic Cable for Underground Monitoring of Geological Stress in British Columbia

S. Hendi[1], **Department of Earth, Ocean and Atmospheric Sciences, The University of British Columbia, Vancouver, British Columbia, shendi@eoas.ubc.ca**

E. Eberhardt, Department of Earth, Ocean and Atmospheric Sciences, The University of British Columbia, Vancouver, British Columbia

M. Gorjian, Department of Earth, Ocean and Atmospheric Sciences, The University of British Columbia, Vancouver, British Columbia

Hendi, S. Eberhardt, E. and Gorjian, M. (2022): Investigating the effect of contributory factors on the response of fibre optic cable for underground monitoring of geological stress in British Columbia; *in* Geoscience BC Summary of Activities 2021: Energy and Water, Geoscience BC, Report 2022-01, p. 73–80.

Introduction

In situ stress is one of the most important boundary conditions in rock-engineering design. It dictates many important design decisions, such as the optimal orientation of horizontal boreholes for energy-development projects (geothermal, oil, gas), as well as the orientation, dimensioning and support design of underground excavations for mining and hydroelectric power infrastructure to ensure stable and safe excavations. However, it is extremely difficult to measure ground stress reliably, resulting in significant uncertainty for, and risk to, these projects. This frequently leads to less than optimum design performance and costly mistakes that, on some projects, represent lost value in the range of tens of millions of dollars.

Despite its importance, it is also the most challenging characteristic to accurately assess in rock-engineering design. As a result, a variety of strategies have been developed, each with its own set of limits and difficulties concerning their reliability (Amadei and Stephansson, 1997; Haimson and Cornet, 2003; Sjöberg and Klasson, 2003):

- most involve point measurements, giving rise to uncertainty owing to geological heterogeneity
- many are destructive, limiting testing to a single measurement, or cause unwanted permanent change to the rock
- most involve a higher per measurement cost.

The emergence of fibre-optic sensing capabilities offers several advantages that can potentially overcome existing challenges. The use of fibre optics in stress-measurement techniques is leading to the development of a nondestructive approach capable of monitoring both in situ stress states as well as any subsequent stress changes in response to engineering activities (e.g., mining). In addition, this technique can also be used to measure the stress state away from a borehole, as well as along the length of the borehole, while being lower cost compared to conventional methods. To use fibre optics in the development of a stress-measurement technique, it is crucial to consider contributory elements that play a critical part in the response of optical fibre sensors. Prior to this work, no attempt to use a fibre-optic cable to measure geological in situ stresses had been undertaken successfully. The aim of this study is to investigate the influence of three different borehole-filling materials and of changes in borehole diameter on a fibre-optic system measuring geological stress.

Distributed Acoustic Sensing

Fibre-optic cable exhibits three scattering mechanisms: Raman, Brillouin and Rayleigh scattering. Since Rayleigh scattering is intrinsically independent of any external fields that may affect the surrounding environment, it is considered a direct-sensing mechanism, as opposed to Raman and Brillouin scattering. Rayleigh scattering is being used in this study to estimate in situ stresses caused by seismic waves propagating in the rock.

Rayleigh-scattering–based, distributed acoustic sensing (DAS) systems could transform a fibre-optic cable into a sensor array, allowing users to detect and monitor many physical factors, such as temperature, vibration and strain, over a long distance, with precise spatial and temporal precision. The DAS system has been developed for a variety of applications, each with different spatial resolutions, spectral ranges and sensing ranges (Bakku, 2015; Miah and Potter, 2017).

A typical DAS system consists of a surface-mounted interrogator unit (IU) coupled to a fibre-optic connection. To

[1]*The lead author is a 2021 Geoscience BC Scholarship recipient.*

This publication is also available, free of charge, as colour digital files in Adobe Acrobat® PDF format from the Geoscience BC website: http://geosciencebc.com/updates/summary-of-activities/.

measure strain in different parts of the fibre, the IU transmits short laser pulses into the fibre and analyses the backscattered energy using optical time-domain reflectometry (OTDR) or optical frequency-domain reflectometry (OFDR). Under the same environmental conditions, the OFDR mode exhibits more sensitivity than the well-known OTDR. The optical power required from the necessary light source for OFDR is lower for the same dynamic range and OFDR successfully exceeds the spatial resolution and signal-to-noise ratio dynamic range of OTDR. In the OFDR system, the source is swept over a certain frequency, but the amplitude is kept virtually constant. Because of the limitations imposed by the sample size as well as the advantages of OFDR over OTDR (e.g., higher spatial resolution), an IU system based on OFDR was used in this research (Hartog, 2017).

Each fibre-optic section serves as a single-component seismic sensor, measuring the axial strain generated by a seismic wave in the optical fibre. One disadvantage of fibre optics is its low broadside sensitivity. As mentioned in Mateeva et al. (2014), applying the DAS technique using a straight fibre-optic cable revealed a directional sensitivity limitation; this limitation is manifested by a reduced sensitivity to broadside waves, or waves that travel perpendicular to the fibre. According to Den Boer et al. (2016), to improve sensitivity on the broadside, a fibre should be wrapped around a mandrel core at a predetermined wrapping angle (α).

Over the past few decades, fibre-optic DAS has been used in numerous settings such as the oil and gas industry as well as mining, civil and environmental engineering due to its capacity to work in confined spaces, measure various parameters over long distances, operate at low-power requirements, withstand harsh environments (high temperature and pressure) and protect itself from potential electromagnetic interference (Nath et al., 2006; Naruse et al., 2007; Molenaar et al., 2012; Kamal, 2014; Mateeva et al., 2014; Miller et al., 2016; Zhao et al., 2016; Zhou et al., 2019). One of the planned outcomes of this extensive research is to develop a stress-measurement technique based on the fibre-optic cable. The emergence of fibre-optic sensing capabilities offers several advantages that can not only help overcome the challenges posed by the currently available techniques but also:

- provide both stress magnitude and orientation in one measurement (other techniques require multiple measurements)
- provide a nondestructive measurement technique (i.e., measurements can be repeated for added precision and confidence)
- be used to measure the stress state of large volumes of rock (i.e., less likely to provide misleading measurements due to heterogeneity)
- be used to measure stress profiles along the borehole and, through repeat surveys, stress changes.

Method

The goal of this study is to investigate the response of helically wound cable (HWC) fibre to three different types of borehole-filling material (cement, polymer-based mud and invert-emulsion mud) and to changes in the borehole diameter. The combination of two distinct analytical methods was used to stimulate the response of fibre-optic cable. By assuming a plane wave travelling through a multilayered media in 2.5 dimensions (Figure 1), it is possible to calculate dynamic strains in the vertical and radial directions as a function of the angle of incidence using this integrated technique (Kuvshinov, 2016; Hendi et al., 2020b).

The first method, presented in Hendi et al. (2020b), is used to calculate the cable's axial strain. The second approach, outlined in Kuvshinov (2016), is applied to calculate the radial strain using the axial strain established in the previous

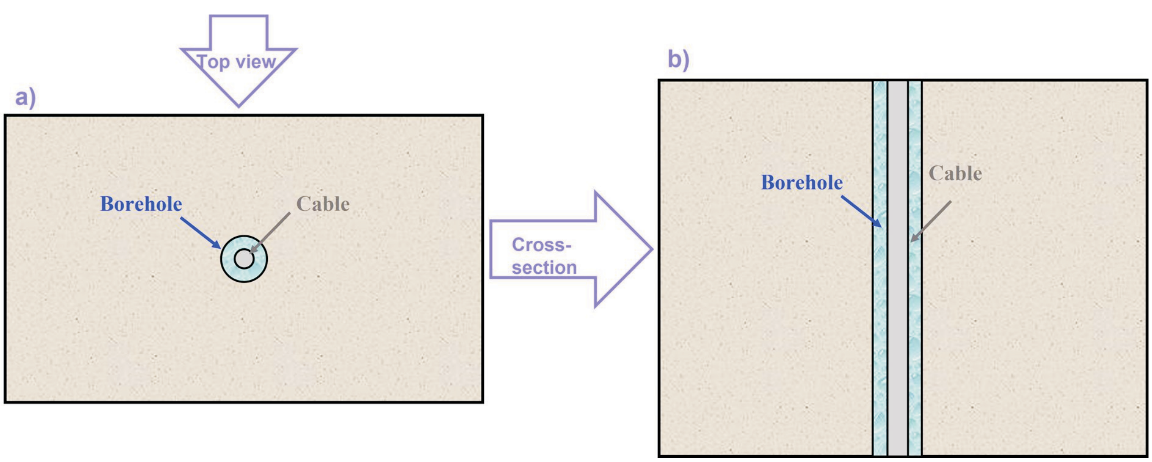

Figure 1. Depiction of the top view and cross-section of the geometry used in different borehole-filling–material scenarios. **a)** A helically wound cable is positioned inside a borehole filled with any of three filling materials. **b)** The diameter of a cement-filled borehole can be modified to examine how the change influences cable-fibre reaction.

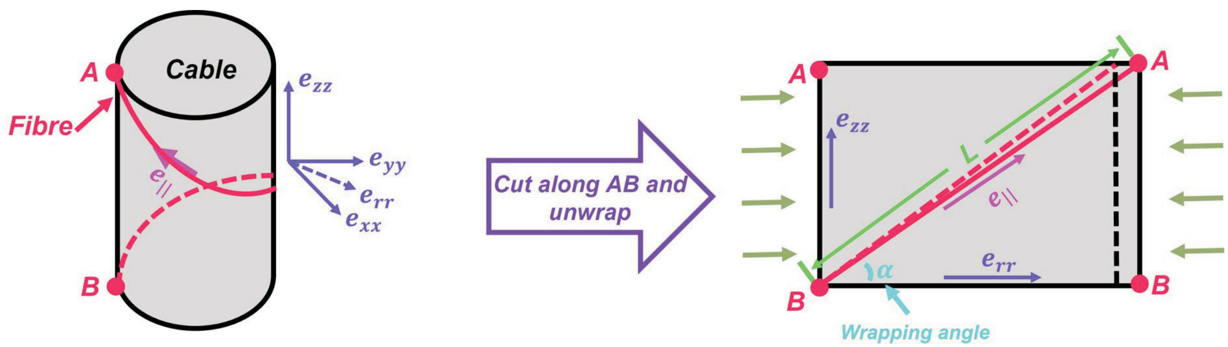

Figure 2. Demonstration of the wrapping angle (α) of helically wound cable (HWC). If the cylindrical surface of a cable (grey) was sliced along AB and unwrapped to a horizontal plane, the fibre trajectory would be represented by the diagonal red line visible in the panel on the right. The wrapping angle (α) is the angle produced by the circumference of the cable and the fibre (BB); the direction of the strain (e) is expressed as being radial ($_{rr}$), axial ($_{zz}$), or occurring in the y-axis ($_{yy}$) or x-axis ($_{xx}$) plane. When a wave strikes the HWC, the cable (dashed black line) deforms and the fibre (red dashed line) deforms as well (after Hornman, 2017).

step. Equation 1 relates the axial and radial strains to the strain of the HWC (Figure 2):

$$e_{ll\,(fibre)} = e_{zz\,(cable)} \cos^2 \alpha + e_{rr\,(cable)} \sin^2 \alpha \tag{1}$$

where e represents strain along the fibre ($_{fibre}$), axial strain in the cable ($_{zz[cable]}$) and radial strain in the cable ($_{rr[cable]}$), respectively, and α represents the wrapping angle of the fibre around the cable.

Two assumptions have been made in this analytical simulation. Firstly, a point source is assumed to be a specific distance away; as a result, the spherical wave can be simplified to a perfect plane wave, with the strains all occurring in the same plane. Secondly, the dominant frequency and amplitude of the point source are 8 kHz and 1 Pa, respectively.

Based on the foregoing, four borehole-filling–material scenarios were developed:

- Scenario 1: a HWC cable is placed in the middle of a cement-filled borehole (Figure 3). To determine how the cement's properties should be defined to obtain an optimum response from the HWC cable, the lower Young's modulus (associated with softer material) of the cement is changed to the higher modulus associated with the surrounding rock (considered as hard cement).

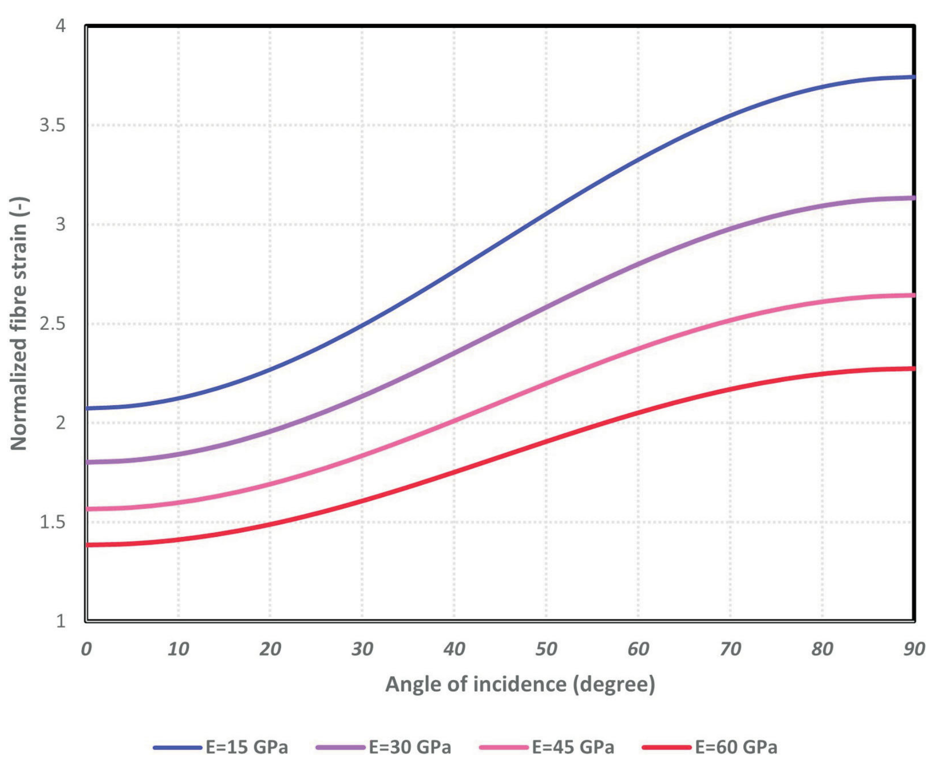

Figure 3. Effect of the properties of cement-filled boreholes (Young's modulus [E]) on the response of helically wound cable as a function of the angle of incidence (scenario 1).

- Scenario 2: a HWC cable is placed in the middle of a mud-filled borehole (Figure 4). To determine how the mud's properties should be defined to obtain an optimum response from the HWC cable, two common types of muds frequently used in industry are used to fill the borehole: polymer-based mud and invert-emulsion mud (mud properties from Hendi et al., 2020a).
- Scenario 3: a HWC cable is placed in the middle of a cement-filled borehole (Figure 5). The diameter of the borehole is altered to examine the sensitivity of HWC-fibre response as a function of borehole diameter.
- Scenario 4: The findings from scenarios 1 and 2 are combined to determine which combination of borehole-filling material and HWC cable is the most efficient. The response of a HWC cable inserted in a borehole, which in one case is filled with hard cement (Young's modulus equivalent to that of the surrounding rock) and, in another, with dense polymer-based mud, is compared (Figure 6).

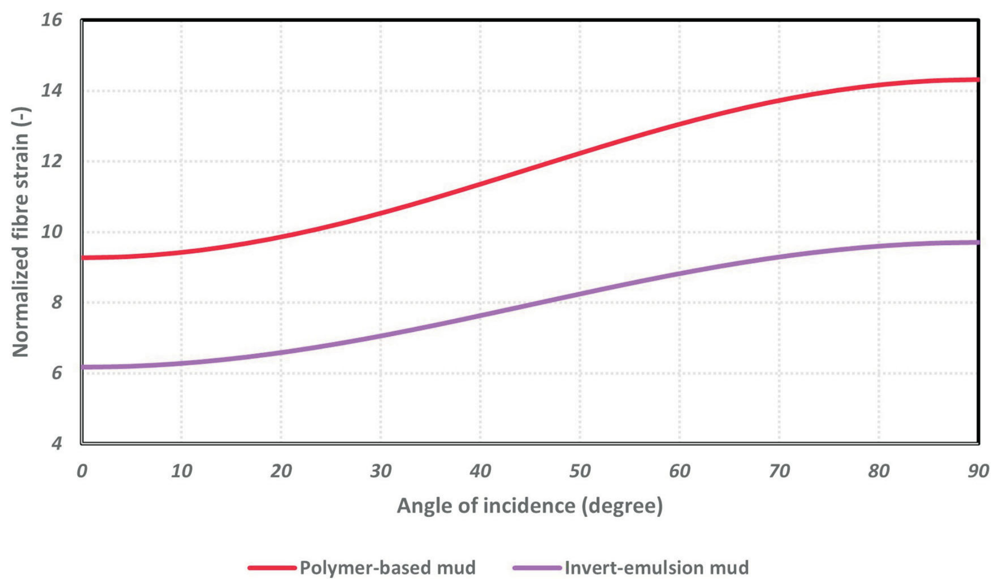

Figure 4. Effect of the properties of mud-filled boreholes on the response of helically wound cable as a function of the angle of incidence (scenario 2).

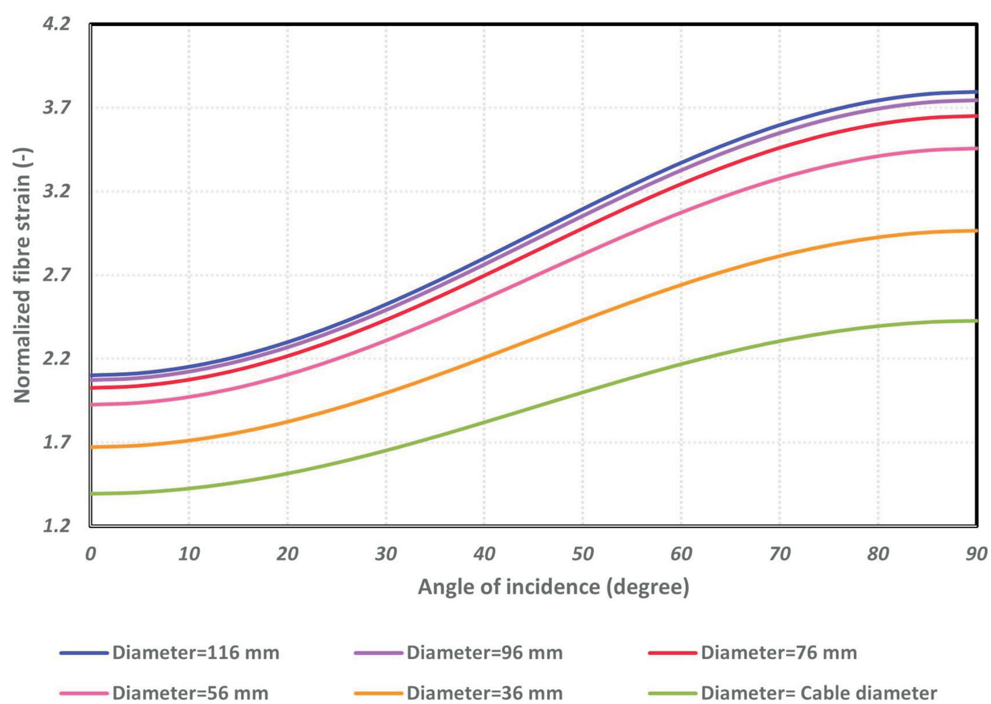

Figure 5. Effect of changes to borehole diameter on the response of helically wound cable as a function of the angle of incidence (scenario 3).

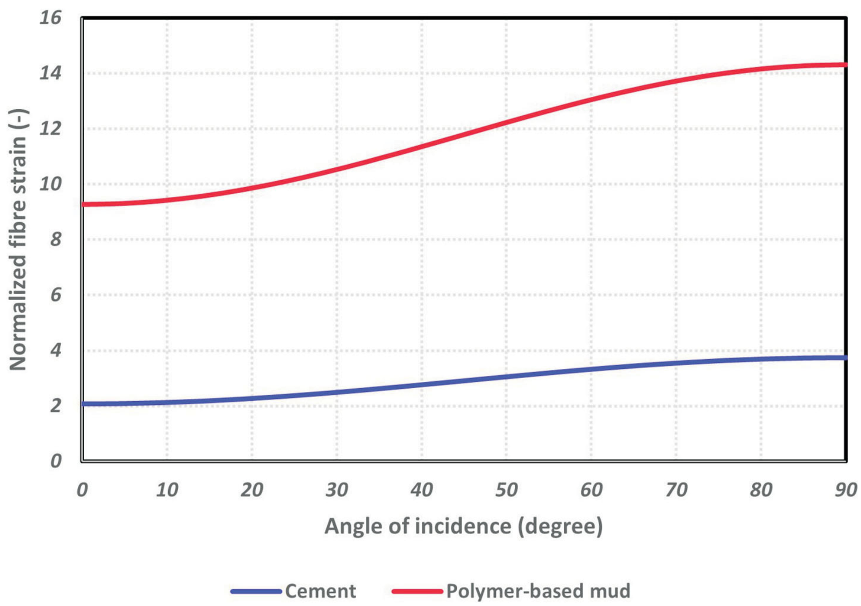

Figure 6. Comparison between the effect of polymer-based mud and cement used as borehole-filling material on the response of helically wound cable fibre.

Tables 1 and 2 show the geometry and characteristics of the materials for the various borehole-filling–material scenarios, respectively (values taken from Hendi et al., 2020a, b).

Results and Discussion

Figures 3 to 5 illustrate the strain distributions computed using the combined analytical technique for scenarios 1 to 3. A comparison of polymer-based mud- and cement-filled boreholes is shown in Figure 6. In all scenarios, the sensitivity of the HWC increases as the angle of incidence increases.

Table 1. Geometric parameters used in analytical stimulation of the response of fibre-optic cable. The cable and borehole diameters are determined using common values found in the field. In this study, the rock formation is assumed to stretch to infinity in both width and height.

Geometric parameters			
Scenario	1	2	3
Borehole diameter (mm)	116	116	25 (cable size)–116
Borehole height (m)	2	2	2
Cable diameter (mm)	25	25	25
Cable length (m)	0.5	0.5	0.5
Formation diameter (mm)	2	2	2
Formation length (m)	2	2	2

Scenario 1

The results of scenario 1 help in determining how cement properties should be designed to obtain the optimum response from HWC. The Young's modulus of the cement has been changed in this scenario from one associated with soft material to one with properties nearer those of the surrounding rock. The results of this study show that, as the layer properties of the cement (Table 1) surrounding the cable near those of the rock formation, the performance of the HWC fibre decreases (Figure 3).

Scenario 2

The results of scenario 2 reveal more about how mud qualities affect HWC optimum response at different angles of incidence. Two common types of mud used frequently in industry (polymer-based mud and invert-emulsion mud) were considered in this scenario and their respective effects are depicted in Figure 4. The results showed that the HWC fibre performed better in the denser polymer-based mud.

Table 2. Layer (domain) properties used for modelling of the response of helically wound cable to different borehole-filling materials and changes in borehole diameter (values from Hendi et al, 2020a, b).

Material	Density (ρ) (kg/m^3)	Compressional velocity (Vp) (m/s)	Young's modulus (E) (GPa)	Poisson's ratio (v) (-)
Rock formation	2734	5736	60	0.28
Cable	1200	1183	1.6	0.15
Cement	2240	2728	15-60	0.2
Invert-emulsion mud	1570	1540	-	-
Polymer-based mud	1830	2350	-	-

Scenario 3

In scenario 3, the impact of borehole diameter on the HWC response in the case of a hard cement-filled borehole (Young's modulus equivalent to that of the surrounding rock) was investigated. In this scenario, boreholes of various diameters were used, varying between 116 mm and 25 mm (i.e., equal to the diameter of the cable; Figure 5). The results indicate that a larger borehole diameter results in better performance of the HWC optical fibre. Responses increase significantly when the borehole diameter is nearly double that of the optic-fibre cable; after that point, borehole diameter has a less significant impact on fibre-optic cable response.

Scenario 4

The performance of HWC fibre was also investigated as a function of surrounding material (cement vs polymer-based mud; Figure 6). Theoretical results indicate that the HWC fibre performs better in polymer-based mud than cement.

Conclusion

Using an integrated analytical technique, strain values in helically wound fibre-optic cable were calculated for three scenarios representing realistic situations, based on the effects of the borehole-filling material and change in borehole diameter on the axial and radial strains of the HWC. The results of this analysis reveal that HWC fibre performs better when the Young's modulus of the cement filling the borehole is low (indicating material softer than the surrounding rock formation). In the case of boreholes filled with polymer-based mud, the performance of the HWC fibre is far higher compared to that achieved using invert-emulsion mud. When HWC is embedded in the denser polymer-based mud, it has a higher sensitivity than when it is embedded in cement. The diameter of the borehole and the sensitivity of the HWC share a direct relationship: when the borehole diameter is approximately two times that of the cable, HWC sensitivity reaches its maximum.

The findings of this study can be considered one of the primary steps in the development of a stress-measurement technique based on fibre-optic cable, which allows for improved precision and accuracy in recording results. By employing stress-measuring techniques, British Columbia mining firms may see a boost in production, while reducing the number of instability events and therefore improving mine safety.

Future Research Directions

The results of this study will be used to build a bench-top experiment to stimulate fibre-optic cable response under simulated field conditions to estimate in situ stresses. The findings will be used as a guideline for installing distributed fibre-optic cable and improving its overall performance. This work will be undertaken in January 2022 and final results published as part of the lead author's doctoral thesis in 2024.

Acknowledgments

The authors thank the Centre for Innovation in Mineral Resource Engineering (CIMRE) and Geoscience BC for their financial support. The authors would also like to thank to A. Mehrabifard for his input and constructive comments on aspects of this work.

References

Amadei, B. and Stephansson, O. (1997): Rock Stress and its Measurement; Springer, Dordrecht, 490 p., URL <https://doi.org/10.1007/978-94-011-5346-1>.

Bakku, S.K. (2015): Fracture characterization from seismic measurements in a borehole; Ph.D. thesis, Massachusetts Institute of Technology, Cambridge, Massachusetts, 227 p.

Den Boer J.J., Mateeva A.A, Pearce J.G., Mestayer J.J., Birch W., Lopez J.L., Hornman, J.C. and Kuvshinov, B.N. (2016): Detecting broadside acoustic signals with a fiber optical distributed acoustic sensing (DAS) assembly; United States Patent and Trademark Office, patent application 15/259348, URL <https://www.uspto.gov> [November 2021].

Haimson, B.C. and Cornet, F.H. (2003): ISRM suggested methods for rock stress estimation—part 3: hydraulic fracturing (HF) and/or hydraulic testing of pre-existing fractures (HTPF); International Journal of Rock Mechanics and Mining Sciences, v. 40, no. 7–8, p. 1011–1020, URL <https://doi.org/10.1016/j.ijrmms.2003.08.002>.

Hartog, A.H. (2017): An Introduction to Distributed Fibre Optic Cable Sensors; Series in Fibre Optic Sensors (A. Mendez, ser. Ed.), 1st edition, CRC Press, Boca Raton, Florida, 471 p., URL <https://doi.org/10.1201/9781315119014>.

Hendi, S., Gorjian, M. and Hawkes, C.D. (2020a). A workflow for predicting the effect of bedding and drilling-induced stresses on borehole sonic logging, with application to the Montney Formation, northeastern British Columbia; 54th U.S. Rock Mechanics/Geomechanics Symposium, June 28–July 1, 2020, virtual event, abstract no. ARMA-2020-2018.

Hendi, S., Gorjian, M., Bellefleur, G., Hawkes, C. D. and White, D. (2020b): Investigation of the effects of surrounding media on the distributed acoustic sensing of helically wound fiber-optic cable with application to the New Afton deposit, British Columbia; Solid Earth Discussions, preprint, 31 p., URL <https://doi.org/10.5194/se-2020-197>.

Hornman, J.C. (2017). Field trial of seismic recording using distributed acoustic sensing with broadside sensitive fibre-optic cables; Geophysical Prospecting, v. 65, no. 1, p. 35–46, URL <https://doi.org/10.1111/1365-2478.12358>.

Kamal, S.Z. (2014): Fiber optic sensing: evolution to value; SPE Intelligent Energy Conference and Exhibition; Society of Petroleum Engineers, April 1–3, 2014, Utrecht, Netherlands, abstract no. SPE-167907-MS, URL <https://doi.org/10.2118/167907-MS>.

Kuvshinov, B.N. (2016): Interaction of helically wound fibre-optic cables with plane seismic waves; Geophysical Prospecting, v. 64, no. 3, p. 671–688.

Mateeva, A., Lopez, J., Potters, H., Mestayer, J., Cox, B., Kiyashchenko, D., Wills, P., Grandi, S., Hornman, K., Kuvshinov, B., Berlang, W, Yang, Z. and Detomo, R. (2014): Distributed acoustic sensing for reservoir monitoring with vertical seismic profiling; *in* Vertical Seismic Profiling and Microseismicity Frontiers, M.N. Alfaraj (ed.); Geophysical Prospecting, v. 62, no. 4, p. 679–692, URL <https://doi.org/10.1111/1365-2478.12116>.

Miah, K. and Potter, D.K. (2017). A review of hybrid fiber-optic distributed simultaneous vibration and temperature sensing technology and its geophysical applications; Sensors, v. 17, no. 11, art. 2511, URL <https://doi.org/10.3390/s17112511>.

Miller, D.E., Daley, T.M., White, D., Freifeld, B.M., Robertson, M., Cocker, J., and Craven, M. (2016). Simultaneous acquisition of distributed acoustic sensing VSP with multi-mode and single-mode fibre-optic cables and 3C-geophones at the Aquistore CO_2 storage site; Canadian Society of Exploration Geophysicists, CSEG Recorder, v. 41, no. 6, p. 28–33.

Molenaar, M.M., Hill, D., Webster, P., Fidan, E., and Birch, B. (2012). First downhole application of distributed acoustic sensing for hydraulic-fracturing monitoring and diagnostics; SPE Drilling & Completion, v. 27, no. 1, p. 32–38, URL <https://doi.org/10.2118/140561-PA>.

Naruse, H., Uehara, H., Deguchi, T., Fujihashi, K., Onishi, M., Espinoza, R., Guzman, C., Pardo, C., Ortega, C. and Pinto, M. (2007). Application of a distributed fibre optic strain sensing system to monitoring changes in the state of an underground mine; Measurement Science and Technology, v. 18, no. 10, art. 3202, URL <https://doi.org/10.1088/0957-0233/18/10/S23>.

Nath, D.K., Finley, D.B. and Kaura, J.D. (2006): Real-time fiber-optic distributed temperature sensing (DTS) – new applications in the oilfield; SPE Annual Technical Conference and Exhibition; Society of Petroleum Engineers, September 24–27, 2006, San Antonio, Texas, abstract no. SPE-103069-MS, URL <https://doi.org 10.2118/103069-MS>.

Sjöberg, J. and Klasson, H. (2003). Stress measurements in deep boreholes using the Borre (SSPB) probe; International Journal of Rock Mechanics and Mining Sciences, v. 40, no. 7, p. 1205–1223, URL <https://doi.org/10.1016/S1365-1609(03)00115-1>.

Zhao, Y., Zhang, N. and Si, G. (2016). A fiber Bragg grating-based monitoring system for roof safety control in underground coal mining; Sensors, v. 16, no. 10, art. 1759, URL <https://doi.org/10.3390/s16101759>.

Zhou, W., Zhang, P., Wu, R. and Hu, X. (2019). Dynamic monitoring the deformation and failure of extra-thick coal seam floor in deep mining; Journal of Applied Geophysics, v. 163, p. 132–138.

Parametric Method for Tailings-Dam Breaches and its Application to the Breach Event at the Mount Polley Mine, South-Central British Columbia (NTS 093A)

D. Adria[1], **The University of British Columbia, Vancouver, British Columbia, dadria@eoas.ubc.ca**

S. McDougall, The University of British Columbia, Vancouver, British Columbia

S.G. Evans, University of Waterloo, Waterloo, Ontario

Adria, D., McDougall, S. and Evans, S.G. (2022): Parametric method for tailings-dam breaches and its application to the breach event at the Mount Polley mine, south-central British Columbia (NTS 093A); *in* Geoscience BC Summary of Activities 2021: Minerals, Geoscience BC, Report 2022-01, p. 81–92.

Introduction

Tailings-dam breach assessments (TDBAs) estimate the inundation area, depths and velocities of a tailings flow that result from a possible tailings-dam breach. These studies inform the potential consequences of a breach of a tailings-storage facility (TSF) and are used in risk assessments and emergency-response planning. Tailings-dam breach assessments involve many uncertainties, as described in the *Guidelines for Tailings Dam Breach Analysis*, prepared and published by the Canadian Dam Association (2021). In recent years, several databases, case-history reviews and statistical analyses (e.g., Ghahramani et al., 2020; Rana et al., 2021) have been developed to address knowledge gaps and to better understand the initiation and field behaviour of tailings flows.

Outflow volumes, runout distances and inundation areas are useful descriptors for statistical analysis of tailings-dam breaches. Most forward analysis (prediction) used in industry relies on numerical models rather than statistical measures to determine consequences. The general procedure includes the development of a breach hydrograph to estimate the volume and flow rate through the tailings-dam breach. A numerical runout model then uses the equations of conservation of mass and momentum to estimate the tailings-flow depth and velocity through the downstream area, for which the breach hydrograph, downstream terrain and flow characteristics (rheology) of the tailings are used as inputs. The modelled depths and velocities give more nuance and detail to consequence estimates than could be achieved by statistical analysis alone. There are numerous numerical methods used for TDBAs, and some model set-ups allow for the breach hydrograph and runout model to be determined concurrently.

[1]The lead author is a 2021 Geoscience BC Scholarship recipient.

This publication is also available, free of charge, as colour digital files in Adobe Acrobat® PDF format from the Geoscience BC website: http://geosciencebc.com/updates/summary-of-activities/.

Tailings-dam breach assessments are relatively new, so the majority of methods or numerical models are borrowed either from landslide modelling (e.g., DAN3D) or from dam-breach studies for hydro dams (e.g., DAMBRK, HEC-RAS), which have a longer history of use (Canadian Dam Association, 2021). The Canadian Dam Association 2007, Washington State 1992 and FEMA 2013 guidelines for hydro-dam breach studies are referred to for TDBAs in particular (Canadian Dam Association, 2021).

The parametric method is well utilized in water-dam breach studies to develop the breach hydrograph (Wahl, 1998, 2004; Froehlich, 2008; Goodell et al., 2018). The parametric method dynamically computes the breach discharge using the common weir equation (Francis, 1868). The breach parameters (ultimate breach size, shape and development time) are defined by the user. The breach width increases and the breach invert decreases to their ultimate values over the duration of the breach development, while the water-surface elevation is recalculated at every time step based on the previous discharge and the defined stage-storage curve. There is limited guidance available from the Canadian Dam Association or International Commission on Large Dams (ICOLD) concerning whether the differences in design, construction and operation of tailings facilities compared to water-retaining dams, and the non-Newtonian flow characteristics of tailings, render the parametric method invalid for TDBAs.

This technical paper explores the application of the parametric-breach method for two tailings-dam breaches and the resultant tailings flows: the Mount Polley event in British Columbia in 2014 and the Feijão event in Brazil in 2019. By comparing the modelled results based on standard practice borrowed from water dams to the field behaviour of historical tailings-breach events, any deficiencies with the method may be identified. Modelling of more than 20 historical events from the Ghahramani et al. (2020) and Rana et al. (2021) databases is in progress, together with physical experiments of tailings-dam breaches, to determine whether trends or observations from the two examples presented are consistent and applicable to observed processes across different cases or various scenarios; however, these more extensive studies are not covered in this paper.

Modelling Methodology

Breach Parameters

A downside commonly noted with the parametric approach (Wahl, 2004; Froehlich, 2008) is the uncertainty in estimating the breach parameters for a dam-breach study. Martin et al. (2015) further noted that common regression equations to predict the parameters are typically based only on water-dam breach events, introducing more uncertainty when applied to TDBAs. Fortunately for back analysis, the breach size and shape can be measured after the event, partially sidestepping this issue. The breach development is defined as the time from initiation of breach until the ultimate size is reached, and is equivalent to breach-formation time (Wahl, 1998; Froehlich, 2008). The development time can also be estimated based on the event narrative, but it has more uncertainty than the other breach parameters for back analysis.

Instant Dam Breaches

The weir equation and parametric approach have been shown to be appropriate for near-instant failures of water-retaining dams, as may be seen in the structural collapse of a concrete-arch dam (e.g., the Malpasset dam failure; Brunner et al., 2018). The breach-development time is set to 0 seconds (s) or some other nominally short time, so the ultimate breach forms almost instantly. In 1892, Ritter derived an analytical set of equations for a perfectly instantaneous breach, ignoring frictional and turbulence losses. The Ritter set can be reduced to the same form as the weir equation, with a weir coefficient of 0.928.

The weir coefficient is used to represent the efficiency of the flow through the weir and varies depending on the size and shape of the weir, upstream conditions and downstream conditions. Typical metric values for constructed weirs in steady-flow conditions range from 1.4 to 2.3 (Brater and King, 1976; Brunner, 2021). Brunner (2014) suggested that breach flow is not efficient and lower coefficient values are thus warranted for erosional breaches, considering that dam breaches have greater turbulence and violence than a constructed weir. Weir coefficients for erosional breaches should therefore be around 1.44 and could range from 1.1 to 1.7 (Goodell and Brunner, 2012). An instantaneous dam breach would be correspondingly more turbulent and, conceptually, the weir coefficient should be lower still. Despite valid criticism that ignoring the losses overpredicts the leading edge of the outflow, the Ritter set of equations matches experimental results closely at the location of the instantaneous breach (Schoklitsch, 1917; Arbuthnot and Strange, 1960).

Khahledi et al. (2015) assessed weir coefficients for non-Newtonian fluids, specifically including kaolin and bentonite mining slurries. They found the non-Newtonian fluids to have coefficients similar to that of water. The experiments were performed under steady-state flow conditions, using flume set-ups similar to constructed weirs and relatively weak rheologies, unlike those of typical tailings deposits within TSFs. Consequently, it is not clear if the conclusions are applicable to liquefied tailings-dam breaches.

Outflow Volumes

Stage-Storage Curves

In the parametric method, the outflow volume can either be represented with a single stage-storage curve, or routed dynamically with a numerical model if reservoir bathymetry data exist. A stage-storage curve can be derived from an idealized shape approximating the reservoir, or a customized curve can be calculated from an irregular shape if bathymetry exists.

The dynamic routing approach is held to be more accurate, but the stage-storage curve approach is attractive for several reasons (Goodell and Wahlin, 2009). The abstraction of the three-dimensional shape of the reservoir into the two-dimensional curve removes the need for conservation equations of momentum and mass, greatly decreasing the computational requirement. With a stage-storage curve, the parametric method could even be implemented in spreadsheet software. Additionally, if bathymetry data are not available for the reservoir, a stage-storage curve can be approximated with an idealized shape, as in Walder and O'Connor (1997).

The downside to the stage-storage curve is the implication that the reservoir has a level water surface during the entirety of the breach (i.e., level-pool routing). If the breach progresses faster than the reservoir is able to self level, then the peak flow of the discharge is overestimated with the level-pool approach. Goodell and Wahlin (2009) provided charts that consider several factors (reservoir length, reservoir depth, development time) to estimate the error associated with level-pool routing for water reservoirs.

Tailings Outflow Volumes and Depressions

The total outflow volumes of historical tailings-dam breach events, which are commonly reported in the investigative work afterwards, have been compiled by Ghahramani et al. (2020) and Rana et al. (2021). Unfortunately, a single value for the volume is insufficient to develop a stage-storage curve. The pond volumes and post-failure depression of the tailings can have varying shapes, and the reported volume is not always distributed between the pond and tailings volumes, which may have different shapes. The shape of the depression and distribution of pond and tailings can be informed by profiles of the depression and photos (if available); however, converting these observations into a stage-storage curve is a qualitative, subjective and difficult task.

A linear relation between the total outflow volume at the dam-crest elevation and zero volume at the breach-invert elevation corresponds to a vertical-prism shape. Intuitively, this shape is not realistic, but it is the quickest and simplest approximation. A valley with constant wall and floor slope (an idealization for many water reservoirs) could be approximated with a tetrahedron, following Walder and O'Connor (1997). A common assumption in TDBAs is that the post-failure depression of the tailings in the facility is a semi-cone with a constant slope (Canadian Dam Association, 2021). These three shapes are shown in Figure 1a, along with a half bowl, funnel and horn for comparison. All of the shapes have the same height of 5 m and are limited to be within an arbitrary boundary of 20 m by 10 m. The general form of the elevation-volume curve for each idealized shape is shown in Figure 1b, where the curves are expressed in relative terms. The semi-cone, tetrahedron and funnel have the same mathematical form and are represented with single curve shape in Figure 1b. It is apparent that, within the same boundary, each shape has a different total volume. Figure 1c shows the actual elevation-volume curve for each shape, demonstrating the difference in shape and volume for all the shapes. The red faces in Figure 1a would be against the breached section and the coloured faces serve to identify the shapes with the corresponding coloured curves in Figure 1c.

Using an idealized shape results in a partial match to many cases in the databases referred to above. A stage-storage curve developed from an ideal shape could be scaled to match the outflow volume from a historical case; however, such an approach is difficult to justify for back analysis if the idealized shape results in a substantially different volume. For example, the failure at Merriespruit in 1994 had a post-failure depression that is a combination of bowl, funnel and horn shapes. Using the average residual slope of 10% (Blight and Fourie, 2003), a hypothetical semi-cone gives an outflow volume of 4.6 million m^3, which is almost 10 times more than the observed value of 0.6 million m^3 (Wagener, 1997).

Schoeman (2018) presented an alternative stage-storage method specifically for tailings-dam breaches, termed the 'inclined slice method'. With any continuous and idealized shape, the volume is sliced at equal intervals at an angle equal to the residual slope of the tailings; the difference in volume between any two elevation intervals represents the volume for that elevation slice. With this method, the majority of the outflow volume is 'placed' at lower elevations, so the peak discharge occurs later and is lower in magnitude compared to a level-pool breach (with constant outflow volumes and breach parameters). The linear curve lies between the level-pool and inclined curves; therefore, its peak discharge magnitude and timing are between the results of the other curves as well.

According to Schoeman, the inclined nature intuitively represents a more realistic representation of the flow of tailings mobilized due to erosion or slumping during a tailings-dam breach. A hybrid stage-storage curve was first proposed by the Canadian Dam Association's Tailings Dam Breach Working Group (Al-Mamun et al., 2019). Conceptually, the volume at higher elevations is sliced horizontally, like a typical stage-storage curve for the pond volume, while the volume at the lower elevations is sliced at an incline for the tailings volume. However, no validation of the main principle or hybrid refinement through comparison to historical tailings-dam breaches or physical experiments has been completed to date.

Example Applications

Mount Polley, British Columbia, Canada

The Mount Polley TSF failed early in the morning on August 4, 2014. The crest of the dam slumped due to foundation failure, resulting in a sudden loss of containment of the large pond within the facility at the time. The flow overtopped and eroded through the slumped centreline dam. Wide-scale tailings liquefaction was not observed, but a large volume was transported out of the facility by the pond discharge (Morgenstern et al., 2015). The location and imagery of the Mount Polley failure are shown in Figure 2.

The dam height was roughly 40 m at the time and location of the failure. The breach width at the invert was 45 m, and 270 m at the dam crest (Morgenstern et al., 2015). The total released volume (water and tailings material) was 25 million m^3, with the majority (almost 70%) being water (Cuervo et al., 2017). There is limited information regarding the development time for the breach; however, the timeline presented in the Chief Inspector of Mines Investigation Report (BC Ministry of Energy, Mines and Low Carbon Innovation, 2015) provides some bounds. Substantial volumes began discharging at 1:08 a.m. when the power lines near the breach location were destroyed. Approximately 3.5 hours later, the V-cut through the dam was observed to be roughly 30 m deep, suggesting a development time of around 4 hours. Video from a helicopter flight at around 7:45 a.m. showed the erosion had fully progressed through the dam and the breach flow was relatively low (Morgenstern et al., 2015). The flow was noted to have fully ceased by around 4:00 p.m. the same day.

The helicopter video and aerial imagery show that dendritic drainage channels almost 2 km long had eroded throughout the tailings deposit, as annotated in Figure 2b. The eroded shape was idealized with a stage-storage curve to a tetrahedron, while the pond was approximated as a vertical prism using the pond volume and surface area from the Mount

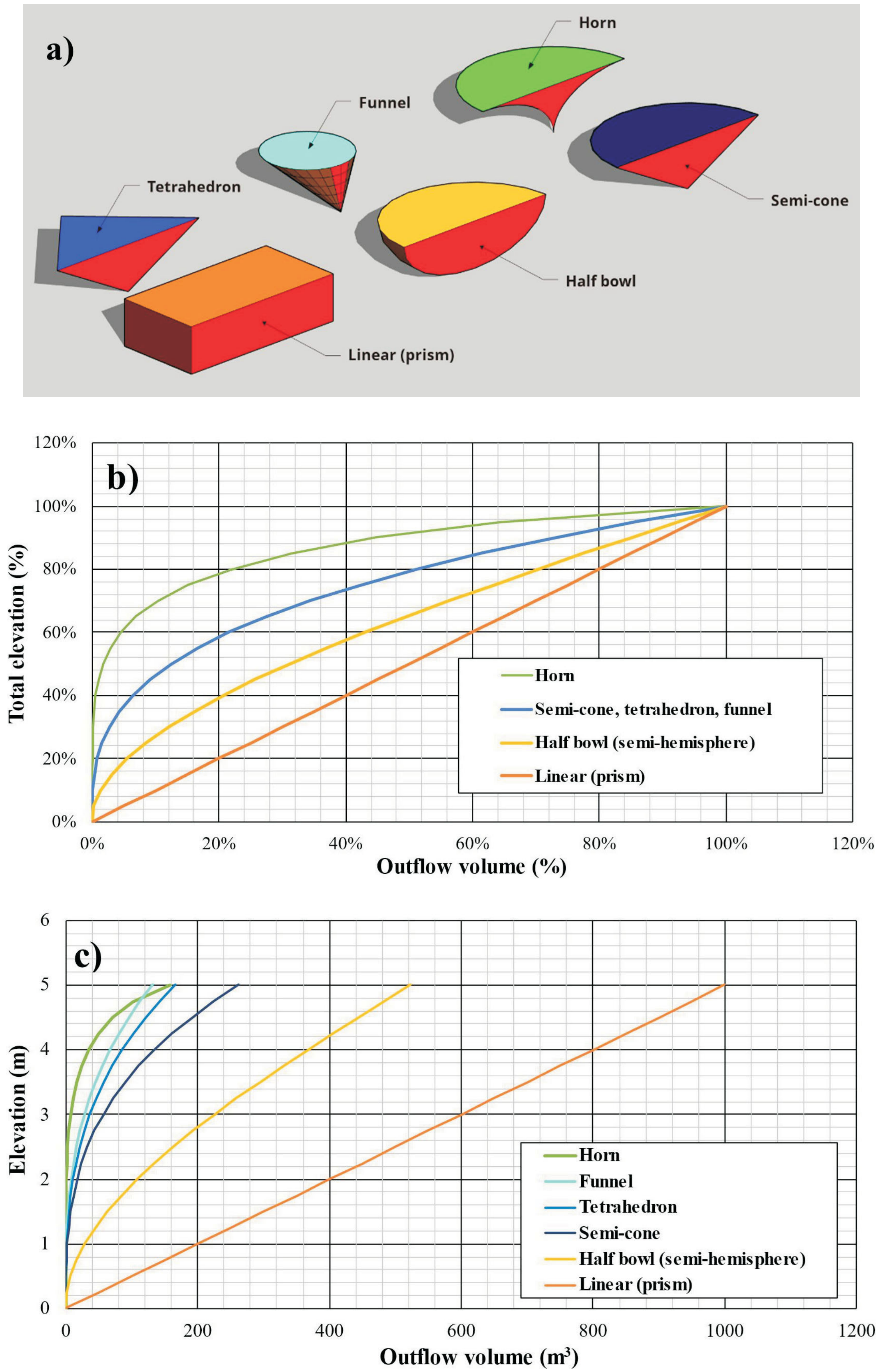

Figure 1. **a)** Six idealized shapes for the post-failure depression of tailings facilities. **b)** Stage-storage curves for the idealized shapes in relative values. **c)** Stage-storage curves for the idealized shapes in real values.

Polley TSF (similar to Petkovšek et al., 2020). Using Schoeman's inclined slice method, an alternative stage-storage curve was generated based on the first curve. A hybrid curve was developed in which the tailings volume was sliced on an incline and the pond volume was level-pool. Lastly, a linear relation was considered as a final comparison. Figure 3 shows the four stage-storage curves. The datum was set as the breach invert. Since the breach was erosional, the weir coefficient was set to the value of 1.44 in the parametric model, representing an 'average' erosional-breach weir scenario (Goodell and Brunner, 2012).

Feijão, Minas Gerais, Brazil

On January 25, 2019, Dam I at the Feijão mine suddenly and instantly collapsed. There was no pond present in the facility at the time of failure but the tailings underwent liquefaction, resulting in a catastrophic failure (Robertson et al., 2019). The location and imagery of the Feijão failure are shown in Figure 4.

Dam I was 80 m high at the time of the failure, and the breach was 580 m and 100 m wide at the dam crest and

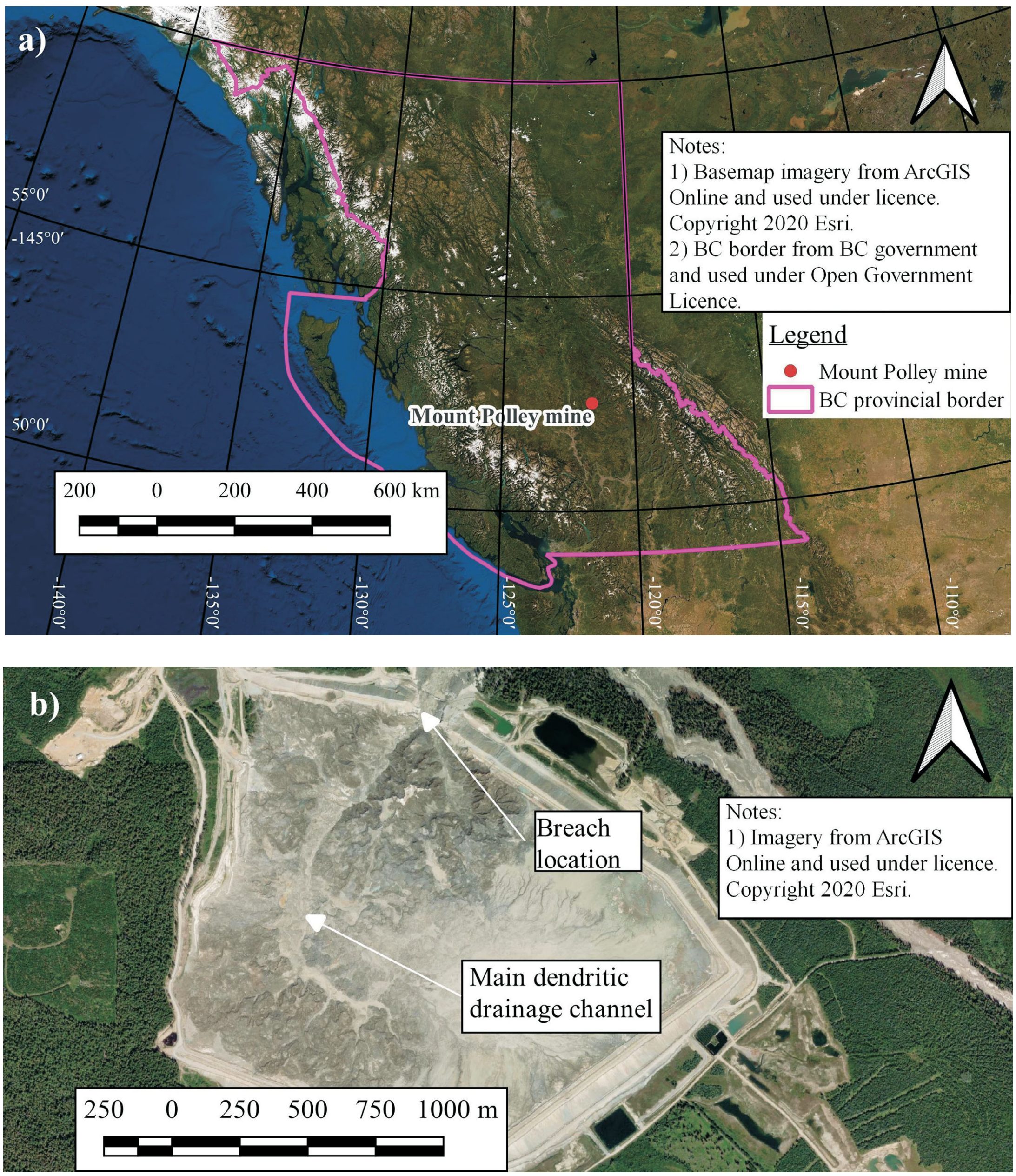

Figure 2. a) Location of the Mount Polley tailings-storage facility. **b)** Post-failure aerial imagery of the Mount Polley tailings-storage facility.

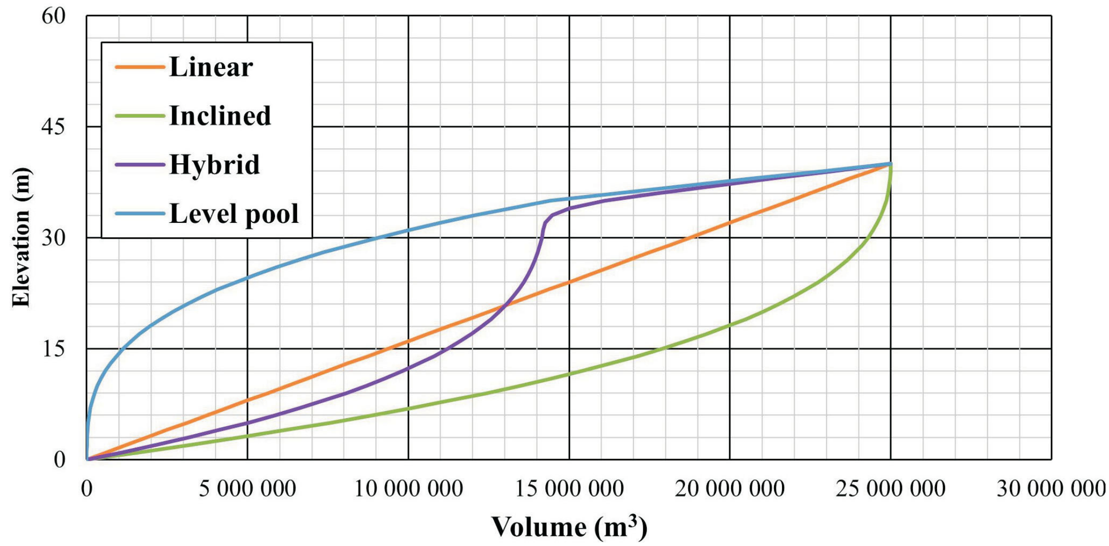

Figure 3. Estimated stage-storage curves for released tailings material and water in the Mount Polley breach event.

breach invert, respectively. LiDAR obtained before and after the failure showed 9.7 million m^3 of tailings discharged (Robertson et al., 2019). The failure was captured on a monitoring camera (CAM1), which showed that the breach had fully progressed to the invert within 6 s and the volume had discharged within 5 min (Robertson et al., 2019). As a simplification, the breach weir was set to be fully formed at the start of the hydrograph, with a weir coefficient of 0.928 based on Ritter (1892).

The photos of the post-failure depression and post-failure LiDAR from Robertson et al. (2019) show that the semi-cone is a reasonable approximation for the remnant tailings deposit behind the crest of the dam. The ideal semi-cone gave an estimate of 6.2 million m^3. Since the volume of the tailings in front of the dam crest was a large portion of the release volume, a separate shape was used. Based on the observed breach shape, dam height and dam slope, an irregular triangular prism shape gave 2.7 million m^3. These two idealized shapes gave a total estimate of 8.9 million m^3, which is quite close to the observed value of 9.7 million m^3; this curve was scaled to the correct value of 9.7 million m^3 A level-pool curve and inclined-slice curve were generated from those idealized shapes, as well as a linear plot for comparison. Figure 5 shows the three stage-storage curves. The datum was set as the breach invert. No hybrid curve was developed as there was no pond in the facility at the time of failure to consider as level-pool while the tailings remained inclined.

Results and Discussion

Mount Polley

Figure 6 shows the four breach hydrographs for the four developed stage-storage curves, with all other inputs remaining constant. The shape of the stage-storage curve has a clear impact on the peak discharge, the shape and the duration of the hydrograph.

The level-pool curve fully discharged the 25 million m^3 volume by 4:00 a.m., almost 12 hours before the actual arrest of the flow around 4:00 p.m. In fact, the development time needs to be increased to more than 16 hrs for the discharge to last until 4:00 p.m. with a level-pool curve (not shown here), contrary to the helicopter video that indicated the breach had essentially progressed to its ultimate size by 8:00 a.m. Inputting the facility dimensions into the charts from Goodell and Wahlin (2009) gives an estimated error (in using a stage-storage curve rather than a dynamic reservoir) only on the order of 3–5% of the peak flow, suggesting the peak flow is not overestimated, due largely to the size of the facility.

It appears that Schoeman's alternate slicing method has some validity for simulating the erosion and slumping of tailings if the tailings are not liquefied. The hydrographs for Mount Polley using the inclined, linear or hybrid curves had flows between 250 m^3/s and 650 m^3/s at 8:00 a.m., and approximately 20 m^3/s at 4:00 p.m., which match the video and timeline much better. The hybrid curve results in a double peak, where the first peak corresponds to the outflow when dominated by the initial pond release and the second peak corresponds to the additional erosion and slumping of tailings. Cuervo et al. (2017) noted that field observations downstream of the breach suggested the erosion occurred in pulses, partially corroborating the hybrid curve. It cannot be confirmed, however, that the pulses originated solely from the breach and not during the runout process.

Feijão

Figure 7 shows the three breach hydrographs for the three developed stage-storage curves, with all other inputs remaining constant.

Since the breach weir was instantly fully formed, there is a discontinuity in the discharge as it jumps to the peak flow. At the first time-step, the discharge is dependant only on the breach geometry; therefore, all stage-storage curves have the same initial peak-flow magnitude of 179 000 m^3/s.

The discharge trails off similarly with all three curves in Figure 7a. Figure 7b gives insight into their fit to the observed event and timing. At 5 min after the initiation of the breach, the level-pool hydrograph has discharged 9.5 million m^3 (98% of the total observed outflow volume), whereas the linear and inclined hydrographs have discharged only 8.3 million m^3 and 6.6 million m^3, respectively. Even when the weir coefficient is increased to 1.7 (a value appropriate for steady-state Newtonian flow over a constructed weir), the predicted hydrograph using the inclined stage-storage curve (not shown here) still discharges only 7.4 million m^3 at 5 min. When the tailings are liquefied, it appears the flow behaviour may be better represented with a stage-storage curve appropriate for water, as shown with the level-pool outflow volumes at 5 min. Schoeman's inclined-slice approach takes more than an

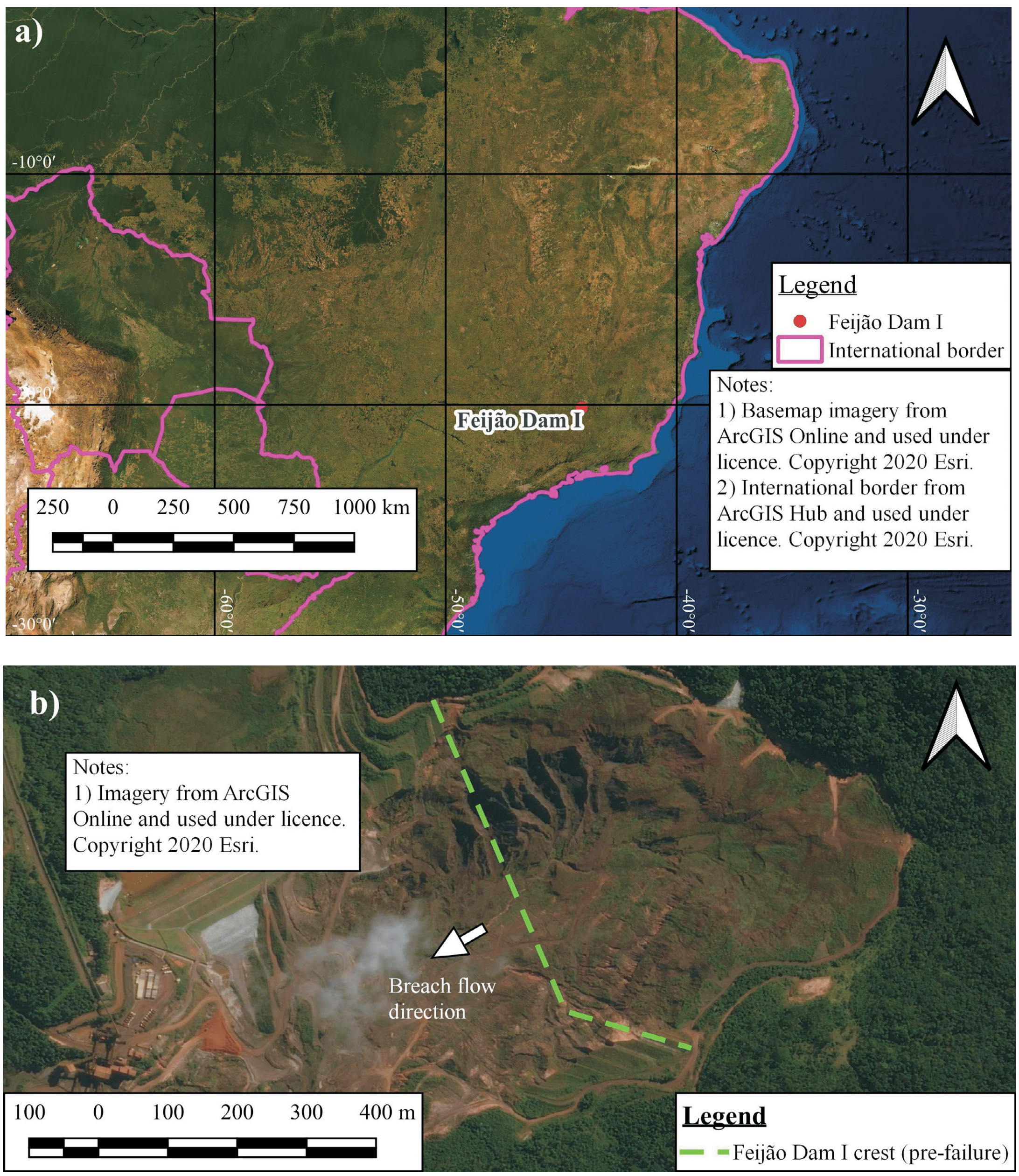

Figure 4. a) Location of Feijão Dam I. **b)** Post-failure aerial imagery of Feijão Dam I.

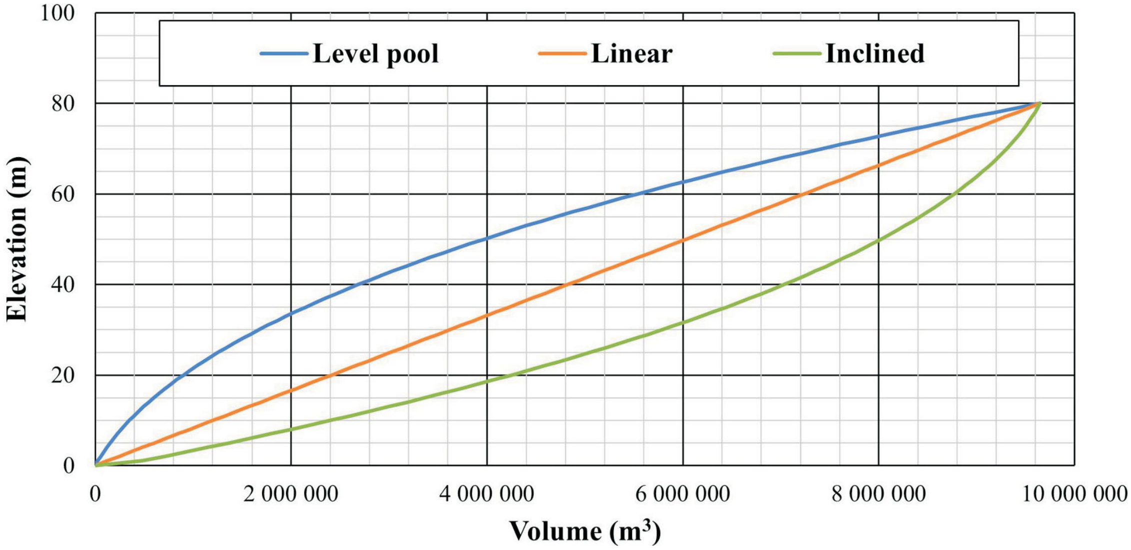

Figure 5. Estimated stage-storage curves for the released tailings in the Feijão breach event.

hour to discharge the observed outflow volume, even when using unrealistically high weir coefficients for an instantaneous breach scenario.

When the level-pool curve is combined with a larger weir coefficient, the peak discharge increases and the hydrograph duration shortens by roughly the same ratio between the larger weir coefficient and the Ritter weir coefficient. For example, using a weir coefficient of 1.44 for the hydrograph (not shown here) rather than 0.928 increases the peak flow to 277 000 m^3/s and 9.5 M m^3 of the outflow volume discharges in 3.2 min. The results presented here suggest that the Ritter weir coefficient matches the observed timing of 5 min for the Feijão event as well, but further comparisons are warranted to confirm this finding.

Concluding Remarks and Future Work

The Mount Polley and Feijão events are among the better documented tailings-dam breach events. Determining the correct sequence of events and the shape and volume of liquefied tailings, non-liquefied tailings and ponds to develop a sophisticated stage-storage curve (e.g., the hybrid curve used in the Mount Polley analysis) is challenging; determining a curve that perfectly recreates the discharge is practically impossible. The process for developing a stage-storage curve is even more uncertain and subjective when there is less information available, which is the case for older events (e.g., the El Cobre event in Chile, 1965; Torres and Brio, 1966) or events with limited impact and reporting (e.g., Tapo Canyon in the United States, 1994; Harder and Stewart, 1996). The linear stage-storage curve hydrographs did not perform the best for either case but were also not the worst. Given the simplicity of the linear stage-storage curve and the uncertainty in the historical events, it appears that it is a reasonable first approximation for any given back analysis with limited information. When observations of historical cases permit, or when conducting forward analysis (prediction) TDBAs of existing or proposed facilities, the more sophisticated stage-storage curve approach or even dynamic numerical models should be used. The au-

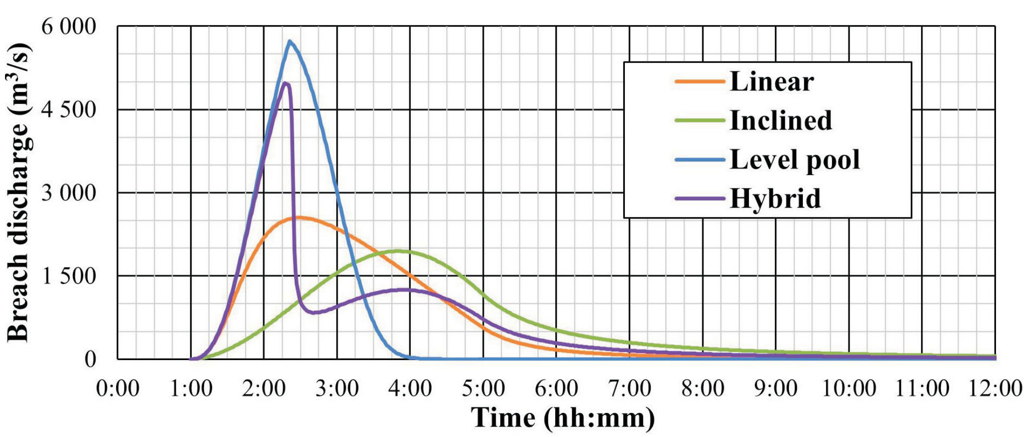

Figure 6. Modelled breach hydrograph for the Mount Polley event.

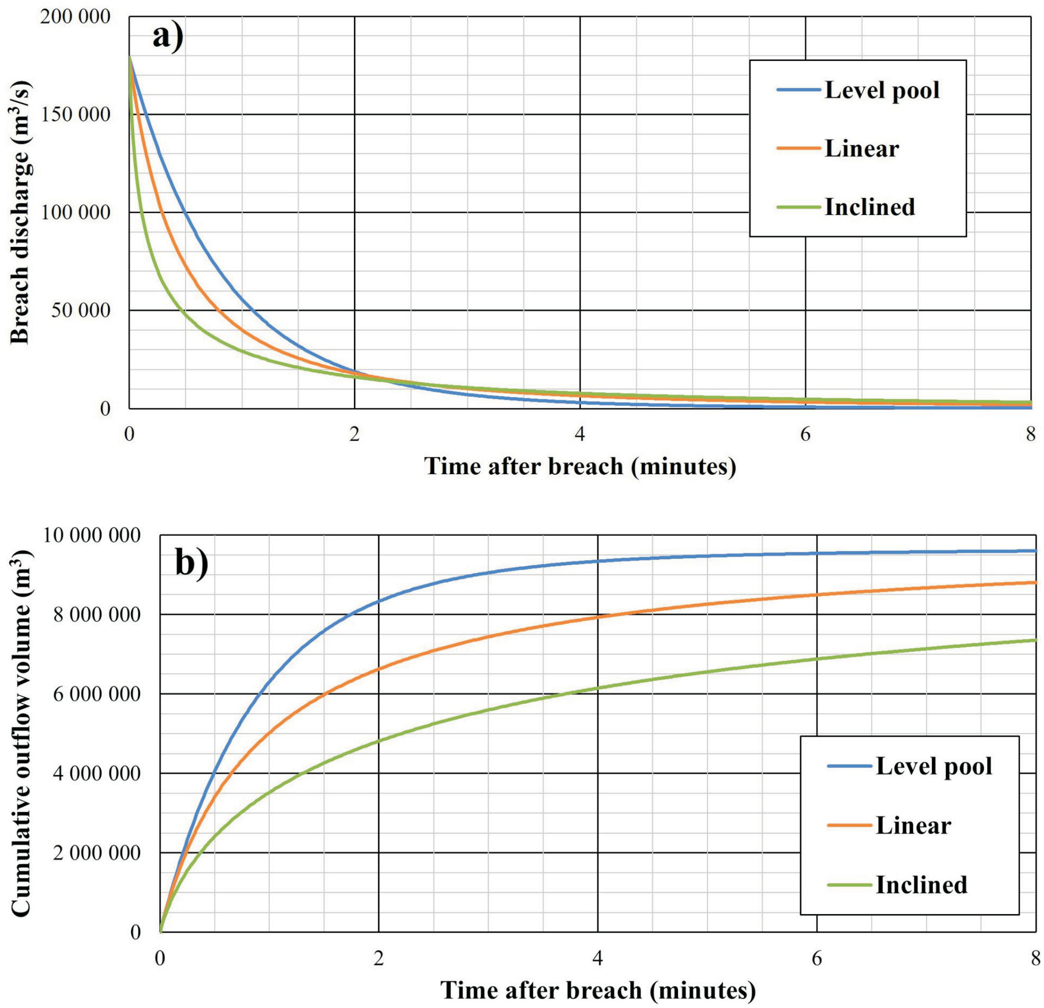

Figure 7. a) Modelled breach hydrographs. **b)** Cumulative outflow volumes for the Feijão event.

thors note that both Mount Polley and Feijão have post-failure LiDAR data, but neither are available to the public, thus preventing the comparison of idealized stage-storage curves to the actual irregular shape or dynamic modelling of the tailings depression during the breach.

The breach modelling outlined here is the first step in validating or refining the parametric dam-breach method for TDBAs; however, the back analysis includes the runout modelling as well. The overall goal of the current modelling is to provide a free and accessible repository of verified inputs for the breach and runout characteristics, numerical model set-ups and calibrated results of historical tailings-dam breaches and resultant tailings flows. Back analysis is informed by focused hindsight; the breach process, extent of tailings liquefaction, breach parameters and outflow volumes are known for the modelled events. For forward analysis, determining these elements is a large part of the challenge associated with TDBAs (Canadian Dam Association, 2021). The uncertainty and sensitivity have not been quantified for TDBAs, but both are needed to reduce the unknown risk in consequence estimates (Adria et al., 2021). The databases from Ghahramani et al. (2020) and Rana et al. (2021) can provide estimates of the uncertainty in the modelled inputs, while the numerical-model database in progress can be used to estimate the sensitivity of consequences to the inputs.

Acknowledgments

The authors thank W.A. Take for his review and helpful comments on this manuscript. The primary author wishes to thank V. Martin and others at Knight Piésold for the mentorship received and knowledge shared over the years. The content of this paper was directly influenced by many discussions with Ms. Martin and project work with Knight Piésold. This research is part of the Canadian Tailings Dam Breach Research (CanBreach) Project, which is supported by funding through an NSERC Collaborative Research Development Grant with the following industrial partners: Imperial Oil Resources Inc., Suncor Energy Inc., BGC Engineering Inc., Golder Associates Ltd. and Klohn Crippen

Berger. Financial support through a scholarship to the lead author was also provided by Geoscience BC.

References

Al-Mamun, M., Martin, V. and Mohseni, O. (2019): CDA Workshop on Tailings Dam Breach Analysis; Canadian Dam Association Annual Conference, Calgary, Alberta.

Arbuthnot, G.L. Jr. and Strange, J.N. (1960): Floods resulting from suddenly breached dams; U.S. Army Corps of Engineers, Waterways Experiment Station, Report No. 1.

BC Ministry of Energy, Mines and Low Carbon Innovation (2015): Investigation report of the Chief Inspector of Mines: Mount Polley mine tailings storage facility breach; BC Ministry of Energy, Mines and Low Carbon Innovation, Mining and Mineral Resources Division, 188 p., URL <https://www2.gov.bc.ca/assets/gov/farming-natural-resources-and-industry/mineral-exploration-mining/documents/directives-alerts-incidents/chief-inspector-s-report-page/m-200_mount_polley_2015-11-30_ci_investigation_report.pdf> [November 2021].

Blight, G.E. and Fourie, A.B. (2003): Catastrophe revisited – disastrous flow failures of mine and municipal solid waste; Geotechnical and Geological Engineering v. 23, p. 219–248.

Brater, E.F. and King, H.W. (1976): Handbook of Hydraulics for the Solution of Hydraulic Engineering Problems (6th edition); McGraw-Hill, New York, New York, 602 p.

Brunner., G.W. (2014): Using HEC-RAS for dam break studies; U.S. Army Corps of Engineers, Institute for Water Resources, Hydrologic Engineering Center, Davis, California.

Brunner., G.W. (2021): HEC-RAS User's Manual; U.S. Army Corps of Engineers, Institute for Water Resources, Hydrologic Engineering Center, Davis, California.

Brunner, G.W., Sanchez, A., Molls, T. and Parr, D.A. (2018): HEC-RAS verification and validation tests; US Army Corps of Engineers, Institute for Water Resources, Hydrologic Engineering Center, Davis, California.

Canadian Dam Association (2021): Tailings Dam Breach Analysis; technical bulletin prepared by the Tailings Dam Breach Working Group of the Canadian Dam Association.

Cuervo, V., Bruge, L., Beaugrand, H., Hendershot, M. and Evans, S.G. (2017): Downstream geomorphic response of the 2014 Mount Polley tailings dam failure, British Columbia; 4th World Landslide Forum, Ljubljana, Slovenia, URL <https://link.springer.com/chapter/10.1007/978-3-319-53483-1_33> [November 2021].

Francis, J.B. (1868): Lowell hydraulic experiments (second edition); D. Van Nostrand, New York, New York, 251 p., URL <https://books.google.ca/books?hl=en&lr=&id=2eZC3fWg2ysC&oi=fnd&pg=PR1&dq=%22Lowell+hydraulic+experiments%22&ots=CwTvBE2nUf&sig=rs8r33re8RHflAqFAhPrXf4_Brk#v=onepage&q=%22Lowell%20hydraulic%20experiments%22&f=false> [November 2021].

Froehlich, D.C. (2008): Embankment dam breach parameters and their uncertainties; Journal of Hydraulic Engineering, v. 134, no. 12, p. 1708–1721.

Ghahramani, N., Mitchell, A., Rana, N.M., McDougall, S., Evans, S.G. and Take, W.A. (2020): Tailings-flow runout analysis: examining the applicability of a semi-physical area-volume relationship using a novel database; Natural Hazards and Earth System Sciences, v. 20, p. 3425–3438.

Goodell, C. and Brunner., G.W. (2012): Flow spike after peak of dam breach floodwave; The RAS Solution: The Place for HEC-RAS Modelers (blog and comments), URL <https://www.kleinschmidtgroup.com/ras-post/flow-spike-after-peak-of-dam-breach-floodwave/> [October 2021].

Goodell, C. and Wahlin, B. (2009): Dynamic and level pool reservoir drawdown – a practical comparison for dam breach modelling; International Association for Hydro-environment Engineering and Research (IAHR), Proceedings of 33rd Congress, Vancouver, Canada.

Goodell, C., Johnson, D., Raeburn, R., Monk, S., Karki, A. and Lee, A. (2018): Probabilistic dam breach modelling using HEC-RAS and McBreach; United States Society on Dams, Proceedings of 38th Annual Conference and Exhibition, Miami, Florida.

Harder, L.F. and Stewart, J.P. (1996): Failure of Tapo Canyon tailings dam; Journal of Performance of Constructed Facilities, v. 10, no. 3, p. 109–114.

Khahledi, M., Haldenwang, R. and Chhabra, R. (2015): Flow rate measurement of non-Newtonian fluids through sharp crested notches; Journal of Hydraulic Engineering, v. 141, no. 1, URL <https://ascelibrary.org/doi/abs/10.1061/(ASCE)HY.1943-7900.0000941> [November 2021].

Martin, V., Fontaine, D. and Cathcart, J. (2015): Challenges with conducting tailings dam breach studies; Proceedings of Tailings and Mine Waste 2015 Conference, Vancouver, British Columbia, URL <https://www.knightpiesold.com/sites/en/assets/File/TMW%202015%20-%20Challenges%20with%20Conducting%20Tailings%20Dam%20Breach%20Studies.pdf> [November 2021].

Morgenstern, N.R., Vick, S.G. and Van Zyl, D. (2015): Report on Mount Polley Tailings Storage Facility Breach; BC Ministry of Energy, Mines and Low Carbon Innovation.

Petkovšek, G., Hassan, M.A.A.M., Lumbroso, D. and Collell, M.R. (2020): A two-fluid simulation of tailings dam breaching; Mine Water and the Environment, v. 40, p. 151–165.

Rana, N.M., Ghahramani, N., Evans, S.G., McDougall, S., Small, A. and Take, W.A. (2021): Catastrophic mass flows resulting from tailings impoundment failures; Engineering Geology, v. 292, p. 1–20.

Ritter, A. (1892): Die fortpflanzung der wasserwellen [The propagation of water waves]; Vereine Deutscher ingenieure zeirschrift, v. 36, no. 2, p. 397–954.

Robertson, P.K., de Melo, L., Williams, D.J. and Wilson, G.W. (2019): Report of the expert panel on the technical causes of the failure of Feijão Dam I; publisher unknown, 71 p., URL <http://www.b1technicalinvestigation.com/report.html> [November 2021].

Schoeman, V. (2018): A conceptual elevation versus volume curve deteration method for tailings dam breach studies; Proceedings of the SANCOLD Annual Conference and AGM, Cape Town, South Africa, URL <https://www.knightpiesold.com/sites/en/assets/File/SANCOLD%202018%20-%20Conceptual%20Elevation%20vs%20Curve%20Deteration%20Model.pdf> [November 2021].

Schoklitsch, A. (1917). Über Dammbuchwellen [On dam breach waves]; Sitzungberichten der Königliche Akademie der Wissenschaften, v. 126 (IIa), p. 1489–1514.

Torres, N.A. and Brio, A.M. (1966): Effects of the March 1965 earthquake on the tailings dams of El Soldado e, province of Valparaiso; Bulletin of the institute of Geological Investigation, Chile.

Wagener, F. (1997): The Merriespruit slimes dam failure: overview and lessons learnt; SAICE Journal, v. 39, no. 3, p. 11–15.

Wahl, T.L. (1998): Prediction of embankment dam breach parameters: a literature review and needs assessment; U.S. Dept. of the Interior, Bureau of Reclamation. Denver, Colorado, Dam Safety Report No. DSO-98-004.

Wahl, T.L. (2004): Uncertainty of predictions of embankment dam breach parameters; Journal of Hydraulic Engineering, v. 130, no. 5, p. 389–397.

Walder, J.S. and O'Connor, J.E. (1997): Methods for predicting peak discharge of floods caused by failure of natural and constructed earthen dams; Water Resources Research, v. 33, no. 10, p. 2337–2348.

Geoscience BC

t: 604 662 4147
e: info@geosciencebc.com

SUITE 1101–750 WEST PENDER ST
VANCOUVER, BC V6C 2T7 CANADA

www.geosciencebc.com